

---

# On the SDEs and Scaling Rules for Adaptive Gradient Algorithms

---

Sadhika Malladi\*    Kaifeng Lyu\*    Abhishek Panigrahi    Sanjeev Arora  
Department of Computer Science  
Princeton University  
{smalladi, klyu, ap34, arora}@cs.princeton.edu

## Abstract

Approximating Stochastic Gradient Descent (SGD) as a Stochastic Differential Equation (SDE) has allowed researchers to enjoy the benefits of studying a continuous optimization trajectory while carefully preserving the stochasticity of SGD. Analogous study of adaptive gradient methods, such as RMSprop and Adam, has been challenging because there were no rigorously proven SDE approximations for these methods. This paper derives the SDE approximations for RMSprop and Adam, giving theoretical guarantees of their correctness as well as experimental validation of their applicability to common large-scaling vision and language settings. A key practical result is the derivation of a *square root scaling rule* to adjust the optimization hyperparameters of RMSprop and Adam when changing batch size, and its empirical validation in deep learning settings.

## 1 Introduction

Distributed synchronous optimization environments have enabled very rapid training of models (in terms of wall-clock time) by allowing a large batch size. Understanding large-batch stochastic optimization is crucial to enjoying the speed-up of this setting. In this context, [1, 2] empirically discovered the *linear scaling rule (LSR)* for Stochastic Gradient Descent (SGD). It calls for scaling learning rate proportionately to the batch size while fixing the number of epochs. It was recognized that the validity of this scaling rule stems from the benefits to generalization due to noise from mini-batch gradient estimation. But naive analysis, as done in [3], suggested that the scaling rule for SGD ought to be *square root* instead of linear. Subsequently, [4] pointed out that since the phenomenon involves varying the LR even down to zero, the correct analysis should invoke a continuous view, namely a stochastic differential equation (SDE). The SDE view helps identify the correct scaling of the noise and leads to a derivation of the linear scaling rule (see Section 2.2).

However, extending the SDE approach—i.e., continuous-time approximations—to popular adaptive optimization algorithms, like RMSprop [5] and Adam [6], has been challenging due to their use of coordinate-wise normalization. By ignoring gradient noise, [7] derived intuitive continuous approximations for full-batch RMSprop and Adam; however, this deterministic view precludes a scaling rule.

Recent papers have suggested a *square root* scaling rule for adaptive algorithms: set the learning rate proportionately to the *square root* of the batch size while fixing the number of epochs. Based on perturbation theory, [8] proposed the square root scaling rule for RMSprop and Adam but could only reason about optimization behavior near convergence, not along the entire trajectory. A square root scaling rule was also empirically discovered for another adaptive gradient method called *LAMB* [9], which is an optimization method with layerwise adaptive learning rates, designed for better optimization and generalization in large-batch training. Instead of tuning learning rates while

increasing batch size, LAMB used the square root scaling rule to automatically adjust the learning rate and achieve strong performance on vision and language tasks.

In this paper, we make the following contributions.

1. We propose new SDE approximations for two popular adaptive optimization algorithms, RMSprop and Adam (Definitions 4.1 and 4.3) in Theorems 4.2 and 4.4. We prove that these approximations are *1st-order weak approximations* (Definition 2.4), providing a calculus-based guarantee of the approximation strength between the SDEs and their corresponding discrete processes as was done for SGD and its SDE in [10].
2. Our SDE approximations immediately yield square-root scaling rules (Definitions 5.1 and 5.2) for adjusting the optimization hyperparameters of Adam and RMSprop when changing batch size to ensure that the resulting discrete trajectories are all 1st-order weak approximations of the same SDE (Theorem 5.3). Experiments (Figures 1 and 2 and Appendix I) validate the scaling rules in the vision and language modeling domains.
3. We provide efficient experimental verification of the validity of the SDE approximation for the adaptive algorithms in realistic deep nets (Definitions 5.1 and 5.2). Direct simulation of the SDE, e.g., Euler-Maruyama, is prohibitively expensive because it requires computing the full gradient and noise covariance at fine-grained intervals. Hence we adapt (Definition 6.2) the new and efficient *SVAG simulation* for SGD [11] for use with our proposed SDEs and rigorously prove its correctness (Theorem 6.3). Using SVAG, we provide evidence that the proposed SDE approximations track the analogous discrete trajectories in many common large-scale vision and language settings (Figure 3 and Appendix H).

## 2 Preliminaries

We use  $\mathbf{v} \odot \mathbf{u}$ ,  $\mathbf{v}^2$ ,  $\sqrt{\mathbf{v}}$  to denote coordinate-wise operators for multiplication, taking squares, taking square roots. For ease of exposition we modify RMSprop and Adam to use  $\mathbf{v}_k$  in the update for  $\boldsymbol{\theta}_k$  instead of using  $\mathbf{v}_{k+1}$ .<sup>1</sup> We also assume that  $\mathbf{v}_0$  is nonzero if  $\epsilon$  is 0 to avoid division by zero.

**Definition 2.1** (RMSprop Algorithm, [5]).

$$\boldsymbol{\theta}_{k+1} = \boldsymbol{\theta}_k - \eta \mathbf{g}_k \odot (\sqrt{\mathbf{v}_k} + \epsilon)^{-1}, \quad \mathbf{v}_{k+1} = \beta \mathbf{v}_k + (1 - \beta) \mathbf{g}_k^2,$$

where  $\boldsymbol{\theta}_k$  is the parameter,  $\mathbf{g}_k$  is the stochastic gradient at step  $k$ , and  $\mathbf{v}_k$  is an estimate for the second moment of  $\mathbf{g}_k$ .

**Definition 2.2** (Adam Algorithm, [6]).

$$\begin{aligned} \mathbf{m}_{k+1} &= \beta_1 \mathbf{m}_k + (1 - \beta_1) \mathbf{g}_k, & \mathbf{v}_{k+1} &= \beta_2 \mathbf{v}_k + (1 - \beta_2) \mathbf{g}_k^2, & \widehat{\mathbf{m}}_{k+1} &= \mathbf{m}_{k+1} \odot (1 - \beta_1^{k+1})^{-1}, \\ \widehat{\mathbf{v}}_{k+1} &= \mathbf{v}_{k+1} \odot (1 - \beta_2^{k+1})^{-1}, & \boldsymbol{\theta}_{k+1} &= \boldsymbol{\theta}_k - \eta \widehat{\mathbf{m}}_{k+1} \odot (\sqrt{\widehat{\mathbf{v}}_{k+1}} + \epsilon)^{-1}, \end{aligned}$$

where  $\boldsymbol{\theta}_k$  is the parameter,  $\mathbf{g}_k$  is the stochastic gradient at step  $k$ ,  $\mathbf{m}_k$  is the momentum, and  $\mathbf{v}_k$  is an estimate for the second moment of  $\mathbf{g}_k$ .

### 2.1 Noisy Gradient Oracle with Scale Parameter

We abstract the stochastic gradient as being provided by a *noisy* oracle for the full gradient. We formulate the oracle to highlight the phenomenon of interest: changing the batch size affects the scale of the noise.

**Definition 2.3.** A *Noisy Gradient Oracle with Scale Parameter* (NGOS) is characterized by a tuple  $\mathcal{G}_\sigma = (f, \Sigma, \mathcal{Z}_\sigma)$ . Given a (noise) scale parameter  $\sigma > 0$ ,  $\mathcal{G}$  takes an input  $\boldsymbol{\theta}$  and returns  $\mathbf{g} = \nabla f(\boldsymbol{\theta}) + \sigma \mathbf{z}$ , where  $\nabla f(\boldsymbol{\theta})$  is the gradient of  $f$  at  $\boldsymbol{\theta}$ ,  $\mathbf{z}$  is the gradient noise drawn from the probability distribution  $\mathcal{Z}_\sigma(\boldsymbol{\theta})$  with mean zero and covariance matrix  $\Sigma(\boldsymbol{\theta})$ . We use  $\mathcal{G}_\sigma(\boldsymbol{\theta})$  to denote the distribution of  $\mathbf{g}$  given  $\sigma$  and  $\boldsymbol{\theta}$ . The probability distribution  $\mathcal{Z}_\sigma(\boldsymbol{\theta})$  can change with the scale  $\sigma$ , but the covariance matrix  $\Sigma(\boldsymbol{\theta})$  is fixed across different noise scales.

For all  $\mathbf{g}_k$  in Definitions 2.1 and 2.2, we assume that  $\mathbf{g}_k$  is drawn from a noisy gradient oracle  $\mathcal{G}_\sigma$ . In our setting, as is common when batches are sampled with replacement,  $\sigma$  is primarily controlled

<sup>1</sup>Experiments in Appendix G.2 show that this change does not significantly impact performance.

through the batch size; in particular,  $\sigma \sim 1/\sqrt{B}$  (see Appendix F.1 for a derivation). For sampling with replacement on a finite dataset of size  $n$ , where  $f_1(\boldsymbol{\theta}), \dots, f_n(\boldsymbol{\theta})$  are the loss functions for the  $n$  data points (and the average of these  $n$  functions is  $f(\boldsymbol{\theta})$ ), this covariance matrix for a given parameter  $\boldsymbol{\theta}$  can be explicitly written as

$$\boldsymbol{\Sigma}(\boldsymbol{\theta}) = \frac{1}{n} \sum_{i=1}^n (\nabla f_i(\boldsymbol{\theta}) - \nabla f(\boldsymbol{\theta})) (\nabla f_i(\boldsymbol{\theta}) - \nabla f(\boldsymbol{\theta}))^\top. \quad (1)$$

## 2.2 SDE Approximation and Scaling Rules

Under appropriate conditions it becomes possible to approximate SGD via an Itô SDE, which uses Brownian motion to model the noise and has the following general form, where  $W_t$  is a Wiener process:  $d\mathbf{X}_t = \mathbf{b}(\mathbf{X}_t)dt + \boldsymbol{\sigma}(\mathbf{X}_t)dW_t$ . The SGD update rule for a loss  $f$  is  $\mathbf{x}_{k+1} = \mathbf{x}_k - \eta \mathbf{g}_k$ , where  $\eta$  is the learning rate and  $\mathbf{g}_k$  is given by the NGOS on input  $\mathbf{x}_k$ . The following is the canonical interpretation of SGD as an SDE:

$$d\mathbf{X}_t = -\nabla f(\mathbf{X}_t)dt + \sqrt{\eta} \boldsymbol{\Sigma}^{1/2}(\mathbf{X}_t)dW_t. \quad (2)$$

Equation (2) hints at a relationship between learning rate and gradient noise—specifically, the *linear scaling rule*—since scaling batch size by factor  $\kappa$  scales the noise covariance by  $1/\kappa$ , which can be canceled by scaling  $\eta$  by  $\kappa$  as well [4]. Therefore, the linear scaling rule ensures the SDE approximation does not change when using a different batch size. With the same methodology, the current paper studies the SDE approximations for adaptive gradient algorithms to derive the square root scaling rule for them.

## 2.3 Quality of SDE Approximation and Theoretical Assumptions

The quality of the SDE approximation can be measured empirically (Section 6) and bounded theoretically using a calculus-based guarantee, which was initiated in the context of deep learning in [10]. In particular, the theoretical guarantee uses the following notion of approximation between discrete and continuous stochastic processes by comparing iteration  $k$  in the discrete process with continuous time  $k\eta_e$ , where  $\eta_e > 0$  is the (effective) step size of the discrete process.

**Definition 2.4** (Order-1 Weak Approximation, [10]). Let  $\{\mathbf{X}_t^{\eta_e} : t \in [0, T]\}$  and  $\{\mathbf{x}_k^{\eta_e}\}_{k=0}^{\lfloor T/\eta_e \rfloor}$  be families of continuous and discrete stochastic processes parametrized by  $\eta_e$ . We say  $\{\mathbf{X}_t^{\eta_e}\}$  and  $\{\mathbf{x}_k^{\eta_e}\}$  are order-1 weak approximations of each other if for every test function  $g$  with at most polynomial growth (Definition B.1), there exists a constant  $C > 0$  independent of  $\eta_e$  such that

$$\max_{k=0, \dots, \lfloor T/\eta_e \rfloor} |\mathbb{E}g(\mathbf{x}_k^{\eta_e}) - \mathbb{E}g(\mathbf{X}_{k\eta_e}^{\eta_e})| \leq C\eta_e$$

A function  $g: \mathbb{R}^d \rightarrow \mathbb{R}$  is said to have *polynomial growth* if there exist positive integers  $\kappa_1, \kappa_2 > 0$  such that  $|g(\mathbf{x})| \leq \kappa_1(1 + \|\mathbf{x}\|_2^{2\kappa_2})$  for all  $\mathbf{x} \in \mathbb{R}^d$  (Definition B.1). The above definition measures the strength of the approximation by the closeness of a test function  $g$  computed on the iterates of both trajectories. The approximation becomes stronger in this sense as  $\eta_e$  becomes smaller. In the SDE approximation of SGD,  $\eta_e = \eta$  and  $k$  steps correspond to continuous time  $k\eta$ . A key difference between SGD and adaptive algorithms is that  $\eta_e = \eta^2$  for both RMSprop and Adam, which means  $k$  steps correspond to continuous time  $k\eta^2$ . We validate this time-scaling theoretically in Section 4.

Now we formalize the assumptions needed in the theory. Since our analysis framework is based upon calculus, it becomes necessary to assume differentiability conditions on the NGOS (Definition 2.5). Similar differentiability conditions also appear in prior SDE works [10, 11], and we note that lately it has become clear that restricting to differentiable losses (via differentiable node activations such as Swish [12]) does not hinder good performance.

**Definition 2.5** (Well-behaved NGOS). The loss function  $f$  and covariance matrix function  $\boldsymbol{\Sigma}$  in a NGOS  $\mathcal{G}_\sigma$  are *well-behaved* if they satisfy<sup>2</sup>: (1)  $\nabla f(\boldsymbol{\theta})$  is Lipschitz and  $\mathcal{C}^\infty$ -smooth; (2) The square root of covariance matrix  $\boldsymbol{\Sigma}^{1/2}(\boldsymbol{\theta})$  is bounded, Lipschitz, and  $\mathcal{C}^\infty$ -smooth; and (3) All partial derivatives of  $\nabla f(\boldsymbol{\theta})$  and  $\boldsymbol{\Sigma}^{1/2}(\boldsymbol{\theta})$  up to and including the 4-th order have polynomial growth. We also say that the NGOS  $\mathcal{G}_\sigma$  is well-behaved if  $f$  and  $\boldsymbol{\Sigma}$  are well-behaved.

<sup>2</sup>Note:  $\mathcal{C}^\infty$ -smoothness can be relaxed using the mollification technique from [10].

Deriving an SDE approximation also requires conditions on the noise distribution in the NGOS. It is allowed to be non-Gaussian, but not heavy-tailed. We require an upper bound on the third moment of the noise so that the distribution is not very skewed. For other higher order moments, we require  $\mathbb{E}_{\mathbf{z} \sim \mathcal{Z}_\sigma} [\|\mathbf{z}\|_2^p]^{1/p}$ , namely the  $L^p$ -norm of random variable  $\|\mathbf{z}\|_2$ , to grow at most linearly as a function of  $\theta$  (which is implied by ensuring an upper bound on all even order moments). We note that the following conditions are standard in prior work using Itô SDEs to study SGD.

**Definition 2.6** (Low Skewness Condition). The NGOS  $\mathcal{G}_\sigma$  is said to satisfy the *low skewness condition* if there is a function  $K_3(\theta)$  of polynomial growth (independent of  $\sigma$ ) such that  $|\mathbb{E}_{\mathbf{z} \sim \mathcal{Z}_\sigma(\theta)}[\mathbf{z}^{\otimes 3}]| \leq K_3(\theta)/\sigma$  for all  $\theta \in \mathbb{R}^d$  and all noise scale parameters  $\sigma$ .

**Definition 2.7** (Bounded Moments Condition). The NGOS  $\mathcal{G}_\sigma$  is said to satisfy the *bounded moments condition* if for all integers  $m \geq 1$  and all noise scale parameters  $\sigma$ , there exists a constant  $C_{2m}$  (independent of  $\sigma$ ) such that  $\mathbb{E}_{\mathbf{z} \sim \mathcal{Z}_\sigma(\theta)}[\|\mathbf{z}\|_2^{2m}]^{\frac{1}{2m}} \leq C_{2m}(1 + \|\theta\|_2)$  for all  $\theta \in \mathbb{R}^d$ .

For well-behaved loss  $f(\theta)$  and covariance  $\Sigma(\theta)$ , the above two conditions are satisfied when  $\mathcal{Z}_\sigma$  is the Gaussian distribution with mean zero and covariance  $\Sigma(\theta)$ . That is, the Gaussian NGOS  $\mathbf{g} \sim \mathcal{N}(\nabla f(\theta), \sigma^2 \Sigma(\theta))$  satisfies the low skewness and bounded moments conditions. The low skewness condition holds because the odd moments of a Gaussian are all zeros, and the bounded moments condition can be verified since  $\mathbb{E}_{\mathbf{z} \sim \mathcal{N}(0, \Sigma(\theta))}[\|\mathbf{z}\|_2^{2m}]^{\frac{1}{2m}} \leq \mathbb{E}_{\mathbf{w} \sim \mathcal{N}(0, \mathbf{I})}[\|\mathbf{w}\|_2^{2m}]^{\frac{1}{2m}} \cdot \|\Sigma^{1/2}(\theta)\|_2$  and  $\Sigma^{1/2}(\theta)$  is Lipschitz.

The Gaussian NGOS with  $\sigma = \frac{1}{\sqrt{B}}$  can be seen as an approximation of the gradient noise in a mini-batch training with batch size  $B$ , if  $\Sigma(\theta)$  is set to match with (1). But this does not directly imply that the gradient noise in mini-batch training satisfies the low skewness and bounded moments conditions, as the noise is not exactly Gaussian. Assuming that the gradient of the loss function  $f_i(\theta)$  at every data point is Lipschitz, these two conditions can indeed be verified for all batch sizes  $B \geq 1$ .

One limitation of our assumptions is that  $K_3(\theta)$  and  $C_{2m}$  could be large in practice, meaning higher order moments of the gradient noise have non-negligible effects on training. [13] and [14] presented experimental evidence that the noise is heavy-tailed<sup>3</sup>. However, [11, 16] highlighted issues with the evidence, noting that the measurements used in [14] are intended only for scalar values. When applied to vector valued distributions the measurement can (incorrectly) identify a multi-dimensional Gaussian distribution as heavy-tailed too [11]. Hence, the heavy-tailedness of real-world gradient noise remains an open question. The success of our empirical validations of the SDE approximations, through the scaling rule and SVAG, suggests that our assumptions are not too strong. We leave it for future work to investigate if and how heavy-tailed noise plays a role in adaptive optimization.

### 3 Related Work

We defer a full discussion of empirical and theoretical works on adaptive gradient methods to Appendix A.1 and only discuss works relevant to SDEs and scaling rules here.

**Applications of SDE Approximations.** There are applications of the SDE approximation beyond the derivation of a scaling rule. [17] and [18] assumed that the loss has some symmetry (i.e., scale invariance) and studied the resulting dynamics. Furthermore, [17] used this property to explain the phenomenon of sudden rising error after LR decay in training. [16] analyzed why SGD favors flat minima using an SDE-motivated diffusion model.

**Past Work on Square Root Scaling Rule.** As mentioned before, square root scaling was incorrectly believed for a few years to be theoretically justified for SGD. [8] decomposed the stochastic Hessian during batch training into a deterministic Hessian and stochastic sampling perturbation and assumes one of the components to be low rank to propose a square root scaling rule. [9] empirically discovered a square root scaling rule for language models trained by LAMB, a layer-wise variant of Adam. [19] heuristically derived, but did not show an approximation bound for, a second-order

<sup>3</sup>This motivated [15] to consider a Lévy SDE approximation (instead of Itô SDE) to study the (worse) generalization behavior of Adam. However, the quality of the Lévy SDE approximation was not formally guaranteed (e.g., in the sense of Definition 2.4), so finding a guaranteed approximation for adaptive optimization algorithms remains an open problem.

SDE for approximating Adam, and they applied the SDE to study the time needed for Adam to escape sharp minima. [19] did not discuss a scaling rule, though their proposed SDE may admit one. Similarly, [15] derived a Lévy SDE for Adam, but no approximation bounds are given in the paper.

## 4 SDEs for Adaptive Algorithms

An SDE approximation operates in continuous time and thus implicitly considers the limit  $\eta \rightarrow 0$ . In adaptive algorithms, the moment averaging parameters  $\beta, \beta_1, \beta_2$  and  $\eta$  must be taken to limits such that the adaptivity and stochasticity can still be studied. For example, if  $\beta, \beta_1, \beta_2$  remain fixed when  $\eta \rightarrow 0$ , then the algorithm computes the moving averages in a very small neighborhood, which averages out the effects of gradient noise and gradient history, causing the flow to turn into deterministic SignGD [7]. We will need to assume  $\beta, \beta_1, \beta_2 \rightarrow 1$  as  $\eta \rightarrow 0$ , which implies the impact of the history grows as the learning rate decreases, and thus the adaptive features of these algorithms can still be studied in the continuous approximation [7]. To keep the stochastic nature of the flow, we require the noise from mini-batching dominate the gradient updates.

### 4.1 Warm-Up: Linear loss

To build intuition for the SDE and the scaling rule, we first study a simplified setting. In particular, consider a linear loss  $f(\boldsymbol{\theta}) = \langle \boldsymbol{\theta}, \bar{\mathbf{g}} \rangle$  and isotropic noise in the NGOS, namely  $\mathbf{g}_k \sim \mathcal{N}(\bar{\mathbf{g}}, \sigma^2 \mathbf{I})$ . The RMSprop update  $\mathbf{v}_{k+1} = \beta \mathbf{v}_k + (1 - \beta) \mathbf{g}_k^2$  can be expanded as  $\mathbf{v}_k = \beta^k \mathbf{v}_0 + (1 - \beta) \sum_{j=0}^{k-1} \beta^j \mathbf{g}_j^2$ . By linearity of expectation,

$$\mathbb{E}[\mathbf{v}_k] = \beta^k \mathbf{v}_0 + (1 - \beta) \sum_{j=0}^{k-1} \beta^j (\bar{\mathbf{g}}^2 + \sigma^2 \mathbf{1}) = \beta^k \mathbf{v}_0 + (1 - \beta^k) (\bar{\mathbf{g}}^2 + \sigma^2 \mathbf{1}).$$

This suggests that  $\mathbb{E}[\mathbf{v}_k]$  is approximately  $\bar{\mathbf{g}}^2 + \sigma^2 \mathbf{1}$  after a sufficient number of steps. Setting  $\mathbf{v}_0 = \bar{\mathbf{g}}^2 + \sigma^2 \mathbf{1}$ , we see that the approximation  $\mathbb{E}[\mathbf{v}_k] = \bar{\mathbf{g}}^2 + \sigma^2 \mathbf{1}$  becomes exact for all  $k \geq 0$ .

Using the linearity of variance (for independent variables), the standard deviation of each coordinate of  $\mathbf{v}_k$  is of scale  $\mathcal{O}((1 - \beta)\sigma^2)$ . Moreover, the expectation  $\mathbb{E}[\mathbf{v}_k]$  is of scale  $\mathcal{O}(\sigma^2)$ , so we know that  $\mathbf{v}_k$  is nearly deterministic and concentrates around its expectation  $\bar{\mathbf{g}}^2 + \sigma^2 \mathbf{1}$  when  $\beta$  is close to 1. Therefore, we take the approximation  $\mathbf{v}_k \approx \bar{\mathbf{g}}^2 + \sigma^2 \mathbf{1}$  for all  $k \geq 0$ . Ignoring  $\epsilon$ , the RMSprop update rule becomes:

$$\boldsymbol{\theta}_{k+1} \approx \boldsymbol{\theta}_k - \eta \mathbf{g}_k \odot (\bar{\mathbf{g}}^2 + \sigma^2 \mathbf{1})^{-1/2}. \quad (3)$$

These dynamics depend on the relative magnitudes of  $\bar{\mathbf{g}}$  and  $\sigma$ . We show that when  $\sigma \ll \|\bar{\mathbf{g}}\|$ , no SDE approximation can exist in Appendix F.2. Here, we explore the case where  $\sigma \gg \|\bar{\mathbf{g}}\|$  which implies  $\boldsymbol{\theta}_{k+1} \approx \boldsymbol{\theta}_k - \frac{\eta}{\sigma} \mathbf{g}_k$ . Noting that  $\mathbf{g}_k \sim \mathcal{N}(\bar{\mathbf{g}}, \sigma^2 \mathbf{I})$  gives  $\boldsymbol{\theta}_{k+1} - \boldsymbol{\theta}_k \sim \mathcal{N}(\frac{\eta}{\sigma} \bar{\mathbf{g}}, \eta^2 \mathbf{I})$  approximately. Since Gaussian variables are additive, we can take a telescoping sum to obtain the marginal distribution of  $\boldsymbol{\theta}_k$ :  $\boldsymbol{\theta}_k \sim \mathcal{N}((k\eta/\sigma)\bar{\mathbf{g}}, k\eta^2 \mathbf{I})$  approximately.

If an SDE approximation of RMSprop exists, then  $\boldsymbol{\theta}_k$  can be closely approximated by a *fixed* random variable from the corresponding stochastic process at a fixed (continuous) time  $t$ . Thus, to keep the SDE unchanged upon changing the noise scale  $\sigma$ , the hyperparameters must be adjusted to keep  $\frac{k\eta}{\sigma}$  and  $k\eta^2$  unchanged, which implies  $\eta \sim \frac{1}{\sigma}$  and  $k \sim \frac{1}{\eta^2}$ . These observations intuitively yield the square root scaling rule: noting that  $\sigma$  changes with mini-batch size  $B$  as  $\sigma \sim 1/\sqrt{B}$  suggests  $\eta \sim \sqrt{B}$ , and  $k \sim 1/B$ .

### 4.2 SDE Approximations for Adaptive Algorithms

Having established intuition in a highly simplified setting for adaptive algorithms, we now return to a more general and realistic setting. We derive the SDEs that are order-1 approximations of the discrete RMSprop and Adam algorithms under Definition 2.5, where the SDE states consist of both the parameters  $\boldsymbol{\theta}$  and moment estimates. From the example of Section 4.1, we see that SDE approximations may exist if  $\sigma \sim 1/\eta^2$  and  $\sigma \gg \|\bar{\mathbf{g}}\|$  (see Appendix G.1 for empirical validation of this assumption). In this case, we can prove that  $k \sim \eta^2$  is true not only for the simple setting above but also in general. This is a key difference to the SDE for SGD — each step in RMSprop or Adam

corresponds to a time interval of  $\eta^2$  in SDEs, but each SGD step corresponds to a time interval of  $\eta$ . In Section 4.1,  $\mathbf{v} \sim \sigma^2 \sim 1/\eta^2$  grows to infinity as  $\eta \rightarrow 0$ . This also happens in the general setting, so we track  $\mathbf{u}_k \triangleq \mathbf{v}_k/\sigma^2$  (instead of  $\mathbf{v}_k$  directly) in the SDEs.

**Definition 4.1** (SDE for RMSprop). Let  $\sigma_0 \triangleq \sigma\eta$ ,  $\epsilon_0 \triangleq \epsilon\eta$ , and  $c_2 \triangleq (1 - \beta)/\eta^2$ . Define the state of the SDE as  $\mathbf{X}_t = (\boldsymbol{\theta}_t, \mathbf{u}_t)$  and the dynamics as

$$d\boldsymbol{\theta}_t = -\mathbf{P}_t^{-1} \left( \nabla f(\boldsymbol{\theta}_t) dt + \sigma_0 \boldsymbol{\Sigma}^{1/2}(\boldsymbol{\theta}_t) d\mathbf{W}_t \right), \quad d\mathbf{u}_t = c_2(\text{diag}(\boldsymbol{\Sigma}(\boldsymbol{\theta}_t)) - \mathbf{u}_t) dt$$

where  $\mathbf{P}_t := \sigma_0 \text{diag}(\mathbf{u}_t)^{1/2} + \epsilon_0 \mathbf{I}$  is a preconditioner matrix, and  $\mathbf{W}_t$  is the Wiener process.

**Theorem 4.2** (Informal version of Theorem C.1). Let  $\mathbf{u}_k \triangleq \mathbf{v}_k/\sigma^2$  and define the state of the discrete RMSprop trajectory with hyperparameters  $\eta, \beta, \epsilon$  (Definition 2.1) as  $\mathbf{x}_k = (\boldsymbol{\theta}_k, \mathbf{u}_k)$ . Then, for a well-behaved NGOS (Definition 2.3) satisfying the skewness and bounded moments conditions (Definitions 2.6 and 2.7), the SDE in Definition 4.1 satisfies

$$\max_{k=0, \dots, \lfloor T/\eta^2 \rfloor} |\mathbb{E}g(\mathbf{x}_k) - \mathbb{E}g(\mathbf{X}_{k\eta^2})| \leq C\eta^2$$

where  $g$  and  $T$  are defined as in Definition 2.4.

*Proof.* We provide a proof sketch here and defer the technical details to Theorem C.1. The proof follows the same steps as [10]: first, we compute the approximation error of the continuous trajectory after one step in discrete time. Then, we use the single step error to bound the error over a finite interval of time. The proof additionally relies on constructing an auxiliary SDE with an equivalent distribution to the desired SDE (Theorem C.3) but with better smoothness conditions, and we prove this SDE to be an order-1 weak approximation of the discrete trajectory.  $\square$

We need to find continuous approximations of the normalization constants in Adam (Definition 2.2). As in the RMSprop case, we take  $(1 - \beta_2)/\eta^2 = c_2$ . Then, we can estimate the normalization constant  $1 - \beta_2^k$  in continuous time  $t = k\eta^2$  as  $1 - \beta_2^k = 1 - (1 - c_2\eta^2)^{t/\eta^2} \approx 1 - \exp(-c_2t)$ . We can do the analogous approximation for the other normalization constant  $1 - \beta_1^k$  in Adam. Taking  $(1 - \beta_1)/\eta^2 = c_1$ , we can approximate it as  $1 - \beta_1^k \approx 1 - \exp(-c_1t)$ . This is a heuristic approach to deal with the normalization constants, but we can indeed justify it in theory.

**Definition 4.3** (Adam SDE). Let  $c_1 \triangleq (1 - \beta_1)/\eta^2$  and define  $\mathbf{u}_k, \sigma_0, c_2, \epsilon_0, \boldsymbol{\Sigma}(\boldsymbol{\theta}_t)$  as in Definition 4.1. Let  $\gamma_1(t) \triangleq 1 - \exp(-c_1t)$  and  $\gamma_2(t) \triangleq 1 - \exp(-c_2t)$ . Define the state of the SDE as  $\mathbf{X}_t = (\boldsymbol{\theta}_t, \mathbf{m}_t, \mathbf{u}_t)$  and the dynamics as

$$d\boldsymbol{\theta}_t = -\frac{\sqrt{\gamma_2(t)}}{\gamma_1(t)} \mathbf{P}_t^{-1} \mathbf{m}_t dt, \quad d\mathbf{m}_t = c_1(\nabla f(\boldsymbol{\theta}_t) - \mathbf{m}_t) dt + \sigma_0 c_1 \boldsymbol{\Sigma}^{1/2}(\boldsymbol{\theta}_t) d\mathbf{W}_t, \\ d\mathbf{u}_t = c_2(\text{diag}(\boldsymbol{\Sigma}(\boldsymbol{\theta}_t)) - \mathbf{u}_t) dt,$$

where  $\mathbf{P}_t := \sigma_0 \text{diag}(\mathbf{u}_t)^{1/2} + \epsilon_0 \sqrt{\gamma_2(t)} \mathbf{I}$  is a preconditioner matrix,  $\mathbf{W}_t$  is the Wiener process.

Our main theorem for Adam is given below. The initial steps of the discrete Adam trajectory can be discontinuous and noisy because of the normalization constants changing drastically. Hence, we introduce a constant  $t_0$  and show that for any  $t_0$ , we can construct an SDE to be a weak approximation for Adam starting from the  $\lceil t_0/\eta^2 \rceil$ -th step of Adam.

**Theorem 4.4** (Informal version of Theorem D.1). Define  $\mathbf{u}_k = \mathbf{v}_k/\sigma^2$  and let  $\mathbf{x}_k = (\boldsymbol{\theta}_k, \mathbf{m}_k, \mathbf{u}_k) \in \mathbb{R}^{3d}$  be the state of the discrete Adam trajectory with hyperparameters  $\eta, \beta_1, \beta_2, \epsilon$ . Then, for a well-behaved NGOS (Definition 2.3) satisfying the skewness and bounded moments conditions (Definitions 2.6 and 2.7) and any  $t_0 > 0$ , the SDE in Definition 4.3 satisfies

$$\max_{k=\lceil t_0/\eta^2 \rceil, \dots, \lfloor T/\eta^2 \rfloor} |\mathbb{E}g(\mathbf{x}_k) - \mathbb{E}g(\mathbf{X}_{k\eta^2})| \leq C\eta^2$$

where  $g$  and  $T$  are defined as in Definition 2.4 and the initial condition of the SDE is  $\mathbf{X}_{t_0} = \mathbf{x}_{\lceil t_0/\eta^2 \rceil}$ .

## 5 Square Root Scaling Rule

The SDE approximations in Definitions 4.1 and 4.3 motivate scaling rules for how to adjust the optimization hyperparameters when changing the batch size. In order for  $\sigma_0, c_1, c_2$ , and  $\epsilon_0$  to remain constant, as required by the SDEs, one needs to change  $\eta, \beta, \beta_1, \beta_2$ , and  $\epsilon$  accordingly.

**Definition 5.1** (RMSprop Scaling Rule). When running RMSprop (Definition 2.1) with batch size  $B' = \kappa B$ , use the hyperparameters  $\eta' = \eta\sqrt{\kappa}$ ,  $\beta' = 1 - \kappa(1 - \beta)$ , and  $\epsilon' = \frac{\epsilon}{\sqrt{\kappa}}$ .

**Definition 5.2** (Adam Scaling Rule). When running Adam (Definition 2.2) with batch size  $B' = \kappa B$ , use the hyperparameters  $\eta' = \eta\sqrt{\kappa}$ ,  $\beta'_1 = 1 - \kappa(1 - \beta_1)$ ,  $\beta'_2 = 1 - \kappa(1 - \beta_2)$ , and  $\epsilon' = \frac{\epsilon}{\sqrt{\kappa}}$ .

**Theorem 5.3** (Validity of the Scaling Rules). *Suppose we have a well-behaved NGOS satisfying the low skewness and bounded moments conditions.*

1. Let  $\mathbf{x}_k^{(B)}$  be the discrete RMSprop (Definition 2.1) trajectory with batch size  $B$  and hyperparameters  $\eta, \beta$ , and  $\epsilon$ . Let  $\mathbf{x}_k^{(\kappa B)}$  be the trajectory with batch size  $\kappa B$  and hyperparameters adjusted according to Definition 5.1. If  $\mathbf{x}_k^{(B)}$  and  $\mathbf{x}_k^{(\kappa B)}$  start from the same initial point, then with  $g$  and  $T$  defined as in Definition 2.4,  $\max_{k=0, \dots, \lfloor T/\eta^2 \rfloor} \left| \mathbb{E}g(\mathbf{x}_k^{(B)}) - \mathbb{E}g(\mathbf{x}_{\lfloor k/\kappa \rfloor}^{(\kappa B)}) \right| \leq C(1 + \kappa)\eta^2$ .
2. Fix  $t_0 > 0$ . Let  $\mathbf{x}_k^{(B)}$  be the discrete Adam (Definition 2.2) trajectory with batch size  $B$  and hyperparameters  $\eta, \beta_1, \beta_2$ , and  $\epsilon$ . Let  $\mathbf{x}_k^{(\kappa B)}$  be the trajectory with batch size  $\kappa B$  and hyperparameters adjusted according to Definition 5.2. If  $\mathbf{x}_{\lceil t_0/\eta^2 \rceil}^{(B)}$  and  $\mathbf{x}_{\lceil \kappa t_0/\eta^2 \rceil}^{(\kappa B)}$  are equal, then with  $g$  and  $T$  defined as in Definition 2.4,  $\max_{k=\lceil t_0/\eta^2 \rceil, \dots, \lfloor T/\eta^2 \rfloor} \left| \mathbb{E}g(\mathbf{x}_k^{(B)}) - \mathbb{E}g(\mathbf{x}_{\lfloor k/\kappa \rfloor}^{(\kappa B)}) \right| \leq C(1 + \kappa)\eta^2$ .

*Proof.* By the linearity of covariance, scaling the batch size by  $\kappa$  only modifies the NGOS by scaling  $\sigma$  by  $1/\sqrt{\kappa}$ . Hence, both scaling rules ensure that  $\sigma_0, c_1, c_2$ , and  $\epsilon_0$  (and thus, the SDEs) are unchanged when the batch size changes. The approximation bounds in Theorems 4.2 and 4.4 are in terms of  $\eta^2$ , and since  $\eta$  is scaled here by  $\sqrt{\kappa}$ , the same method gives an upper bound  $C\kappa\eta^2$ . Adding the approximation bounds for  $\eta$  and  $\sqrt{\kappa}\eta$  together gives  $C(1 + \kappa)\eta^2$ .  $\square$

*Remark 5.4.* The  $t_0$  condition on the Adam rule, a holdover from the condition in Theorem 4.4, implies that our theory only directly applies when there is a warm-start phase of  $\lceil t_0/\eta^2 \rceil$ , where the marginal distribution of the trainable parameters at the end of the phase is the same across different learning rates  $\eta$ . Regardless, the scaling rules are shown to work in practice even without this phase.

The scaling rules depend on maintaining the same SDE approximation, so the bounded moments and low skewness conditions are sufficient (but not necessary) for this scaling rule to work. [11] provided an analogous discussion for SGD, and they show the scaling rule can hold even if there is heavy-tailed noise. We leave a study of heavy-tailed gradient noise in adaptive algorithms as future work.

**Experiments.** Figures 1 and 2 show the square root scaling rule applied to ResNet-50 [20] and VGG-16 [21] trained on CIFAR-10 [22], RoBERTa-large [23] trained on the Wiki+Books corpus [24], 12-layer GPT [25] on WikiText-103 [26] and ResNet-50 trained on ImageNet [27]. We use the efficient language model pre-training recipe outlined in [28]. Appendix I has many additional settings, including ablations against other scaling rules (Appendix I.1).

## 6 SVAG for Adaptive Algorithms

Validating the approximation strength captured in Definition 2.4 involves comparing the discrete algorithms and their SDEs on a set of test functions. However, obtaining the SDE solution through traditional simulations, e.g., Euler-Maruyama, is computationally intractable.<sup>4</sup>

[11] proposed an efficient simulation, SVAG, of the SDE for SGD in the finite LR regime: scale the constant LR by  $1/\ell$  and take the limit  $\ell \rightarrow \infty$ . In practice the simulation converges for a small

<sup>4</sup>One can also simulate the SDE by constructing 1st-order weak approximations while taking  $\eta \rightarrow 0$  along the scaling rules, but the batch size cannot be smaller than 1 and hence  $\eta$  cannot go arbitrarily close to the limit.

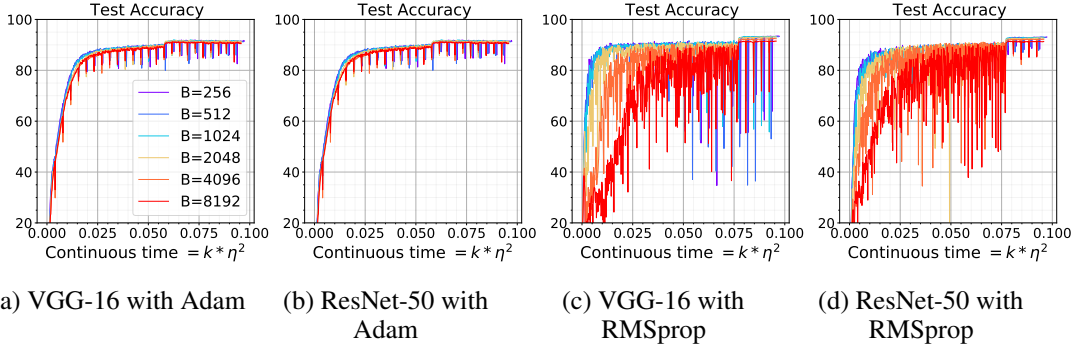


Figure 1: Square root scaling rule experiments on CIFAR-10 with VGG-16 and ResNet-50 (details in Appendix J). Same color legend has been used across all the plots. The performance gap between  $B = 256$  and  $B = 8192$  is at most 3% in all cases.

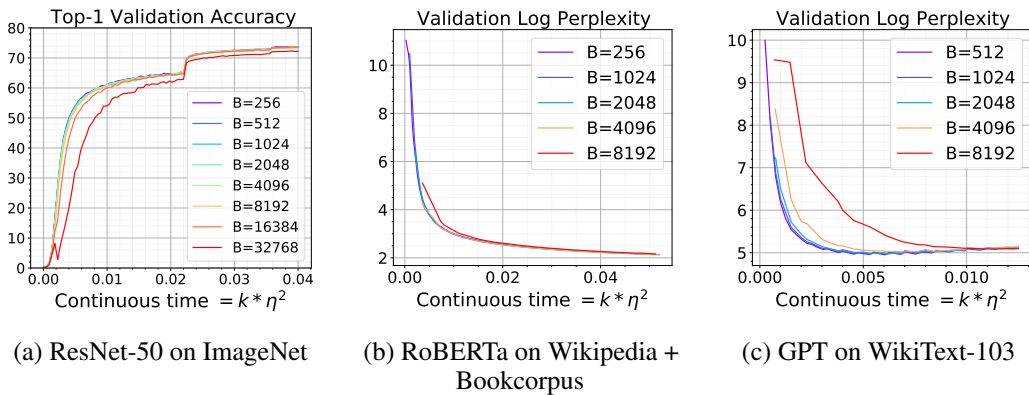


Figure 2: Large scale square root scaling rule experiments (details in Appendix J). Small and large batch models differ by at most 1.5% test accuracy in vision and 0.5 perplexity in language.

value of  $\ell$ . We adapt SVAG technique to simulate our proposed SDEs, which requires additionally adjusting the moment averaging hyperparameters (i.e.,  $\beta, \beta_1, \beta_2$ ) and  $\epsilon$ .

**Definition 6.1** (SVAG Operator). Given an NGOS  $\mathcal{G}_\sigma = (f, \Sigma, \mathcal{Z}_\sigma)$  with scale  $\sigma$  (Definition 2.3) and hyperparameter  $\ell \geq 1$ , the SVAG operator transforms  $\mathcal{G}_\sigma$  into an NGOS  $\hat{\mathcal{G}}_{\ell\sigma} = (f, \Sigma, \hat{\mathcal{Z}}_{\ell\sigma})$  with scale  $\ell\sigma$ . The NGOS  $\hat{\mathcal{G}}_{\ell\sigma}$  takes an input  $\theta$  and returns  $\hat{g} = r_1(\ell)g_1 + r_2(\ell)g_2$ , where  $g_1, g_2$  are two stochastic gradients from  $\mathcal{G}_\sigma(\theta)$  and  $r_i(\ell) = \frac{1}{2}(1 + (-1)^i\sqrt{2\ell^2 - 1})$  for  $i \in \{1, 2\}$ . The probability distribution  $\hat{\mathcal{Z}}_{\ell\sigma}$  is defined such that  $\hat{g}$  has the same distribution as  $\nabla f(\theta) + \ell\sigma z$  when  $z \sim \hat{\mathcal{Z}}_{\ell\sigma}(\theta)$ .

Lemma E.1 verifies that  $\hat{\mathcal{G}}_{\ell\sigma}$  does indeed compute stochastic gradients for  $f$  with covariance  $\Sigma$ . Applying the SVAG operator to mini-batch training amplifies the noise scale by  $\ell$ . We then apply the square root scaling rule to adjust the learning rates and other hyperparameters accordingly, which yields the SVAG algorithm.

**Definition 6.2** (SVAG Algorithm). For a loss  $f$ , SVAG operator hyperparameter  $\ell > 0$ , and optimization hyperparameters  $\eta, \beta, \beta_1, \beta_2$ , and  $\epsilon$ , compute the stochastic gradient as  $\hat{g} = r_1(\ell)g_{\gamma_1} + r_2(\ell)g_{\gamma_2}$ , where  $r_1$  and  $r_2$  are defined as in Definition 6.1, and scale the optimization hyperparameters:

1. For RMSprop, set  $\eta \leftarrow \eta/\ell$ ,  $\beta \leftarrow 1 - (1 - \beta)/\ell^2$ , and  $\epsilon \leftarrow \epsilon\ell$  and apply updates as in Definition 2.1.
2. For Adam, set  $\eta \leftarrow \eta/\ell$ ,  $\beta_1 \leftarrow 1 - (1 - \beta_1)/\ell^2$ ,  $\beta_2 \leftarrow 1 - (1 - \beta_2)/\ell^2$  and  $\epsilon \leftarrow \epsilon\ell$  and apply updates as in Definition 2.2.

The SVAG algorithm describes a discrete trajectory that is a 1st-order approximation of the corresponding SDE (Definitions 4.1 and 4.3), thereby providing an efficient simulation of the SDEs.



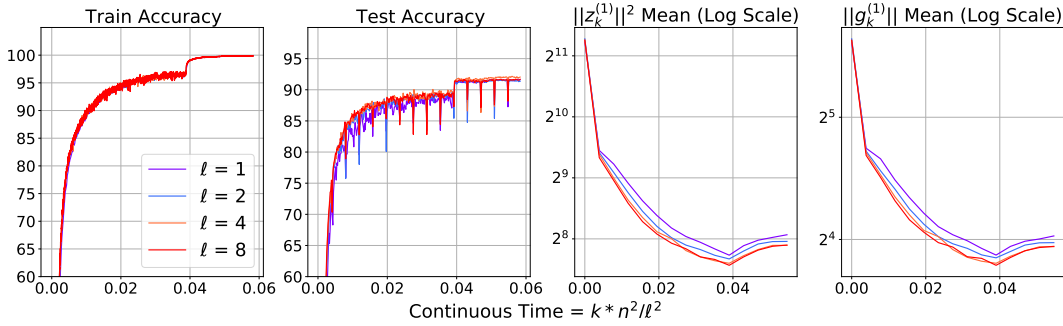


Figure 3: SVAG on the Adam trajectory when training ResNet-50 on CIFAR-10 matches the discrete trajectory ( $\ell = 1$ ) on various test functions (see Appendix J for details). The closeness of the trajectories with respect to various test functions for different values of  $\ell$  implies the SDE approximation (Definition 4.3) is a 1st-order weak approximation of Adam (Theorem 4.4).

**Theorem 6.3** (SVAG algorithm approximates SDE). *Assume the NGOS is well-behaved and satisfies the bounded moments condition (Definitions 2.5 and 2.7).*

1. Let  $\mathbf{X}_t$  be the state of the RMSprop SDE (Definition 4.1) with hyperparameters  $\eta$ ,  $\beta$ , and  $\epsilon$ . Let  $\mathbf{x}_k$  be the state of the analogous discrete SVAG algorithm with hyperparameter  $\ell$ .
2. Let  $\mathbf{X}_t$  be the state of the Adam SDE (Definition 4.3) with hyperparameters  $\eta$ ,  $\beta_1$ ,  $\beta_2$ , and  $\epsilon$ . Let  $\mathbf{x}_k$  be the state of the analogous discrete SVAG algorithm with hyperparameter  $\ell$ .

In both 1 and 2, following holds for  $g$  and  $T$  as in Definition 2.4.

$$\max_{k=0, \dots, \lfloor \ell^2 T / \eta^2 \rfloor} |\mathbb{E}g(\mathbf{x}_k) - \mathbb{E}g(\mathbf{X}_{k\eta^2/\ell^2})| \leq C\eta^2/\ell^2$$

*Proof.* The main idea of the proof is to show that the SVAG operator transforms the noise distribution of a well-behaved NGOS satisfying the bounded moments condition into one that is well-behaved and satisfies the bounded moments and the low skewness conditions (Lemma E.2). With these three conditions satisfied, we can directly apply Theorems 4.2 and 4.4 to complete the proof.  $\square$

Because the SDE scales time as  $k = t/\eta^2$ , we must run SVAG for  $\ell^2$  steps to match a single step of the discrete trajectories. Nevertheless, we note that in our setting and in [11], the approximation guarantee is strong enough for small  $\ell$ , so this simulation is still more efficient than Euler-Maruyama.

**Experiments.** Figure 3 compares the Adam SVAG trajectories (Definition 6.2) up to  $\ell = 8$  to the discrete one ( $\ell = 1$ ) on CIFAR-10 [22] with ResNet-50 [29]. We use  $\text{Tr}(\Sigma(\theta_k))$  and  $\|g_k\|$  as mathematically well-behaved test functions to test the approximation strength (see Definition 2.4). We also measure the train and test accuracies, even though they are not differentiable (and hence, not covered by the theory). The converged SVAG trajectories are close to the discrete ones under these test functions, suggesting the SDE approximations are applicable to realistic deep learning settings. Additional details and settings, including large language models, are in Appendix H.

## 7 Conclusion

We derive SDEs that are provable 1st-order approximations of the RMSprop and Adam trajectories, immediately yielding formal derivations of square root scaling rules: increase the learning rate by  $\sqrt{\kappa}$  and adjust the adaptive hyperparameters when increasing batch size by  $\kappa$ . Experiments in the vision and language domains verify that applying these rules ensures that the values of several test functions, including test accuracy, are preserved. We furthermore design an efficient simulation for the SDEs, allowing us to directly validate the applicability of these SDEs to common vision and language settings. These SDEs can lead to a deeper understanding of how adaptivity and stochasticity impact optimization and generalization, and we hope to extend our results to formal identification of necessary and sufficient conditions for the approximation and its consequences to hold.

## References

- [1] Alex Krizhevsky. One weird trick for parallelizing convolutional neural networks. *arXiv preprint arXiv:1404.5997*, 2014.
- [2] Priya Goyal, Piotr Dollár, Ross Girshick, Pieter Noordhuis, Lukasz Wesolowski, Aapo Kyrola, Andrew Tulloch, Yangqing Jia, and Kaiming He. Accurate, large minibatch sgd: Training imagenet in 1 hour. *arXiv preprint arXiv:1706.02677*, 2017.
- [3] Elad Hoffer, Itay Hubara, and Daniel Soudry. Train longer, generalize better: closing the generalization gap in large batch training of neural networks. In I. Guyon, U. V. Luxburg, S. Bengio, H. Wallach, R. Fergus, S. Vishwanathan, and R. Garnett, editors, *Advances in Neural Information Processing Systems 30*, pages 1731–1741. Curran Associates, Inc., 2017.
- [4] Stanisław Jastrzębski, Zachary Kenton, Devansh Arpit, Nicolas Ballas, Asja Fischer, Yoshua Bengio, and Amos Storkey. Three factors influencing minima in SGD. *arXiv preprint arXiv:1711.04623*, 2017.
- [5] Tijmen Tieleman and Geoffrey Hinton. Lecture 6.5-rmsprop: Divide the gradient by a running average of its recent magnitude., 2012.
- [6] Diederik P Kingma and Jimmy Ba. Adam: A method for stochastic optimization. *arXiv preprint arXiv:1412.6980*, 2014.
- [7] Chao Ma, Lei Wu, and Weinan E. A qualitative study of the dynamic behavior of adaptive gradient algorithms. *CoRR*, abs/2009.06125, 2020.
- [8] Diego Granzio, Stefan Zohren, and Stephen Roberts. Learning rates as a function of batch size: A random matrix theory approach to neural network training, 2021.
- [9] Yang You, Jing Li, Sashank Reddi, Jonathan Hseu, Sanjiv Kumar, Srinadh Bhojanapalli, Xiaodan Song, James Demmel, Kurt Keutzer, and Cho-Jui Hsieh. Large batch optimization for deep learning: Training bert in 76 minutes. In *International Conference on Learning Representations*, 2020.
- [10] Qianxiao Li, Cheng Tai, and Weinan E. Stochastic modified equations and dynamics of stochastic gradient algorithms i: Mathematical foundations. *Journal of Machine Learning Research*, 20(40):1–47, 2019.
- [11] Zhiyuan Li, Sadhika Malladi, and Sanjeev Arora. On the validity of modeling sgd with stochastic differential equations (sdes). *arXiv preprint arXiv:2102.12470*, 2021.
- [12] Prajit Ramachandran, Barret Zoph, and Quoc V. Le. Searching for activation functions. *CoRR*, abs/1710.05941, 2017.
- [13] Jingzhao Zhang, Sai Praneeth Karimireddy, Andreas Veit, Seungyeon Kim, Sashank J Reddi, Sanjiv Kumar, and Suvrit Sra. Why are adaptive methods good for attention models?, 2020.
- [14] Umut Simsekli, Levent Sagun, and Mert Gurbuzbalaban. A tail-index analysis of stochastic gradient noise in deep neural networks. In Kamalika Chaudhuri and Ruslan Salakhutdinov, editors, *Proceedings of the 36th International Conference on Machine Learning*, volume 97 of *Proceedings of Machine Learning Research*, pages 5827–5837. PMLR, 09–15 Jun 2019.
- [15] Pan Zhou, Jiashi Feng, Chao Ma, Caiming Xiong, Steven C. H. Hoi, and Weinan E. Towards theoretically understanding why SGD generalizes better than ADAM in deep learning. *CoRR*, abs/2010.05627, 2020.
- [16] Zeke Xie, Issei Sato, and Masashi Sugiyama. A diffusion theory for deep learning dynamics: Stochastic gradient descent exponentially favors flat minima, 2021.
- [17] Zhiyuan Li, Kaifeng Lyu, and Sanjeev Arora. Reconciling modern deep learning with traditional optimization analyses: The intrinsic learning rate. In Hugo Larochelle, Marc’Aurelio Ranzato, Raia Hadsell, Maria-Florina Balcan, and Hsuan-Tien Lin, editors, *Advances in Neural Information Processing Systems 33: Annual Conference on Neural Information Processing Systems 2020, NeurIPS 2020, December 6-12, 2020, virtual*, 2020.
- [18] Daniel Kunin, Javier Sagastuy-Brena, Surya Ganguli, Daniel L. K. Yamins, and Hidenori Tanaka. Neural mechanics: Symmetry and broken conservation laws in deep learning dynamics, 2020.

- [19] Zeke Xie, Xinrui Wang, Huishuai Zhang, Issei Sato, and Masashi Sugiyama. Adai: Separating the effects of adaptive learning rate and momentum inertia. *CoRR*, abs/2006.15815, 2020.
- [20] Kaiming He, Xiangyu Zhang, Shaoqing Ren, and Jian Sun. Deep residual learning for image recognition. In *Proceedings of the IEEE conference on computer vision and pattern recognition*, pages 770–778, 2016.
- [21] Karen Simonyan and Andrew Zisserman. Very deep convolutional networks for large-scale image recognition. *arXiv preprint arXiv:1409.1556*, 2014.
- [22] Alex Krizhevsky, Vinod Nair, and Geoffrey Hinton. Cifar-10 (canadian institute for advanced research).
- [23] Yinhan Liu, Myle Ott, Naman Goyal, Jingfei Du, Mandar Joshi, Danqi Chen, Omer Levy, Mike Lewis, Luke Zettlemoyer, and Veselin Stoyanov. Roberta: A robustly optimized BERT pretraining approach. *CoRR*, abs/1907.11692, 2019.
- [24] Yukun Zhu, Ryan Kiros, Richard Zemel, Ruslan Salakhutdinov, Raquel Urtasun, Antonio Torralba, and Sanja Fidler. Aligning books and movies: Towards story-like visual explanations by watching movies and reading books, 2015.
- [25] Tom Brown, Benjamin Mann, Nick Ryder, Melanie Subbiah, Jared D Kaplan, Prafulla Dhariwal, Arvind Neelakantan, Pranav Shyam, Girish Sastry, Amanda Askell, et al. Language models are few-shot learners. *Advances in neural information processing systems*, 33:1877–1901, 2020.
- [26] Stephen Merity, Caiming Xiong, James Bradbury, and Richard Socher. Pointer sentinel mixture models. *arXiv preprint arXiv:1609.07843*, 2016.
- [27] Jia Deng, Wei Dong, Richard Socher, Li-Jia Li, Kai Li, and Li Fei-Fei. Imagenet: A large-scale hierarchical image database. In *2009 IEEE Conference on Computer Vision and Pattern Recognition*, pages 248–255, 2009.
- [28] Peter Izsak, Moshe Berchansky, and Omer Levy. How to train BERT with an academic budget. *CoRR*, abs/2104.07705, 2021.
- [29] Kaiming He, Xiangyu Zhang, Shaoqing Ren, and Jian Sun. Delving deep into rectifiers: Surpassing human-level performance on ImageNet classification. In *The IEEE International Conference on Computer Vision (ICCV)*, December 2015.
- [30] Sashank J. Reddi, Satyen Kale, and Sanjiv Kumar. On the convergence of adam and beyond. In *International Conference on Learning Representations*, 2018.
- [31] Manzil Zaheer, Sashank Reddi, Devendra Sachan, Satyen Kale, and Sanjiv Kumar. Adaptive methods for nonconvex optimization. In S. Bengio, H. Wallach, H. Larochelle, K. Grauman, N. Cesa-Bianchi, and R. Garnett, editors, *Advances in Neural Information Processing Systems*, volume 31. Curran Associates, Inc., 2018.
- [32] John Duchi, Elad Hazan, and Yoram Singer. Adaptive subgradient methods for online learning and stochastic optimization. *Journal of Machine Learning Research*, 12(Jul):2121–2159, 2011.
- [33] Jinghui Chen, Dongruo Zhou, Yiqi Tang, Ziyang Yang, Yuan Cao, and Quanquan Gu. Closing the generalization gap of adaptive gradient methods in training deep neural networks. In *Proceedings of the Twenty-Ninth International Joint Conference on Artificial Intelligence, IJCAI’20*, 2021.
- [34] Timothy Dozat. Incorporating nesterov momentum into adam. 2016.
- [35] Ilya Loshchilov and Frank Hutter. Decoupled weight decay regularization. In *International Conference on Learning Representations*, 2019.
- [36] Liangchen Luo, Yuanhao Xiong, and Yan Liu. Adaptive gradient methods with dynamic bound of learning rate. In *International Conference on Learning Representations*, 2019.
- [37] Juntang Zhuang, Tommy Tang, Yifan Ding, Sekhar C Tatikonda, Nicha Dvornek, Xenophon Papademetris, and James Duncan. Adabelief optimizer: Adapting stepsizes by the belief in observed gradients. *Advances in neural information processing systems*, 33:18795–18806, 2020.
- [38] Jerry Ma and Denis Yarats. Quasi-hyperbolic momentum and adam for deep learning. In *International Conference on Learning Representations*, 2019.
- [39] Emma Strubell, Ananya Ganesh, and Andrew McCallum. Energy and policy considerations for deep learning in nlp. *arXiv preprint arXiv:1906.02243*, 2019.

- [40] Alex Wang, Amanpreet Singh, Julian Michael, Felix Hill, Omer Levy, and Samuel R Bowman. Glue: A multi-task benchmark and analysis platform for natural language understanding. *arXiv preprint arXiv:1804.07461*, 2018.
- [41] Kaiming He, Xiangyu Zhang, Shaoqing Ren, and Jian Sun. Delving deep into rectifiers: Surpassing human-level performance on ImageNet classification. In *The IEEE International Conference on Computer Vision (ICCV)*, December 2015.
- [42] Zhiyuan Li and Sanjeev Arora. An exponential learning rate schedule for deep learning. *arXiv preprint arXiv:1910.07454*, 2019.
- [43] Alexander Wettig, Tianyu Gao, Zexuan Zhong, and Danqi Chen. Should you mask 15% in masked language modeling? *arXiv preprint arXiv:2202.08005*, 2022.

## A Contextualizing our Work

### A.1 Additional Recent Works

Variations of Adam have been proposed to improve its speed of convergence, generalization, and stability during training. [30] observed that Adam does not collect long-term memory of past gradients and therefore the effective learning rate could be increasing in some cases. Hence, they propose AMSGrad that maintains a maximum over the exponential running average of the squared gradients. [31] proposed a more controlled increase in the effective learning rate by switching to additive updates, using a more refined version of AdaGrad[32]. [33] unified the generalization ability of vanilla SGD and the convergence speed of Adam by introducing a new adaptive parameter  $p \in (0, \frac{1}{2}]$  that can be hypertuned for each setting. Other variations include (a) Nadam[34] that uses Nesterov momentum, (b) AdamW[35] that decouples the weight decay from the optimization step, (c) AdaBound [36] that maintains a dynamic upper and lower bound on the step size, (d) AdaBelief[37] uses a decaying average of estimated variance in the gradient in place of the running average of the squared gradients, (e) QHAdam[38] that replaces both momentum estimators in Adam with quasi-hyperbolic terms, etc. LAMB[9] used a layerwise adaptive version of Adam to pretrain large language models efficiently.

### A.2 Broader Impact

Our work is primarily theoretical in nature, but we discuss its broader impacts here. [39] highlighted the environmental impact of training large language models. Formal scaling rules remove the need to grid search over hyperparameters: in the case of adaptive algorithms, the grid search is over an even larger space because of the additional adaptivity hyperparameters. Hence, our work reduces the number of times researchers need to train very large models to find ones that work just as well as their smaller, slower counterparts. At the same time, we recognize that the presence of a formal scaling rule may encourage people who were otherwise discouraged by the daunting grid search to train very large models.

## B SDE Approximation Theorem

In this section, we introduce a theorem in aid of our analysis for approximating Stochastic Gradient Algorithm (SGA) with Stochastic Differential Equation (SDE).

We consider Stochastic Gradient Algorithm (SGA) of the following form:

$$\mathbf{x}_{k+1} = \mathbf{x}_k + \eta_e \mathbf{h}_k(\mathbf{x}_k, \boldsymbol{\xi}_k, \eta_e), \quad (4)$$

where  $\mathbf{x}_k \in \mathbb{R}^D$  is the parameter vector,  $\eta_e$  is the learning rate,  $\mathbf{h}_k$  is a vector-valued function that can depend on the current step  $k$ , the current parameter  $\mathbf{x}_k$ , a random vector  $\boldsymbol{\xi}_k$ , and the learning rate  $\eta_e$ . The random vector  $\boldsymbol{\xi}_k$  is sampled from certain distribution  $\Xi(\mathbf{x}_k, \eta_e)$  in every step.

We consider Stochastic Differential Equation (SDE) of the following form:

$$d\mathbf{X}_t = \mathbf{b}(X_t, t)dt + \boldsymbol{\sigma}(X_t, t)d\mathbf{W}_t, \quad (5)$$

where  $\mathbf{b} : \mathbb{R}^D \times \mathbb{R} \rightarrow \mathbb{R}^D$  is the drift vector function,  $\boldsymbol{\sigma} : \mathbb{R}^D \times \mathbb{R} \rightarrow \mathbb{R}^{D \times D}$  is the diffusion matrix function.

Let  $\mathcal{P}_X(\mathbf{x}, s, t)$  be the probability distribution of  $\mathbf{X}_t$  in (5) when the initial condition is  $\mathbf{X}_s = \mathbf{x}$ . Now we define the following random variables to characterize the one-step changes of SGA and SDE.

$$\Delta(\mathbf{x}, k) := \eta_e \mathbf{h}_k(\mathbf{x}, \boldsymbol{\xi}, \eta_e), \quad \text{where } \boldsymbol{\xi} \sim \Xi(\mathbf{x}, \eta_e). \quad (6)$$

$$\tilde{\Delta}(\mathbf{x}, k) := \mathbf{X}_{(k+1)\eta_e} - \mathbf{x}, \quad \text{where } \mathbf{X}_{(k+1)\eta_e} \sim \mathcal{P}_X(\mathbf{x}, k\eta_e, (k+1)\eta_e). \quad (7)$$

The following regularity condition is needed for our main theorem.

**Definition B.1.** A function  $g : \mathbb{R}^d \rightarrow \mathbb{R}$  is said to have *polynomial growth* if there exist positive integers  $\kappa_1, \kappa_2 > 0$  such that

$$|g(\mathbf{x})| \leq \kappa_1(1 + \|\mathbf{x}\|_2^{2\kappa_2}),$$

for all  $\mathbf{x} \in \mathbb{R}^d$ . We let  $G$  denote the set of all such functions. For each integer  $\alpha \geq 1$ ,  $G^\alpha$  denotes the set of  $\alpha$ -times continuously differentiable functions  $\mathbb{R}^d \rightarrow \mathbb{R}$  which, together with its partial derivatives up to and including order  $\alpha$ , belong to  $G$ . If  $g$  depends on additional parameters, we say  $g \in G^\alpha$  uniformly if the constants  $\kappa_1, \kappa_2$  are independent of those parameters.

Now we are ready to introduce the main theorem for the order of approximation by modeling SGA as SDE. We follow the same proof strategy as [10]. First, we show that the moments of the one-step difference for the SGA and for the SDE of our interest are close to each other. Then, under some regularity conditions, we translate the one-step error to an error over a finite interval of time to get the final result. The following is our main theorem to achieve such translation, and it is adapted from Theorem 3 in [10] with slightly different conditions to match our need in the analysis of adaptive gradient methods.

**Theorem B.2** (Adaption of Theorem 3 in [10]). *Let  $T > 0$ ,  $\eta_e \in (0, 1 \wedge T)$  and  $N = \lfloor T/\eta_e \rfloor$ . Consider an SDE with drift vector  $\mathbf{b}(\mathbf{x}, \eta_e)$  and diffusion matrix  $\boldsymbol{\sigma}(\mathbf{x}, \eta_e)$ , and a stochastic gradient algorithm with initial point  $\mathbf{x}_0 \in \mathbb{R}^D$  and update rule  $\mathbf{x}_{k+1} = \mathbf{x}_k + \eta_e \mathbf{h}(\mathbf{x}_k, \boldsymbol{\xi}_k, \eta_e)$ . Let  $\mathcal{X}_k$  be the support of the random variable  $\mathbf{x}_k$  given  $\mathbf{x}_0$ . If the following conditions hold:*

1. *The drift function  $\mathbf{b}$  and diffusion function  $\boldsymbol{\sigma}$  are Lipschitz and belong to  $G^4$ ;*
2. *The moments of  $\boldsymbol{\Delta} \in \mathbb{R}^D$  and  $\tilde{\boldsymbol{\Delta}} \in \mathbb{R}^D$  satisfy the following. There is a function  $K_1 \in G$  (independent of  $\eta_e$ ) such that for all  $\mathbf{x} \in \mathcal{X}_k$ ,*

$$\begin{aligned} \left| \mathbb{E}[\Delta_i(\mathbf{x}, k) - \tilde{\Delta}_i(\mathbf{x}, k)] \right| &\leq K_1(\mathbf{x})\eta_e^2 \quad \text{for all } 1 \leq i \leq D, \\ \left| \mathbb{E}[\Delta_i(\mathbf{x}, k)\Delta_j(\mathbf{x}, k) - \tilde{\Delta}_i(\mathbf{x}, k)\tilde{\Delta}_j(\mathbf{x}, k)] \right| &\leq K_1(\mathbf{x})\eta_e^2 \quad \text{for all } 1 \leq i, j \leq D, \\ \left| \mathbb{E}[\Delta_i(\mathbf{x}, k)\Delta_j(\mathbf{x}, k)\Delta_l(\mathbf{x}, k) - \tilde{\Delta}_i(\mathbf{x}, k)\tilde{\Delta}_j(\mathbf{x}, k)\tilde{\Delta}_l(\mathbf{x}, k)] \right| &\leq K_1(\mathbf{x})\eta_e^2 \quad \text{for all } 1 \leq i, j, l \leq D. \end{aligned}$$

3. *There exists a subset  $P$  of indices set  $\{1, 2, \dots, D\}$  such that the following holds. Let  $\|\mathbf{x}\|_P := \sqrt{\sum_{i \in P} x_i^2}$  and  $\|\mathbf{x}\|_R := \sqrt{\sum_{i \notin P} x_i^2}$ . There are constants  $C_1 > 0, \omega_1 > 0$  (independent of  $\eta_e$ ) so that*

$$\|\mathbb{E}\boldsymbol{\Delta}(\mathbf{x}, k)\|_P \leq C_1\eta_e(1 + \|\mathbf{x}\|_P), \quad \|\mathbb{E}\boldsymbol{\Delta}(\mathbf{x}, k)\|_R \leq C_1\eta_e(1 + \|\mathbf{x}\|_P^{\omega_1})(1 + \|\mathbf{x}\|_R),$$

for all  $k \leq N$  and  $\mathbf{x} \in \mathcal{X}_k$ . For all  $m \geq 1$ , there are constants  $C_{2m}, \omega_{2m} > 0$  (independent of  $\eta_e$ ) so that

$$\|\mathbb{E}\boldsymbol{\Delta}(\mathbf{x}, k)\|_P^{2m} \leq C_{2m}\eta_e^m(1 + \|\mathbf{x}\|_P^{2m}), \quad \|\mathbb{E}\boldsymbol{\Delta}(\mathbf{x}, k)\|_R^{2m} \leq C_{2m}\eta_e^m(1 + \|\mathbf{x}\|_P^{\omega_{2m}})(1 + \|\mathbf{x}\|_R^{2m}),$$

for all  $k \leq N$  and  $\mathbf{x} \in \mathcal{X}_k$ .

Then for each function  $g \in G^4$ , there exists a constant  $C > 0$  (independent of  $\eta_e$ ) such that

$$\max_{0 \leq k \leq N} |\mathbb{E}[g(\mathbf{x}_k)] - \mathbb{E}[g(\mathbf{X}_{k\eta_e})]| \leq C\eta_e, \quad (8)$$

when the SDE starts from the same initial point  $\mathbf{x}_0$  as SGA. That is, the SGA is a first-order weak approximation of the SDE.

To apply Theorem B.2, the major condition to verify is that  $\boldsymbol{\Delta}$  and  $\tilde{\boldsymbol{\Delta}}$  match in moments. The following lemma computes the moments for  $\tilde{\boldsymbol{\Delta}}$ :

**Lemma B.3.** *For drift function  $b$  and diffusion function  $\boldsymbol{\sigma}$  that belong to  $G^4$ , there is a function  $K_2 \in G$  (independent of  $\eta_e$ ) such that for all  $\mathbf{x} \in \mathbb{R}^D$ ,*

$$\begin{aligned} \left| \mathbb{E}[\tilde{\Delta}_i(\mathbf{x}, k)] - \eta_e b_i(\mathbf{x}, k\eta_e) \right| &\leq K_2(\mathbf{x})\eta_e^2, \quad \text{for all } 1 \leq i \leq D, \\ \left| \mathbb{E}[\tilde{\Delta}_i(\mathbf{x}, k)\tilde{\Delta}_j(\mathbf{x}, k)] - \eta_e^2 \sum_{k=1}^D \sigma_{i,k}(\mathbf{x}, k\eta_e)\sigma_{j,k}(\mathbf{x}, k\eta_e) \right| &\leq K_2(\mathbf{x})\eta_e^2, \quad \text{for all } 1 \leq i, j \leq D, \\ \left| \mathbb{E}[\tilde{\Delta}_i(\mathbf{x}, k)\tilde{\Delta}_j(\mathbf{x}, k)\tilde{\Delta}_l(\mathbf{x}, k)] \right| &\leq K_2(\mathbf{x})\eta_e^2, \quad \text{for all } 1 \leq i, j, l \leq D. \end{aligned}$$

## B.1 Proof for Theorem B.2

To prove Theorem B.2, we need the following lemma from [10]. However, the original version of the lemma does not apply to time-dependent SDEs, i.e.,  $\mathbf{b}$  and  $\boldsymbol{\sigma}$  cannot change with time  $t$ . By carefully scrutinizing the proof, we find that the proof is indeed applicable to time-dependent SDEs.

**Lemma B.4** (Adaption of Proposition 25, [10]). *Suppose that the drift function  $\mathbf{b}$  and diffusion function  $\boldsymbol{\sigma}$  are Lipschitz and belong to  $G^\alpha$  for some  $\alpha \geq 1$ . Let  $s \in [0, T]$  and  $g \in G^\alpha$ . For  $t \in [s, T]$ , define*

$$u(\mathbf{x}, s, t) := \mathbb{E}_{\mathbf{X}_t \sim \mathcal{P}_{\mathbf{X}}(\mathbf{x}, s, t)}[g(\mathbf{X}_t)],$$

Then  $u(\cdot, s, t) \in G^\alpha$  uniformly in  $s, t$ .

We need the following lemma to bound the growth of  $\mathbf{x}_k$ .

**Lemma B.5.** *Under Condition (3) in Theorem B.2, given the initial point  $\mathbf{x}_0$  and any  $m \geq 1$ , there exists a constant  $C'_{2m} > 0$  (depending on  $\mathbf{x}_0$  but independent of  $\eta_e$ ) such that the parameters  $\{\mathbf{x}_k\}$  of SGA starting from  $\mathbf{x}_0$  can be uniformly bounded by  $\mathbb{E}[\|\mathbf{x}_k\|_2^{2m}] \leq C'_{2m}$  for all  $k \leq N := \lfloor T/\eta_e \rfloor$ .*

*Proof.* First, we show that  $\mathbb{E}[(1 + \|\mathbf{x}_k\|_P^2)^m]$  is uniformly bounded. For all  $2 \leq j \leq 2m$ , there exists a constant  $\hat{C}_1 > 0$  so that

$$\mathbb{E} \left[ \|\Delta(\mathbf{x}_k, k)\|_P^j \mid \mathbf{x}_k \right] \leq \mathbb{E} \left[ \|\Delta(\mathbf{x}_k, k)\|_P^{2m} \mid \mathbf{x}_k \right]^{\frac{j}{2m}} \leq C_{2m}^{\frac{j}{2m}} \eta_e^{j/2} (1 + \|\mathbf{x}_k\|_P^{2m})^{\frac{j}{2m}} \leq \hat{C}_1 \eta_e (1 + \|\mathbf{x}_k\|_P^2)^{\frac{j}{2}} \quad (9)$$

For two vector  $\mathbf{x}, \mathbf{y} \in \mathbb{R}^D$ , we use the notation  $\langle \mathbf{x}, \mathbf{y} \rangle_P := \sum_{i \in P} x_i y_i$  to denote the inner product of  $\mathbf{x}$  and  $\mathbf{y}$  restricting on coordinates in  $P$ . Now we expand  $(1 + \|\mathbf{x}_{k+1}\|_P^2)^m$  using the update rule, then there is a constant  $\hat{C}_2$  (independent of  $\eta_e, \|\mathbf{x}_k\|_P$ ) such that

$$\begin{aligned} \mathbb{E} \left[ (1 + \|\mathbf{x}_{k+1}\|_P^2)^m \mid \mathbf{x}_k \right] &= \mathbb{E} \left[ (1 + \|\mathbf{x}_k\|_P^2 + 2\langle \mathbf{x}_k, \Delta(\mathbf{x}_k, k) \rangle_P + \|\Delta(\mathbf{x}_k, k)\|_P^2)^m \mid \mathbf{x}_k \right] \\ &= (1 + \|\mathbf{x}_k\|_P^2)^m + 2m \langle \mathbf{x}_k, \mathbb{E}[\Delta(\mathbf{x}_k, k) \mid \mathbf{x}_k] \rangle_P (1 + \|\mathbf{x}_k\|_P^2)^{m-1} \\ &\quad + m \mathbb{E}[\|\Delta(\mathbf{x}_k, k)\|_P^2 \mid \mathbf{x}_k] (1 + \|\mathbf{x}_k\|_P^2)^{m-1} \\ &\quad + \sum_{j=2}^m \binom{m}{j} \mathbb{E} \left[ (2\langle \mathbf{x}_k, \Delta(\mathbf{x}_k, k) \rangle_P + \|\Delta(\mathbf{x}_k, k)\|_P^2)^j \mid \mathbf{x}_k \right] (1 + \|\mathbf{x}_k\|_P^2)^{m-j} \\ &\leq (1 + \|\mathbf{x}_k\|_P^2)^m + 2m \langle \mathbf{x}_k, \mathbb{E}[\Delta(\mathbf{x}_k, k) \mid \mathbf{x}_k] \rangle_P (1 + \|\mathbf{x}_k\|_P^2)^{m-1} \\ &\quad + \hat{C}_2 \eta_e (1 + \|\mathbf{x}_k\|_P^2)^m, \end{aligned}$$

where the last line is due to (9). By Condition (3),  $\|\mathbb{E}[\Delta(\mathbf{x}_k, k) \mid \mathbf{x}_k]\|_P \leq C_1 \eta_e (1 + \|\mathbf{x}_k\|_P)$ . Thus, there exists a constant  $\hat{C}_3$  (independent of  $\eta_e, \|\mathbf{x}_k\|_P$ ) such that

$$\mathbb{E} \left[ (1 + \|\mathbf{x}_{k+1}\|_P^2)^m \mid \mathbf{x}_k \right] \leq (1 + \hat{C}_3 \eta_e) (1 + \|\mathbf{x}_k\|_P^2)^m.$$

Taking the expectation over  $\mathbf{x}_k$  and using the inequality  $1 + z \leq \exp(z)$  gives

$$\mathbb{E} \left[ (1 + \|\mathbf{x}_{k+1}\|_P^2)^m \right] \leq (1 + \hat{C}_3 \eta_e) \mathbb{E}[(1 + \|\mathbf{x}_k\|_P^2)^m] \leq \exp(\hat{C}_3 \eta_e) \mathbb{E}[(1 + \|\mathbf{x}_k\|_P^2)^m].$$

Taking a telescoping product proves that

$$\mathbb{E}[(1 + \|\mathbf{x}_k\|_P^2)^m] \leq \exp(\hat{C}_3 k \eta_e) (1 + \|\mathbf{x}_0\|_P^2)^m \leq \exp(\hat{C}_3 T) (1 + \|\mathbf{x}_0\|_P^2)^m.$$

for all  $k \leq N$ . So  $\mathbb{E}[(1 + \|\mathbf{x}_k\|_P^2)^m]$  is uniformly bounded (independent of  $\eta_e, k$ ).

Now we show that  $\mathbb{E}[(1 + \|\mathbf{x}_k\|_R^2)^m]$  is uniformly bounded. We can repeat the argument above to bound  $\mathbb{E}[(1 + \|\mathbf{x}_k\|_R^2)^m]$ , while utilizing the bounds  $\|\mathbb{E}[\Delta(\mathbf{x}, k)]_R \leq C_1 \eta_e (1 + \|\mathbf{x}\|_P^{\omega_1}) (1 + \|\mathbf{x}\|_R)$ ,  $\mathbb{E}[\|\Delta(\mathbf{x}, k)\|_R^{2m}] \leq C_{2m} \eta_e^m (1 + \|\mathbf{x}\|_P^{2\omega_2}) (1 + \|\mathbf{x}\|_R^{2m})$ . In the end we can obtain the following for some real constant  $\hat{C}_4 > 0$  and some integer constant  $\hat{\omega} > 0$ :

$$\mathbb{E} \left[ (1 + \|\mathbf{x}_{k+1}\|_R^2)^m \right] \leq \exp \left( \hat{C}_3 \eta_e \mathbb{E}[1 + \|\mathbf{x}_k\|_P^{2\hat{\omega}}] \right) \mathbb{E} \left[ (1 + \|\mathbf{x}_k\|_R^2)^m \right].$$

As we have shown,  $\mathbb{E}[1 + \|\mathbf{x}_k\|_P^{2\hat{\omega}}]$  is uniformly bounded by a constant. Taking a telescoping product proves that  $\mathbb{E}[(1 + \|\mathbf{x}_k\|_R^2)^m]$  is uniformly bounded (independent of  $\eta_e, k$ ). As  $\mathbb{E}[(1 + \|\mathbf{x}_k\|_P^2)^m]$  is also uniformly bounded, we can conclude that so it  $\mathbb{E}[\|\mathbf{x}_k\|_2^{2m}]$ .  $\square$

We also need the following lemma adapted from Lemma C.2, [11].

**Lemma B.6** (Adaption of Lemma C.2, [11]). *Let  $u_1, \dots, u_N$  be a set of functions that belong to  $G^4$  uniformly. Under Condition (2), (3) in Theorem B.2, if the drift function  $\mathbf{b}$  and the diffusion function  $\boldsymbol{\sigma}$  are Lipschitz, then there exists a function  $K'_1 \in G$  (independent of  $\eta_e$ ) such that*

$$\left| \mathbb{E}[u_j(\mathbf{x} + \boldsymbol{\Delta}(\mathbf{x}, k))] - \mathbb{E}[u_j(\mathbf{x} + \tilde{\boldsymbol{\Delta}}(\mathbf{x}, k))] \right| \leq K'_1(\mathbf{x})\eta_e^2,$$

for all  $1 \leq j \leq N$ ,  $1 \leq k \leq N$  and  $\mathbf{x} \in \mathcal{X}_k$ .

*Proof.* Since  $u_1, \dots, u_N \in G^4$  uniformly, we can find  $K_0 \in G$  such that  $u_j(\mathbf{x})$  is bounded by  $K_0(\mathbf{x})$  and so are all the partial derivatives of  $u_j$  up to order 4.

By Taylor's Theorem with Lagrange Remainder, for all  $1 \leq j \leq N$ ,  $1 \leq k \leq N$  we have

$$\begin{aligned} & u_j(\mathbf{x} + \boldsymbol{\Delta}(\mathbf{x}, k)) - u_j(\mathbf{x} + \tilde{\boldsymbol{\Delta}}(\mathbf{x}, k)) \\ &= \underbrace{\sum_{s=1}^3 \frac{1}{s!} \sum_{1 \leq i_1, \dots, i_s \leq D} \frac{\partial^s u_j}{\partial x_{i_1} \dots \partial x_{i_s}}(\mathbf{x}) \prod_{r=1}^s (\Delta_{i_r}(\mathbf{x}, k) - \tilde{\Delta}_{i_r}(\mathbf{x}, k))}_{=: M_j} + R_j - \tilde{R}_j, \end{aligned}$$

where the remainders  $R_j, \tilde{R}_j$  are

$$\begin{aligned} R_j &:= \frac{1}{4!} \sum_{1 \leq i_1, \dots, i_4 \leq D} \frac{\partial^4 u_j}{\partial x_{i_1} \dots \partial x_{i_4}}(\mathbf{x} + a\boldsymbol{\Delta}(\mathbf{x}, k)) \prod_{r=1}^4 \Delta_{i_r}(\mathbf{x}, k). \\ \tilde{R}_j &:= \frac{1}{4!} \sum_{1 \leq i_1, \dots, i_4 \leq D} \frac{\partial^4 u_j}{\partial x_{i_1} \dots \partial x_{i_4}}(\mathbf{x} + \tilde{a}\tilde{\boldsymbol{\Delta}}(\mathbf{x}, k)) \prod_{r=1}^4 \tilde{\Delta}_{i_r}(\mathbf{x}, k). \end{aligned}$$

for some  $a, \tilde{a} \in [0, 1]$ .

For  $M_j$  we have

$$\mathbb{E}[M_j] \leq \sum_{s=1}^3 \frac{1}{s!} \sum_{1 \leq i_1, \dots, i_s \leq D} \left| \frac{\partial^s u_j}{\partial x_{i_1} \dots \partial x_{i_s}}(\mathbf{x}) \right| \cdot K_1(\mathbf{x})\eta_e^2 \leq \sum_{s=1}^3 \frac{D^s}{s!} K_0(\mathbf{x})K_1(\mathbf{x})\eta_e^2,$$

so  $\frac{1}{\eta_e^2} \mathbb{E}[M_j]$  is uniformly bounded by a function in  $G$ .

Now let  $\kappa_0, m$  be the constants so that  $K_0(\mathbf{x})^2 \leq \kappa_0^2(1 + \|\mathbf{x}\|_2^{2m})$ . For  $R_j$ , by Cauchy-Schwarz inequality we have

$$\begin{aligned} \mathbb{E}[R_j] &\leq \frac{1}{4!} \left( \sum_{1 \leq i_1, \dots, i_4 \leq D} \mathbb{E} \left[ \left| \frac{\partial^4 u_j}{\partial x_{i_1} \dots \partial x_{i_4}}(\mathbf{x} + a\boldsymbol{\Delta}(\mathbf{x}, k)) \right|^2 \right] \right)^{1/2} \cdot \left( \sum_{1 \leq i_1, \dots, i_4 \leq D} \mathbb{E} \left[ \left| \prod_{r=1}^4 \Delta_{i_r}(\mathbf{x}, k) \right|^2 \right] \right)^{1/2} \\ &\leq \frac{1}{4!} \left( \sum_{1 \leq i_1, \dots, i_4 \leq D} \mathbb{E} \left[ \left| \frac{\partial^4 u_j}{\partial x_{i_1} \dots \partial x_{i_4}}(\mathbf{x} + a\boldsymbol{\Delta}(\mathbf{x}, k)) \right|^2 \right] \right)^{1/2} \cdot \mathbb{E} [\|\boldsymbol{\Delta}_{i_r}(\mathbf{x}, k)\|_2^8]^{1/2} \\ &\leq \frac{1}{4!} (D^2 \cdot K_0(\mathbf{x} + a\boldsymbol{\Delta}(\mathbf{x}, k))) \cdot (\eta_e^4 K_8(\mathbf{x}))^{1/2}, \end{aligned}$$

where the last line uses Condition (3) and  $K_8$  is a function of polynomial growth. For  $K_0(\mathbf{x} + a\boldsymbol{\Delta}(\mathbf{x}, k))$ , we can bound it by

$$\begin{aligned} K_0(\mathbf{x} + a\boldsymbol{\Delta}(\mathbf{x}, k)) &\leq \kappa_0 \mathbb{E} [1 + \|\mathbf{x} + a\boldsymbol{\Delta}(\mathbf{x}, k)\|_2^{2m}]^{1/2} \\ &\leq \kappa_0 (1 + 2^{2m-1} \mathbb{E}[\|\mathbf{x}\|_2^{2m} + \mathbb{E}\|\boldsymbol{\Delta}(\mathbf{x}, k)\|_2^{2m}])^{1/2} \\ &\leq \kappa_0 (1 + 2^{2m-1} (\|\mathbf{x}\|_2^{2m} + C_{2m}\eta_e^{2m}(1 + \|\mathbf{x}\|_2^{2m})))^{1/2}. \end{aligned}$$



Combining this with our bound for  $\mathbb{E}[R_j]$ , we have

$$\mathbb{E}[R_j] \leq \eta_e^2 \cdot \frac{1}{4!} \cdot D^4 \cdot \kappa_0 \left(1 + 2^{2m-1} (\|\mathbf{x}\|_2^{2m} + C_{2m} \eta_e^{2m} (1 + \|\mathbf{x}\|_2^{2m}))\right)^{1/2} \cdot K_8^{1/2}(\mathbf{x}).$$

so  $\frac{1}{\eta_e} \mathbb{E}[R_j]$  is uniformly bounded by a function in  $G$ .

Since  $\mathbf{b}, \boldsymbol{\sigma}$  are Lipschitz, we can apply a similar argument as in Lemma 26 of [10] to show that for all  $s \geq 1$  there exists a function  $\tilde{K} \in G$  such that

$$\mathbb{E} \left[ \left| \prod_{r=1}^s \tilde{\Delta}_{i_r}(\mathbf{x}, k) \right| \right] \leq \tilde{K}(\mathbf{x}) \eta^s \quad \text{for all } 1 \leq i_1, \dots, i_s \leq D.$$

Then we can repeat the above argument for  $R_j$  while replacing  $\Delta$  as  $\tilde{\Delta}$ , which implies that  $\frac{1}{\eta_e} \mathbb{E}[\tilde{R}_j]$  is also uniformly bounded by a function in  $G$ .

Therefore, we can conclude that there exists a function  $K'_1 \in G$  such that  $\mathbb{E}[M_j] \leq \frac{1}{3} K'_1(\mathbf{x}) \eta_e^2$ ,  $\mathbb{E}[R_j] \leq \frac{1}{3} K'_1(\mathbf{x}) \eta_e^2$ ,  $\mathbb{E}[\tilde{R}_j] \leq \frac{1}{3} K'_1(\mathbf{x}) \eta_e^2$ . So  $\mathbb{E}[u_j(\mathbf{x} + \boldsymbol{\Delta}(\mathbf{x}, k))] - \mathbb{E}[u_j(\mathbf{x} + \tilde{\boldsymbol{\Delta}}(\mathbf{x}, k))] \leq K'_1(\mathbf{x}) \eta_e^2$ .  $\square$

Now we are ready to present our proof for Theorem C.1.

*Proof for Theorem B.2.* For  $0 \leq j \leq k$ , let  $\hat{\mathbf{x}}_{j,k}$  be a random variable that is distributed as the probability distribution  $\mathcal{P}_X(\mathbf{x}_j, j\eta_e, k\eta_e)$  conditioned on  $\mathbf{x}_j$ . By definition,  $\Pr[\hat{\mathbf{x}}_{k,k} = \mathbf{x}_k] = 1$ ,  $\hat{\mathbf{x}}_{0,k} \sim \mathbf{X}_{k\eta_e}$ . Let  $u(\mathbf{x}, s, t) := \mathbb{E}_{\mathbf{X}_t \sim \mathcal{P}_X(\mathbf{x}, s, t)}[g(\mathbf{X}_t)]$ .

$$\begin{aligned} |\mathbb{E}[g(\mathbf{x}_k)] - \mathbb{E}[g(\mathbf{X}_{k\eta_e})]| &= |\mathbb{E}[g(\hat{\mathbf{x}}_{k,k})] - \mathbb{E}[g(\hat{\mathbf{x}}_{0,k})]| \\ &\leq \sum_{j=0}^{k-1} |\mathbb{E}[g(\hat{\mathbf{x}}_{j+1,k})] - \mathbb{E}[g(\hat{\mathbf{x}}_{j,k})]| \\ &= \sum_{j=0}^{k-1} |\mathbb{E}[u(\hat{\mathbf{x}}_{j+1,j+1}, (j+1)\eta_e, k\eta_e)] - \mathbb{E}[u(\hat{\mathbf{x}}_{j,j+1}, (j+1)\eta_e, k\eta_e)]|. \end{aligned}$$

Let  $u_{j+1}(\mathbf{x}) := u(\mathbf{x}, (j+1)\eta_e, k\eta_e)$ . Note that  $\hat{\mathbf{x}}_{j+1,j+1} \sim \mathbf{x}_j + \boldsymbol{\Delta}(\mathbf{x}_j, j)$ ,  $\hat{\mathbf{x}}_{j,j+1} \sim \mathbf{x}_j + \tilde{\boldsymbol{\Delta}}(\mathbf{x}_j, j)$ . We can rewrite the above formula as

$$|\mathbb{E}[g(\mathbf{x}_k)] - \mathbb{E}[g(\mathbf{X}_{k\eta_e})]| \leq \sum_{j=0}^{k-1} \left| \mathbb{E}[u_{j+1}(\mathbf{x}_j + \boldsymbol{\Delta}(\mathbf{x}_j, j))] - \mathbb{E}[u_{j+1}(\mathbf{x}_j + \tilde{\boldsymbol{\Delta}}(\mathbf{x}_j, j))] \right|.$$

By Lemma B.4,  $u \in G^4$  uniformly in  $s, t$ , so  $u_1, \dots, u_N \in G^4$  uniformly. Then by Lemma B.6, we know that there exists a function  $K'_1(\mathbf{x}) = \kappa_1(1 + \|\mathbf{x}\|_2^{2m}) \in G$  such that

$$\left| \mathbb{E}[u_{j+1}(\mathbf{x}_j + \boldsymbol{\Delta}(\mathbf{x}_j, j))] - \mathbb{E}[u_{j+1}(\mathbf{x}_j + \tilde{\boldsymbol{\Delta}}(\mathbf{x}_j, j))] \right| \leq \mathbb{E}[K'_1(\mathbf{x}_j) \eta_e^2],$$

for all  $0 \leq j < N$ . Combining this with Lemma B.5, we can bound  $|\mathbb{E}[g(\mathbf{x}_k)] - \mathbb{E}[g(\mathbf{X}_{k\eta_e})]|$  by

$$\begin{aligned} |\mathbb{E}[g(\mathbf{x}_k)] - \mathbb{E}[g(\mathbf{X}_{k\eta_e})]| &\leq \sum_{j=0}^{k-1} \mathbb{E}[K'_1(\mathbf{x}_j) \eta_e^2] \leq \eta_e^2 \sum_{j=0}^{k-1} \mathbb{E}[\kappa_1(1 + \|\mathbf{x}_j\|_2^{2m})] \leq \eta_e^2 \sum_{j=0}^{k-1} \kappa_1(1 + C'_{2m}) \\ &\leq \kappa_1(1 + C'_{2m}) T \eta_e. \end{aligned}$$

We can complete the proof by noting that  $\kappa_1, C'_{2m}, T$  are independent of  $\eta_e$ .  $\square$

## B.2 Proof for Lemma B.3

To prove Lemma B.3, we only need to verify the following lemma using Itô-Taylor expansion.

**Lemma B.7.** Let  $\psi : \mathbb{R}^D \rightarrow \mathbb{R}$  be a function in  $G^4$ . Define

$$\mathcal{A}_t \psi(\mathbf{x}) := \sum_{i \in [D]} b_i(\mathbf{x}, t) \partial_i \psi(\mathbf{x}) + \frac{1}{2} \sum_{i, j \in [D]} \left( \sum_{l \in [D]} \sigma_{i,l}(\mathbf{x}, t) \sigma_{l,j}(\mathbf{x}, t) \right) \partial_{i,j}^2 \psi(\mathbf{x}).$$

Then there exists a function  $\hat{K} \in G$  such that

$$\left| \mathbb{E} \left[ \psi(\mathbf{x} + \tilde{\Delta}(\mathbf{x}, k)) \right] - \psi(\mathbf{x}) - \eta_e \mathcal{A}_{k\eta_e} \psi(\mathbf{x}) \right| \leq \hat{K}(\mathbf{x}) \eta_e^2. \quad (10)$$

*Proof.* WLOG we prove the case of  $k = 0$ , then all the other cases can be proved by shifting the time. Let  $\Lambda_t \psi(\mathbf{x}) := \boldsymbol{\sigma}(\mathbf{x}, t)^\top \nabla \psi(\mathbf{x})$ .

$$\psi(\mathbf{X}_\eta) = \psi(\mathbf{x}) + \int_0^{\eta_e} \mathcal{A}_s \psi(\mathbf{X}_s) ds + \int_0^{\eta_e} \langle \Lambda_s \psi(\mathbf{X}_s), d\mathbf{W}_s \rangle.$$

Now we further apply the above formula to  $\mathcal{A}_s \psi(\mathbf{X}_s)$ . Then we have

$$\begin{aligned} \psi(\mathbf{X}_\eta) &= \psi(\mathbf{x}) + \int_0^{\eta_e} \left( \mathcal{A}_s \psi(\mathbf{x}) + \int_0^s \mathcal{A}_r \mathcal{A}_s \psi(\mathbf{X}_r) dr + \int_0^s \langle \Lambda_r \mathcal{A}_s \psi(\mathbf{X}_r), d\mathbf{W}_r \rangle \right) ds + \int_0^{\eta_e} \langle \Lambda_s \psi(\mathbf{X}_s), d\mathbf{W}_s \rangle \\ &= \psi(\mathbf{x}) + \int_0^{\eta_e} \mathcal{A}_s \psi(\mathbf{x}) ds + \int_0^{\eta_e} \int_0^s \mathcal{A}_r \mathcal{A}_s \psi(\mathbf{X}_r) dr ds \\ &\quad + \int_0^{\eta_e} \int_0^s \langle \Lambda_r \mathcal{A}_s \psi(\mathbf{X}_r), d\mathbf{W}_r \rangle ds + \int_0^{\eta_e} \langle \Lambda_s \psi(\mathbf{X}_s), d\mathbf{W}_s \rangle. \end{aligned}$$

Taking expectation, the last two integrals vanish. So we have

$$\mathbb{E} \psi(\mathbf{X}_\eta) = \psi(\mathbf{x}) + \int_0^{\eta_e} \mathcal{A}_s \psi(\mathbf{x}) ds + \int_0^{\eta_e} \int_0^s \mathbb{E} [\mathcal{A}_r \mathcal{A}_s \psi(\mathbf{X}_r)] dr ds.$$

By Lipschitzness of  $\mathbf{b}$  and  $\boldsymbol{\sigma}$ ,  $\frac{1}{\eta_e} (\mathcal{A}_s \psi(\mathbf{x}) - \mathcal{A}_0 \psi(\mathbf{x}))$  is bounded by a function of  $\mathbf{x}$  with polynomial growth. Also,  $\mathcal{A}_r \mathcal{A}_s \psi(\cdot)$  is in  $G$  uniformly, then Theorem 19 in [10] implies that  $\mathbb{E} [\mathcal{A}_r \mathcal{A}_s \psi(\mathbf{X}_r)]$  is also in  $G$  uniformly. Then we know that there exists two functions  $\hat{K}_1, \hat{K}_2 \in G$  such that

$$|\mathbb{E} [\psi(\mathbf{X}_{\eta_e})] - \psi(\mathbf{x}) - \eta_e \mathcal{A}_0 \psi(\mathbf{x})| \leq \int_0^{\eta_e} \eta_e \hat{K}_1(\mathbf{x}) ds + \int_0^{\eta_e} \int_0^s \hat{K}_2(\mathbf{x}) dr ds \leq \eta_e^2 (\hat{K}_1(\mathbf{x}) + \hat{K}_2(\mathbf{x})).$$

We can conclude the proof by setting  $\hat{K}(\mathbf{x}) := \hat{K}_1(\mathbf{x}) + \hat{K}_2(\mathbf{x})$ .  $\square$

*Proof for Lemma B.3.* We can prove the lemma by applying Lemma B.7 with  $\psi(\mathbf{x})$  being  $\psi(\tilde{\mathbf{x}}) = \prod_{r=1}^s (\tilde{x}_{i_r} - x_{i_r})$  for any tuple  $(i_1, \dots, i_s) \in [D]^s$  with  $s \leq 3$  elements.  $\square$

## C RMSProp SDE Proof

In this section, we prove the following theorem for the SDE approximation of RMSprop.

**Theorem C.1.** Fix  $\sigma_0, c_2 > 0$ ,  $\epsilon_0 \geq 0$ . Let  $T > 0$ ,  $\eta^2 \in (0, 1 \wedge T \wedge \frac{1}{2c_2})$  and set  $N = \lfloor T/\eta^2 \rfloor$ . Let  $\mathbf{u}_k \triangleq \mathbf{v}_k/\sigma^2$  and  $\mathbf{x}_k \triangleq (\boldsymbol{\theta}_k, \mathbf{u}_k) \in \mathbb{R}^{2d}$ . Let  $\{\mathbf{x}_k : k \geq 0\}$  be the discrete RMSprop iterations defined in Definition 2.1. Set  $\sigma, \epsilon, \beta$  so that  $\sigma_0 = \sigma\eta$ ,  $\epsilon_0 = \epsilon\eta$  and  $c_2 = (1 - \beta)/\eta^2$ .

For well-behaved NGOS that satisfies the bounded moments and low skewness conditions, the SDE  $d\mathbf{X}_t = \mathbf{b}(\mathbf{X}_t)dt + \boldsymbol{\sigma}(\mathbf{X}_t)d\mathbf{W}_t$ , where  $\mathbf{W}_t$  is the standard Wiener process and with  $\mathbf{b}$  and  $\boldsymbol{\sigma}$  defined by

$$\begin{aligned} b_i(\boldsymbol{\theta}, \mathbf{u}) &:= -\frac{1}{\sigma_0 \sqrt{u_i} + \epsilon_0} \cdot \partial_i f(\boldsymbol{\theta}), & b_{d+i}(\boldsymbol{\theta}, \mathbf{u}) &:= c_2 (\boldsymbol{\Sigma}(\boldsymbol{\theta})_{i,i} - u_i). \\ \sigma_{i,j}(\boldsymbol{\theta}, \mathbf{u}) &:= \frac{1}{\sqrt{u_i} + \epsilon_0/\sigma} \cdot \left( \boldsymbol{\Sigma}(\boldsymbol{\theta})^{1/2} \right)_{i,j}, & \sigma_{i,d+j}(\boldsymbol{\theta}, \mathbf{u}) &:= 0, \\ \sigma_{d+i,j}(\boldsymbol{\theta}, \mathbf{u}) &:= 0, & \sigma_{d+i,d+j}(\boldsymbol{\theta}, \mathbf{u}) &:= 0. \end{aligned}$$

for all  $i, j \in [d]$ , is an order-1 weak approximation (Definition 2.4) of discrete RMSprop.

The basic idea is to apply the general theorem (Theorem B.2) with  $\eta_e := \eta^2$ . However, the SDE above does not satisfy Condition (1) in Theorem B.2 because the denominators such as  $\sigma_0 \sqrt{u_i} + \epsilon_0$  can be unbounded. To solve this issue, the first step is to reduce Theorem C.1 to proving the order-1 weak approximation for the following auxiliary SDE:

**Definition C.2.** Define  $\tau : \mathbb{R} \rightarrow \mathbb{R}$  to be the following smooth transition function:

$$\tau(z) = \begin{cases} 1 & \text{if } z \geq 1, \\ \frac{e^{-1/z}}{e^{-1/z} + e^{-1/(1-z)}} & \text{if } z \in (0, 1), \\ 0 & \text{if } z \leq 0. \end{cases} \quad (11)$$

**Theorem C.3.** In the setting of Theorem C.1, let  $u_{\min} = 2^{-c_2 T} \min_{i \in [d]} u_{0,i}$  and  $\mu(u)$  be the following function

$$\mu(u) := \frac{1}{2} u_{\min} + \tau\left(\frac{2u}{u_{\min}} - 1\right) \cdot \left(u - \frac{1}{2} u_{\min}\right). \quad (12)$$

The SDE  $d\mathbf{X}_t = \mathbf{b}(\mathbf{X}_t)dt + \boldsymbol{\sigma}(\mathbf{X}_t)d\mathbf{W}_t$ , where  $\mathbf{W}_t$  is the standard Wiener process and with  $\mathbf{b}$  and  $\boldsymbol{\sigma}$  defined by

$$\begin{aligned} b_i(\boldsymbol{\theta}, \mathbf{u}) &:= -\frac{1}{\sigma_0 \sqrt{\mu(u_i)} + \epsilon_0} \cdot \partial_i f(\boldsymbol{\theta}), & b_{d+i}(\boldsymbol{\theta}, \mathbf{u}) &:= c_2(\Sigma(\boldsymbol{\theta})_{i,i} - u_i). \\ \sigma_{i,j}(\boldsymbol{\theta}, \mathbf{u}) &:= \frac{1}{\sqrt{\mu(u_i)} + \epsilon_0/\sigma_0} \cdot \left(\Sigma(\boldsymbol{\theta})^{1/2}\right)_{i,j}, & \sigma_{i,d+j}(\boldsymbol{\theta}, \mathbf{u}) &:= 0, \\ \sigma_{d+i,j}(\boldsymbol{\theta}, \mathbf{u}) &:= 0, & \sigma_{d+i,d+j}(\boldsymbol{\theta}, \mathbf{u}) &:= 0. \end{aligned}$$

for all  $i, j \in [d]$ , is an order-1 weak approximation (Definition 2.4) of discrete RMSprop (Definition 2.1).

*Proof for Theorem C.1.* Given Theorem C.3, we only need to show that  $\mathbf{X}_t$  has the same distribution in the original and auxiliary SDEs for all  $t \in [0, T]$ , when  $\mathbf{X}_0 = (\boldsymbol{\theta}_0, \mathbf{u}_0)$ . To see this, we only need to note that in the original SDE

$$\frac{du_{t,i}}{dt} = c_2(\Sigma(\boldsymbol{\theta}_t)_{i,i} - u_{t,i}) \geq -c_2 u_{t,i}.$$

Thus,  $u_{t,i} \geq \exp(-c_2 t) u_{0,i} \geq u_{\min}$ , which means  $\Pr[u_{t,i} = \mu(u_{t,i})] = 1$  for all  $t \in [0, T]$ .  $\square$

It remains to prove Theorem C.3 by applying Theorem B.2. In the rest of this section, we verify the three conditions in Theorem B.2 respectively.

Below we use the notations  $\mathbf{x}_k, \mathbf{X}_t, \mathbf{b}, \boldsymbol{\sigma}$  defined as in Theorem C.3. Let  $D = 2d$ . Every  $\mathbf{x}_k \in \mathbb{R}^D$  is a concatenation of two  $\mathbb{R}^d$ -vectors  $\boldsymbol{\theta}_k$  and  $\mathbf{u}_k$ . According to the update rule of RMSprop,  $\mathbf{x}_k$  can be seen as SGA  $\mathbf{x}_{k+1} = \mathbf{x}_k - \eta_e \mathbf{h}_k(\mathbf{x}_k, \mathbf{z}_k, \eta_e)$ , where  $\eta_e = \eta^2$ ,  $\mathbf{z}_k \sim \mathcal{Z}_\sigma(\boldsymbol{\theta}_k)$ , and  $\mathbf{h}_k$  is defined below:

$$\mathbf{h}_k(\boldsymbol{\theta}, \mathbf{u}, \mathbf{z}, \eta_e) := \begin{bmatrix} -(\nabla f(\boldsymbol{\theta}) + \sigma \mathbf{z}) \odot (\sigma_0 \sqrt{\mathbf{u}} + \epsilon_0)^{-1} \\ c_2 \left( (\nabla f(\boldsymbol{\theta})/\sigma + \mathbf{z})^2 - \mathbf{u} \right) \end{bmatrix}.$$

We define  $\Delta$  and  $\tilde{\Delta}$  as in (6) and (7).

Fix  $\mathbf{x}_0 = (\boldsymbol{\theta}_0, \mathbf{u}_0)$  with  $u_{0,j} > 0$  for all  $j \in [d]$ . Define  $u_{\min}$  as in Theorem C.3. Let  $\mathcal{X}_k$  be the support of the random variable  $\mathbf{x}_k$  given  $\mathbf{x}_0$ , then it is easy to show that  $\mathcal{X}_k$  is a subset of  $\{(\boldsymbol{\theta}, \mathbf{u}) : u_j \geq u_{\min} \text{ for all } j \in [d]\}$ .

### C.1 Verifying Condition 1

**Lemma C.4.** The drift function  $\mathbf{b}$  and diffusion function  $\boldsymbol{\sigma}$  are Lipschitz and belong to  $G^4$ .

*Proof.*  $\Sigma^{1/2}(\boldsymbol{\theta})$  is bounded and Lipschitz, so  $\Sigma(\boldsymbol{\theta})$  is Lipschitz. Note that the denominators in the fractions in the formulas of  $\mathbf{b}$  and  $\boldsymbol{\sigma}$  are always lower bounded by a constant. Then the Lipschitz property of  $\mathbf{b}$  and  $\boldsymbol{\sigma}$  can be implied by the Lipschitz property of  $\nabla f(\boldsymbol{\theta})$ ,  $\Sigma(\boldsymbol{\theta})$ ,  $\Sigma^{1/2}(\boldsymbol{\theta})$ , and  $\mathbf{b}, \boldsymbol{\sigma} \in G^4$  can be implied by  $\nabla f, \Sigma^{1/2}, \mu \in G^4$ .  $\square$

## C.2 Verifying Condition 2

To verify Condition 2, we only need to compute the moments of  $\mathbf{\Delta}$  and  $\tilde{\mathbf{\Delta}}$  for the discrete RMSprop and the auxiliary SDE, and show that they are close to each other. We compute them by the following two lemmas.

**Lemma C.5.** *Let  $\mathbf{\Delta}(\mathbf{x}, k) := \mathbf{x}_{k+1} - \mathbf{x}$  be the one-step difference of discrete RMSprop starting from  $\mathbf{x} = (\boldsymbol{\theta}, \mathbf{u}) \in \mathcal{X}_k$  at step  $k$ . Write  $\mathbf{\Delta}$  instead of  $\mathbf{\Delta}(\mathbf{x}, k)$  for notational convenience. If the NGOS is well-behaved and  $\mathcal{Z}_\sigma$  satisfies the bounded moments and low skewness condition, then the moments of  $\mathbf{\Delta}$  can be written as below.*

1. The first moments are given by

$$\begin{aligned} \mathbb{E}[\Delta_i] &= -\frac{\eta^2}{\sigma_0\sqrt{u_i} + \epsilon_0} \partial_i f(\boldsymbol{\theta}), & \mathbb{E}[\Delta_{d+i}] &= \eta^2 c_2 (\Sigma_{ii}(\boldsymbol{\theta}) - u_i) + \frac{\eta^4 c_2}{\sigma_0^2} (\partial_i f(\boldsymbol{\theta}))^2 \\ & & &= \eta^2 c_2 (\Sigma_{ii}(\boldsymbol{\theta}) - u_i) + \mathcal{O}(\eta^4). \end{aligned}$$

for all  $i \in [d]$ .

2. The second moments are given by

$$\begin{aligned} \mathbb{E}[\Delta_i \Delta_j] &= \frac{\eta^2 \Sigma_{ij}(\boldsymbol{\theta})}{(\sqrt{u_i} + \epsilon_0/\sigma_0)(\sqrt{u_j} + \epsilon_0/\sigma_0)} + \mathcal{O}(\eta^4) & \mathbb{E}[\Delta_i \Delta_{d+j}] &= \mathcal{O}(\eta^4) \\ \mathbb{E}[\Delta_{d+i} \Delta_j] &= \mathcal{O}(\eta^4) & \mathbb{E}[\Delta_{d+i} \Delta_{d+j}] &= \mathcal{O}(\eta^4). \end{aligned}$$

for all  $i, j \in [d]$ .

3. The third moments are bounded by  $\mathbb{E}[\mathbf{\Delta}^{\otimes 3}] = \mathcal{O}(\eta^4)$ .

Here the big-O notation  $\mathcal{O}(\cdot)$  is used in a way that  $\mathcal{O}(1)$  hides constants (independent of  $\eta$  and  $\mathbf{x}$ ) and values that are bounded by a function of  $\mathbf{x}$  with polynomial growth.

*Proof.* We note that

$$\Delta_i = -\frac{\eta^2}{\sigma_0\sqrt{u_i} + \epsilon_0} (\partial_i f(\boldsymbol{\theta}) + \sigma z_i), \quad \Delta_{d+i} = (1 - \beta) ((\partial_i f(\boldsymbol{\theta})/\sigma + z_i)^2 - u_i).$$

Let  $\nu_i := \frac{1}{\sigma_0\sqrt{u_i} + \epsilon_0}$ . Since  $\mathbf{x} \in \mathcal{X}_k$ ,  $\nu_i \leq \frac{1}{\sigma_0\sqrt{u_{\min}} + \epsilon_0} = \mathcal{O}(1)$ . Writing  $1 - \beta$  as  $c_2\eta^2$ , we have

$$\Delta_i = -\nu_i \eta^2 (\partial_i f(\boldsymbol{\theta}) + \sigma z_i), \quad \Delta_{d+i} = c_2 \eta^2 ((\partial_i f(\boldsymbol{\theta})/\sigma + z_i)^2 - u_i). \quad (13)$$

We can now compute the first moments:

$$\begin{aligned} \mathbb{E}[\Delta_i] &= -\nu_i \eta^2 \partial_i f(\boldsymbol{\theta}) & (\mathbb{E}[z_i] = 0) \\ \mathbb{E}[\Delta_{d+i}] &= c_2 \eta^2 (\mathbb{E}[(\partial_i f(\boldsymbol{\theta})/\sigma)^2] + \mathbb{E}[z_i^2] - \mathbb{E}[u_i]) \\ &= c_2 \eta^2 ((\partial_i f(\boldsymbol{\theta})/\sigma)^2 + \Sigma_{ii} - u_i). \end{aligned}$$

Now we observe that  $1/\sigma = \mathcal{O}(\eta)$ , so we can write

$$\mathbb{E}[\Delta_{d+i}] = \eta^2 c_2 (\Sigma_{ii} - u_i) + \mathcal{O}(\eta^4).$$

Let  $\boldsymbol{\delta} := \mathbf{\Delta} - \mathbb{E}[\mathbf{\Delta}]$ . That is,

$$\begin{aligned} \delta_i &= -\nu_i \eta^2 \sigma z_i & \delta_{d+i} &= c_2 \eta^2 (z_i^2 - \Sigma_{ii} + 2z_i \partial_i f(\boldsymbol{\theta})/\sigma) \\ &= -\nu_i \sigma_0 \eta z_i. & &= c_2 \eta^2 (z_i^2 - \Sigma_{ii}) + 2c_2 (\partial_i f(\boldsymbol{\theta})/\sigma_0) \eta^3 z_i. \end{aligned}$$

For convenience we also define  $w_i = (z_i^2 - \Sigma_{ii}) + 2(\partial_i f(\boldsymbol{\theta})/\sigma_0) \eta z_i$  and write  $\delta_{d+i} = c_2 \eta^2 w_i$ .

For the second moments we have

$$\mathbb{E}[\Delta_p \Delta_q] = \mathbb{E}[\delta_p \delta_q] + \mathbb{E}[\Delta_p] \mathbb{E}[\Delta_q] = \mathbb{E}[\delta_p \delta_q] + \mathcal{O}(\eta^4) \quad \text{for all } 1 \leq p, q \leq 2d.$$

Then it suffices to compute the second moments for  $\boldsymbol{\delta}$ . For  $\mathbb{E}[\delta_i \delta_j]$  we have

$$\mathbb{E}[\delta_i \delta_j] = \nu_i \nu_j \eta^4 \sigma^2 \mathbb{E}[z_i z_j] = \nu_i \nu_j \sigma_0^2 \Sigma_{ij}.$$

For  $\mathbb{E}[\delta_i \delta_{d+j}]$  we have

$$\begin{aligned}\mathbb{E}[\delta_i \delta_{d+j}] &= -c_2 \nu_i \sigma_0 \eta^3 \mathbb{E}[z_i w_j] \\ &= -c_2 \nu_i \sigma_0 \eta^3 \mathbb{E}[z_i z_j^2] + \mathcal{O}(\eta^4) \\ &= \mathbb{E}[z_i z_j^2] \cdot \mathcal{O}(\eta^3) + \mathcal{O}(\eta^4).\end{aligned}$$

Similarly, we have  $\mathbb{E}[\Delta_{d+i} \Delta_j] = \mathbb{E}[z_i^2 z_j] \cdot \mathcal{O}(\eta^3) + \mathcal{O}(\eta^4)$ .

For  $\mathbb{E}[\delta_{d+i} \delta_{d+j}]$ , we note that  $\mathbf{z} \sim \mathcal{Z}_\sigma(\boldsymbol{\theta})$  has bounded 4th-order moments, so  $\mathbb{E}[g(\mathbf{z})] = \mathcal{O}(1)$  for any polynomial  $g$  of degree at most 4, if the coefficients of  $g$  are bounded by  $\mathcal{O}(1)$ . Then we have

$$\mathbb{E}[\delta_{d+i} \delta_{d+j}] = c_2^2 \eta^4 \mathbb{E}[w_i w_j] = \mathcal{O}(\eta^4).$$

Now we can check the third moments.

$$\begin{aligned}\mathbb{E}[\Delta_p \Delta_q \Delta_r] &= \mathbb{E}[\delta_p \delta_q \delta_r] + (\mathbb{E}[\delta_p \delta_q] \mathbb{E}[\Delta_r] + \mathbb{E}[\delta_p \delta_r] \mathbb{E}[\Delta_q] + \mathbb{E}[\delta_q \delta_r] \mathbb{E}[\Delta_p]) + \mathbb{E}[\Delta_p] \mathbb{E}[\Delta_q] \mathbb{E}[\Delta_r] \\ &= \mathbb{E}[\delta_p \delta_q \delta_r] + \mathcal{O}(\eta^2) \cdot \mathcal{O}(\eta^2) + \mathcal{O}(\eta^6) \\ &= \mathbb{E}[\delta_p \delta_q \delta_r] + \mathcal{O}(\eta^4).\end{aligned}$$

Note that  $\delta_p \delta_q \delta_r$  is a polynomial of  $\mathbf{z}$ . For  $p = i, q = j, r = k$ , by the low skewness condition for  $\mathcal{Z}_\sigma$  we have

$$\mathbb{E}[\delta_i \delta_j \delta_k] = -\nu_i^3 \sigma_0^3 \eta^3 \mathbb{E}[z_i z_j z_k] = K_3(\boldsymbol{\theta}) / \sigma \cdot \mathcal{O}(\eta^3) = \mathcal{O}(\eta^4).$$

Except the above case, it can be shown that  $\delta_p \delta_q \delta_r$  is a polynomial with coefficients bounded by  $\mathcal{O}(\eta^4)$ . Combining this with the fact that  $\mathbf{z} \sim \mathcal{Z}_\sigma(\boldsymbol{\theta})$  has bounded moments of any order, we have  $\mathbb{E}[\delta_p \delta_q \delta_r] = \mathcal{O}(\eta^4)$ .  $\square$

**Lemma C.6.** *Let  $\tilde{\Delta}(x, k) = \mathbf{X}_{(k+1)\eta^2} - \mathbf{x}$  be the one-step difference of the auxiliary SDE of RMSprop starting from  $\mathbf{x} = (\boldsymbol{\theta}, \mathbf{u}) \in \mathcal{X}_k$  at time  $k\eta^2$ . Write  $\tilde{\Delta}$  instead of  $\tilde{\Delta}(x, k)$  for notational convenience. If the NGOS is well-behaved, then the moments of  $\tilde{\Delta}$  can be written as below.*

1. The first moments are given by

$$\mathbb{E}[\tilde{\Delta}_i] = -\frac{\eta^2}{\sigma_0 \sqrt{\mu(u_i)} + \epsilon_0} \partial_i f(\boldsymbol{\theta}), \quad \mathbb{E}[\tilde{\Delta}_{d+i}] = \eta^2 c_2 (\Sigma_{ii}(\boldsymbol{\theta}) - u_i) + \mathcal{O}(\eta^4).$$

for all  $i \in [d]$ .

2. The second moments are given by

$$\begin{aligned}\mathbb{E}[\tilde{\Delta}_i \tilde{\Delta}_j] &= \frac{\eta^2 \Sigma_{ij}(\boldsymbol{\theta})}{(\sqrt{\mu(u_i)} + \epsilon_0 / \sigma_0)(\sqrt{\mu(u_j)} + \epsilon_0 / \sigma_0)} + \mathcal{O}(\eta^4) & \mathbb{E}[\tilde{\Delta}_i \tilde{\Delta}_{d+j}] &= \mathcal{O}(\eta^4) \\ \mathbb{E}[\tilde{\Delta}_{d+i} \tilde{\Delta}_j] &= \mathcal{O}(\eta^4) & \mathbb{E}[\tilde{\Delta}_{d+i} \tilde{\Delta}_{d+j}] &= \mathcal{O}(\eta^4).\end{aligned}$$

for all  $i, j \in [d]$ .

3. The third moments are bounded by  $\mathbb{E}[\tilde{\Delta}^{\otimes 3}] = \mathcal{O}(\eta^4)$ .

Here the big- $\mathcal{O}$  notation  $\mathcal{O}(\cdot)$  is used in a way that  $\mathcal{O}(1)$  hides constants (independent of  $\eta$  and  $\mathbf{x}$ ) and values that are bounded by a function of  $\mathbf{x}$  with polynomial growth.

*Proof.* Applying Lemma B.3 gives

$$\mathbb{E}[\tilde{\Delta}] = \eta^2 \mathbf{b}(\mathbf{x}) + \mathcal{O}(\eta^4), \quad \mathbb{E}[\tilde{\Delta} \tilde{\Delta}^\top] = \eta^2 \boldsymbol{\sigma}(\mathbf{x}) \boldsymbol{\sigma}(\mathbf{x})^\top + \mathcal{O}(\eta^4), \quad \mathbb{E}[\tilde{\Delta}^{\otimes 3}] = \mathcal{O}(\eta^4).$$

Splitting up the formula by indices proves the claim.  $\square$

### C.3 Verifying Condition 3

**Lemma C.7.** *Let  $P := \{1, 2, \dots, d\}$ . Then*

1. *There is a constant  $C_1 > 0$  (independent of  $\eta_e$ ) so that*

$$\|\mathbb{E}\Delta(\mathbf{x}, k)\|_P \leq C_1 \eta_e (1 + \|\mathbf{x}\|_P), \quad \|\mathbb{E}\Delta(\mathbf{x}, k)\|_R \leq C_1 \eta_e (1 + \|\mathbf{x}\|_P^2)(1 + \|\mathbf{x}\|_R),$$

for all  $k \leq N$  and  $\mathbf{x} \in \mathcal{X}_k$ .

2. *For all  $m \geq 1$ , there is a constant  $C_{2m}$  (independent of  $\eta_e$ ) so that*

$$\mathbb{E}\|\Delta(\mathbf{x}, k)\|_P^{2m} \leq C_{2m} \eta_e^m (1 + \|\mathbf{x}\|_P^{2m}), \quad \mathbb{E}\|\Delta(\mathbf{x}, k)\|_R^{2m} \leq C_{2m} \eta_e^m (1 + \|\mathbf{x}\|_P^{4m})(1 + \|\mathbf{x}\|_R^{2m}),$$

for all  $k \leq N$  and  $\mathbf{x} \in \mathcal{X}_k$ .

*Proof.* By Lemma C.5, for all  $i \in [d]$ ,

$$\mathbb{E}[\Delta_i] = -\frac{\eta^2}{\sigma_0 \sqrt{u_i} + \epsilon_0} \partial_i f(\boldsymbol{\theta}), \quad \mathbb{E}[\Delta_{d+i}] = \eta^2 c_2 (\Sigma_{ii}(\boldsymbol{\theta}) - u_i) + \frac{\eta^4 c_2}{\sigma_0^2} (\partial_i f(\boldsymbol{\theta}))^2.$$

Combining this with the Lipschitzness of  $\nabla f(\boldsymbol{\theta})$  and the boundedness of  $\Sigma(\boldsymbol{\theta})$  proves Item 1.

By (13), for all  $i \in [d]$ ,

$$|\Delta_i| = \nu_i \eta^2 |\partial_i f(\boldsymbol{\theta}) + \sigma z_i| \leq \eta^2 \nu_i (1 + |\partial_i f(\boldsymbol{\theta})|)(1 + \sigma |z_i|) \leq \eta \nu_i (1 + |\partial_i f(\boldsymbol{\theta})|)(1 + \sigma_0 |z_i|)$$

$$|\Delta_{d+i}| = c_2 \eta^2 |(\partial_i f(\boldsymbol{\theta})/\sigma + z_i)^2 - u_i| \leq c_2 \eta^2 (1 + (\partial_i f(\boldsymbol{\theta})/\sigma + z_i)^2)(1 + u_i)$$

By the Lipschitzness of  $\nabla f(\boldsymbol{\theta})$  and the bounded moments condition for  $\mathcal{Z}_\sigma$ , we can prove Item 2 by taking powers and expectations on both sides of the above inequalities.  $\square$

## D Adam SDE Proof

In this section, we prove the following theorem for the SDE approximation of Adam.

**Theorem D.1.** *Fix  $\sigma_0, c_1, c_2 > 0, \epsilon_0 \geq 0$ . Let  $T > 0, \eta^2 \in (0, 1 \wedge T \wedge \frac{1}{2c_2})$  and set  $N = \lfloor T/\eta^2 \rfloor$ . Let  $\mathbf{u}_k \triangleq \mathbf{v}_k/\sigma^2$  and  $\mathbf{x}_k \triangleq (\boldsymbol{\theta}_k, \mathbf{m}_k, \mathbf{u}_k) \in \mathbb{R}^{3d}$ . Let  $\{\mathbf{x}_k : k \geq 0\}$  be the discrete Adam iterations defined in Definition 2.2. Set  $\sigma, \epsilon, \beta_1, \beta_2$  so that  $\sigma_0 = \sigma\eta, \epsilon_0 = \epsilon\eta, c_1 = (1 - \beta_1)/\eta^2$  and  $c_2 = (1 - \beta_2)/\eta^2$ .*

*For well-behaved NGOS that satisfies the bounded moments and low skewness conditions, consider the SDE  $d\mathbf{X}_t = \mathbf{b}(\mathbf{X}_t)dt + \boldsymbol{\sigma}(\mathbf{X}_t)d\mathbf{W}_t$ , where  $\mathbf{W}_t$  is the standard Wiener process and with  $\mathbf{b}$  and  $\boldsymbol{\sigma}$  defined by*

$$b_i(\mathbf{x}, t) := -\frac{\sqrt{\gamma_2(t)}}{\gamma_1(t)} \cdot \frac{m_i}{\sigma_0 \sqrt{u_i} + \epsilon_0 \sqrt{\gamma_2(t)}}, \quad \text{where } \gamma_1(t) := 1 - e^{-c_1 t}, \gamma_2(t) := 1 - e^{-c_2 t},$$

$$b_{d+i}(\mathbf{x}, t) := c_1 (\partial_i f(\boldsymbol{\theta}) - m_i),$$

$$b_{2d+i}(\mathbf{x}, t) := c_2 (\Sigma(\boldsymbol{\theta})_{i,i} - u_i).$$

$$\sigma_{d+i, d+j}(\mathbf{x}, t) := \sigma_0 c_1 \left( \Sigma^{1/2}(\boldsymbol{\theta}) \right)_{i,j},$$

for all  $i, j \in [d]$ , and all other entries of  $\boldsymbol{\sigma}$  is zero. For any constant  $t_0 > 0$ , the solution  $\mathbf{X}_t$  ( $t \in [t_0, T]$ ) of the above SDE is an order-1 weak approximation (Definition 2.4) of the sequence of Adam iterates  $\mathbf{x}_k$  starting from  $k_0 = \lceil t_0/\eta^2 \rceil$ , if the initial condition of the SDE is set to  $\mathbf{X}_{t_0} = \mathbf{x}_{k_0}$ .

The proof strategy is essentially the same as that for RMSprop. Similar to what we have done for RMSprop, we turn to prove the approximation order for the following auxiliary SDE.

**Theorem D.2.** *In the setting of Theorem D.1, let  $u_{\min} = 2^{-(T-t_0)} \min_{i \in [d]} u_{k_0, i}$ , and  $\mu(u)$  be the following function*

$$\mu(u) := \frac{1}{2} u_{\min} + \tau \left( \frac{2u}{u_{\min}} - 1 \right) \cdot \left( u - \frac{1}{2} u_{\min} \right). \quad (14)$$

Consider the SDE  $d\mathbf{X}_t = \mathbf{b}(\mathbf{X}_t)dt + \boldsymbol{\sigma}(\mathbf{X}_t)d\mathbf{W}_t$ , where  $\mathbf{W}_t$  is the standard Wiener process and with  $\mathbf{b}$  and  $\boldsymbol{\sigma}$  defined by

$$\begin{aligned} b_i(\mathbf{x}, t) &:= -\frac{\sqrt{\bar{\gamma}_2(t)}}{\bar{\gamma}_1(t)} \cdot \frac{m_i}{\sigma_0 \sqrt{\mu(u_i)} + \epsilon_0 \sqrt{\bar{\gamma}_2(t)}}, \quad \text{where } \bar{\gamma}_1(t) := 1 - e^{-c_1 t}, \bar{\gamma}_2(t) := 1 - e^{-c_2 t}, \\ b_{d+i}(\mathbf{x}, t) &:= c_1(\partial_i f(\boldsymbol{\theta}) - m_i), \\ b_{2d+i}(\mathbf{x}, t) &:= c_2(\Sigma(\boldsymbol{\theta})_{i,i} - u_i). \\ \sigma_{d+i, d+j}(\mathbf{x}, t) &:= \sigma_0 c_1 \left( \boldsymbol{\Sigma}^{1/2}(\boldsymbol{\theta}) \right)_{i,j}, \end{aligned}$$

for all  $i, j \in [d]$ , and all other entries of  $\boldsymbol{\sigma}$  is zero. For any constant  $t_0 > 0$ , the solution  $\mathbf{X}_t$  ( $t \in [t_0, T]$ ) of the above SDE is an order-1 weak approximation (Definition 2.4) of the sequence of Adam iterates  $\mathbf{x}_k$  starting from  $k_0 = \lceil t_0/\eta^2 \rceil$ , if the initial condition of the SDE is set to  $\mathbf{X}_{t_0} = \mathbf{x}_{k_0}$ .

*Proof for Theorem D.1.* Given Theorem D.2, we only need to show that  $\mathbf{X}_t$  has the same distribution in the original and auxiliary SDEs for all  $t \in [0, T]$ , when  $\mathbf{X}_0 = (\boldsymbol{\theta}_0, \mathbf{m}_0, \mathbf{u}_0)$ . To see this, we only need to note that in the original SDE

$$\frac{du_{t,i}}{dt} = c_2(\Sigma(\boldsymbol{\theta}_t)_{i,i} - u_{t,i}) \geq -c_2 u_{t,i}.$$

Thus,  $u_{t,i} \geq \exp(-c_2 t)u_{0,i} \geq u_{\min}$ , which means  $\Pr[u_{t,i} = \mu(u_{t,i})] = 1$  for all  $t \in [0, T]$ .  $\square$

It remains to prove Theorem D.2 by applying Theorem B.2. In the rest of this section, we verify the three conditions in Theorem B.2 respectively.

Below we use the notations  $\mathbf{x}_k, \mathbf{X}_t, \mathbf{b}, \boldsymbol{\sigma}$  defined as in Theorem D.2. Let  $D = 3d$ . Every  $\mathbf{x}_k \in \mathbb{R}^D$  is a concatenation of three  $\mathbb{R}^d$ -vectors  $\boldsymbol{\theta}_k, \mathbf{m}_k$  and  $\mathbf{u}_k$ . According to the update rule of Adam,  $\mathbf{x}_k$  can be seen as SGA  $\mathbf{x}_{k+1} = \mathbf{x}_k - \eta_e \mathbf{h}_k(\mathbf{x}_k, \mathbf{z}_k, \eta_e)$ , where  $\eta_e = \eta^2$ ,  $\mathbf{z}_k \sim \mathcal{Z}_\sigma(\boldsymbol{\theta}_k)$ , and  $\mathbf{h}_k$  is defined below:

$$\mathbf{h}_k(\boldsymbol{\theta}, \mathbf{u}, \mathbf{z}, \eta_e) := \begin{bmatrix} -\frac{\sqrt{1-\beta_2^k}}{1-\beta_1^{k+1}} \mathbf{m} \odot \left( \sigma_0 \sqrt{\mathbf{u}} + \epsilon_0 \sqrt{1-\beta_2^k} \right)^{-1} \\ c_1(\nabla f(\boldsymbol{\theta}) + \sigma \mathbf{z} - \mathbf{m}) \\ c_2 \left( (\nabla f(\boldsymbol{\theta})/\sigma + \mathbf{z})^2 - \mathbf{u} \right) \end{bmatrix}.$$

We define  $\boldsymbol{\Delta}$  and  $\tilde{\boldsymbol{\Delta}}$  as in (6) and (7).

Fix  $\mathbf{x}_0 = (\boldsymbol{\theta}_0, \mathbf{m}_0, \mathbf{u}_0)$  with  $u_{0,j} > 0$  for all  $j \in [d]$ . Define  $u_{\min}$  as in Theorem D.2. Let  $\mathcal{X}_k$  be the support of the random variable  $\mathbf{x}_k$  given  $\mathbf{x}_0$ , then it is easy to show that  $\mathcal{X}_k$  is a subset of  $\{(\boldsymbol{\theta}, \mathbf{m}, \mathbf{u}) : u_j \geq u_{\min} \text{ for all } j \in [d]\}$ .

## D.1 Verifying Condition 1

**Lemma D.3.** *The drift function  $\mathbf{b}$  and diffusion function  $\boldsymbol{\sigma}$  are Lipschitz and belong to  $G^4$ .*

*Proof.* Same argument as for Lemma C.4.  $\square$

## D.2 Verifying Condition 2

Let  $\mathbf{x} = (\boldsymbol{\theta}, \mathbf{m}, \mathbf{u}) \in \mathbb{R}^{3d}$ . For ease of notation, let  $\gamma_1 = 1 - \beta_1^{k+1}$  and  $\gamma_2 = 1 - \beta_2^k$ . These are not constants across time steps like the other constants, but they are deterministic and upper bounded by constants for  $k \geq t_0/\eta^2$ . Let

To verify Condition 2, we only need to compute the moments of  $\boldsymbol{\Delta}$  and  $\tilde{\boldsymbol{\Delta}}$  for the discrete Adam and the auxiliary SDE, and show that they are close to each other. We compute them by the following two lemmas.

**Lemma D.4.** *Let  $\boldsymbol{\Delta}(\mathbf{x}, k) := \mathbf{x}_{k+1} - \mathbf{x}$  be the one-step difference of discrete Adam starting from  $\mathbf{x} = (\boldsymbol{\theta}, \mathbf{u}) \in \mathcal{X}_k$  at step  $k$ . Write  $\tilde{\boldsymbol{\Delta}}$  instead of  $\boldsymbol{\Delta}(\mathbf{x}, k)$  for notational convenience. If the NGOS is well-behaved and  $\mathcal{Z}_\sigma$  satisfies the bounded moments and low skewness condition, then the moments of  $\boldsymbol{\Delta}$  can be written as below.*

1. The first moments are given by

$$\begin{aligned}\mathbb{E}[\Delta_i] &= -\frac{\sqrt{\gamma_2}}{\gamma_1} \cdot \frac{\eta^2}{\sigma_0\sqrt{u_i} + \epsilon_0\sqrt{\gamma_2}} (m_i + c_1\eta^2(\partial_i f(\boldsymbol{\theta}) - m_i)) \\ &= -\frac{\sqrt{\gamma_2}}{\gamma_1} \cdot \frac{\eta^2 m_i}{\sigma_0\sqrt{u_i} + \epsilon_0\sqrt{\gamma_2}} + \mathcal{O}(\eta^4) \\ \mathbb{E}[\Delta_{d+i}] &= c_1\eta^2(\partial_i f(\boldsymbol{\theta}) - m_i) \\ \mathbb{E}[\Delta_{2d+i}] &= c_2\eta^2((\partial_i f(\boldsymbol{\theta})/\sigma)^2 + \Sigma_{ii} - u_i) \\ &= c_2\eta^2(\Sigma_{ii} - u_i) + \mathcal{O}(\eta^4).\end{aligned}$$

for all  $i \in [d]$ .

2. The second moments are given by

$$\mathbb{E}[\Delta_p \Delta_q] = \begin{cases} c_1^2 \sigma_0^2 \eta^2 \Sigma_{ij} + \mathcal{O}(\eta^4) & \text{if } p = d+i, q = d+j \text{ for some } i, j \in [d] \\ \mathcal{O}(\eta^4) & \text{otherwise.} \end{cases}$$

for all  $p, q \in [3d]$ .

3. The third moments are bounded by  $\mathbb{E}[\Delta^{\otimes 3}] = \mathcal{O}(\eta^4)$ .

Here the big-O notation  $\mathcal{O}(\cdot)$  is used in a way that  $\mathcal{O}(1)$  hides constants (independent of  $\eta$  and  $\mathbf{x}$ ) and values that are bounded by a function of  $\mathbf{x}$  with polynomial growth.

*Proof.* For notational convenience, we write  $\Delta, \Sigma$  instead of  $\Delta(\mathbf{x}), \Sigma(\boldsymbol{\theta})$ . We note that

$$\begin{aligned}\Delta_i &= -\frac{\sqrt{\gamma_2}}{\gamma_1} \cdot \frac{\eta^2 m_i + \eta^2(1 - \beta_1)(\partial_i f(\boldsymbol{\theta}) + \sigma z_i - m_i)}{\sigma_0\sqrt{u_i} + \epsilon_0\sqrt{\gamma_2}} \\ \Delta_{d+i} &= (1 - \beta_1)(\partial_i f(\boldsymbol{\theta}) + \sigma z_i - m_i) \\ \Delta_{2d+i} &= (1 - \beta_2)((\partial_i f(\boldsymbol{\theta})/\sigma + z_i)^2 - u_i)\end{aligned}$$

Let  $\nu_i := \frac{\sqrt{\gamma_2}}{\gamma_1} \cdot \frac{1}{\sigma_0\sqrt{u_i} + \epsilon_0\sqrt{\gamma_2}}$ . And we write  $1 - \beta = c_2\eta^2$ . Then we have

$$\begin{aligned}\Delta_i &= -\nu_i \eta^2 (m_i + c_1 \eta^2 (\partial_i f(\boldsymbol{\theta}) + \sigma z_i - m_i)) \\ \Delta_{d+i} &= c_1 \eta^2 (\partial_i f(\boldsymbol{\theta}) + \sigma z_i - m_i) \\ \Delta_{2d+i} &= c_2 \eta^2 ((\partial_i f(\boldsymbol{\theta})/\sigma + z_i)^2 - u_i)\end{aligned} \tag{15}$$

The first moments follow directly:

$$\begin{aligned}\mathbb{E}[\Delta_i] &= -\nu_i \eta^2 (m_i + c_1 \eta^2 (\partial_i f(\boldsymbol{\theta}) - m_i)) = -\nu_i \eta^2 m_i + \mathcal{O}(\eta^4) \\ \mathbb{E}[\Delta_{d+i}] &= c_1 \eta^2 (\partial_i f(\boldsymbol{\theta}) - m_i) \\ \mathbb{E}[\Delta_{2d+i}] &= c_2 \eta^2 ((\partial_i f(\boldsymbol{\theta})/\sigma)^2 + \Sigma_{ii} - u_i) = c_2 \eta^2 (\Sigma_{ii} - u_i) + \mathcal{O}(\eta^4).\end{aligned}$$

Let  $\boldsymbol{\delta} := \boldsymbol{\Delta} - \mathbb{E}[\boldsymbol{\Delta}]$ . That is,

$$\begin{aligned}\delta_i &= -\nu_i c_1 \eta^4 \sigma z_i = -\nu_i c_1 \sigma_0 \eta^3 z_i \\ \delta_{d+i} &= c_1 \eta^2 \sigma z_i = c_1 \sigma_0 \eta z_i \\ \delta_{2d+i} &= c_2 \eta^2 (z_i^2 - \Sigma_{ii} + 2z_i \partial_i f(\boldsymbol{\theta})/\sigma) \\ &= c_2 \eta^2 (z_i^2 - \Sigma_{ii}) + 2c_2 (\partial_i f(\boldsymbol{\theta})/\sigma_0) \eta^3 z_i.\end{aligned}$$

For convenience we also define  $w_i = (z_i^2 - \Sigma_{ii}) + 2(\partial_i f(\boldsymbol{\theta})/\sigma_0) \eta z_i$  and write  $\delta_{d+i} = c_2 \eta^2 w_i$ .

Similar as the proof for Lemma C.5, for the second moments we have

$$\mathbb{E}[\Delta_p \Delta_q] = \mathbb{E}[\delta_p \delta_q] + \mathbb{E}[\Delta_p] \mathbb{E}[\Delta_q] = \mathbb{E}[\delta_p \delta_q] + \mathcal{O}(\eta^4) \quad \text{for all } 1 \leq p, q \leq 2d.$$



Then it suffices to compute the second order moments for  $\delta$ . A direct computation gives the following:

$$\begin{aligned}
\mathbb{E}[\delta_i \delta_j] &= \nu_i \nu_j c_1^2 \sigma_0^2 \eta^6 \mathbb{E}[z_i z_j] = \mathcal{O}(\eta^6). \\
\mathbb{E}[\delta_i \delta_{d+j}] &= -\nu_i c_1^2 \sigma_0^2 \eta^4 \mathbb{E}[z_i z_j] = \mathcal{O}(\eta^4). \\
\mathbb{E}[\delta_i \delta_{2d+j}] &= -\nu_i c_1 c_2 \sigma_0 \eta^5 \mathbb{E}[z_i w_j] = \mathcal{O}(\eta^5). \\
\mathbb{E}[\delta_{d+i} \delta_{d+j}] &= c_1^2 \sigma_0^2 \eta^2 \mathbb{E}[z_i z_j] = c_1^2 \sigma_0^2 \eta^2 \Sigma_{ij}. \\
\mathbb{E}[\delta_{d+i} \delta_{2d+j}] &= c_1 c_2 \sigma_0 \eta^3 \mathbb{E}[z_i w_j] = c_1 c_2 \sigma_0 \eta^3 \mathbb{E}[z_i z_j^2] + \mathcal{O}(\eta^4). \\
\mathbb{E}[\delta_{2d+i} \delta_{2d+j}] &= c_2^2 \eta^4 \mathbb{E}[w_i w_j] = \mathcal{O}(\eta^4).
\end{aligned}$$

Now we check the third moments. Similar as the proof for Lemma C.5,  $\mathbb{E}[\Delta_p \Delta_q \Delta_r] = \mathbb{E}[\delta_p \delta_q \delta_r] + \mathcal{O}(\eta^4)$ . Note that  $\delta_p \delta_q \delta_r$  is a polynomial of  $\mathbf{z}$ . For  $p = d + i, q = d + j, r = d + k$ , by the low skewness condition for  $\mathcal{Z}_\sigma$  we have

$$\mathbb{E}[\delta_{d+i} \delta_{d+j} \delta_{d+k}] = c_1^3 \sigma_0^3 \eta^3 \mathbb{E}[z_i z_j z_k] = K_3(\boldsymbol{\theta})/\sigma \cdot \mathcal{O}(\eta^3) = \mathcal{O}(\eta^4).$$

Except the above case, it can be shown that  $\delta_p \delta_q \delta_r$  is a polynomial with coefficients bounded by  $\mathcal{O}(\eta^4)$ . Combining this with the fact that  $\mathbf{z} \sim \mathcal{Z}_\sigma(\boldsymbol{\theta})$  has bounded moments of any order, we have  $\mathbb{E}[\delta_p \delta_q \delta_r] = \mathcal{O}(\eta^4)$ .  $\square$

**Lemma D.5.** *Let  $\tilde{\Delta}(x, k) = \mathbf{X}_{(k+1)\eta^2} - \mathbf{x}$  be the one-step difference of the auxiliary SDE of RMSprop starting from  $\mathbf{x} = (\boldsymbol{\theta}, \mathbf{u}) \in \mathcal{X}_k$  at time  $k\eta^2$ . Write  $\tilde{\Delta}$  instead of  $\tilde{\Delta}(x, k)$  for notational convenience. If the NGOS is well-behaved, then the moments of  $\tilde{\Delta}$  can be written as below.*

1. *The first moments are given by*

$$\begin{aligned}
\mathbb{E}[\Delta_i] &= -\frac{\sqrt{\gamma_2}}{\gamma_1} \cdot \frac{\eta^2 m_i}{\sigma_0 \sqrt{u_i} + \epsilon_0 \sqrt{\gamma_2}} + \mathcal{O}(\eta^4) \\
\mathbb{E}[\Delta_{d+i}] &= c_1 \eta^2 (\partial_i f(\boldsymbol{\theta}) - m_i) + \mathcal{O}(\eta^4) \\
\mathbb{E}[\Delta_{2d+i}] &= c_2 \eta^2 (\Sigma_{ii} - u_i) + \mathcal{O}(\eta^4).
\end{aligned}$$

for all  $i \in [d]$ .

2. *The second moments are given by*

$$\mathbb{E}[\Delta_p \Delta_q] = \begin{cases} c_1^2 \sigma_0^2 \eta^2 \Sigma_{ij} + \mathcal{O}(\eta^4) & \text{if } p = d + i, q = d + j \text{ for some } i, j \in [d] \\ \mathcal{O}(\eta^4) & \text{otherwise.} \end{cases}$$

for all  $p, q \in [3d]$ .

3. *The third moments are bounded by  $\mathbb{E}[\Delta^{\otimes 3}] = \mathcal{O}(\eta^4)$ .*

Here the big-O notation  $\mathcal{O}(\cdot)$  is used in a way that  $\mathcal{O}(1)$  hides constants (independent of  $\eta$  and  $\mathbf{x}$ ) and values that are bounded by a function of  $\mathbf{x}$  with polynomial growth.

*Proof.* Applying Lemma B.3 gives

$$\mathbb{E}[\tilde{\Delta}] = \eta^2 \mathbf{b}(\mathbf{x}) + \mathcal{O}(\eta^4), \quad \mathbb{E}[\tilde{\Delta} \tilde{\Delta}^\top] = \eta^2 \boldsymbol{\sigma}(\mathbf{x}) \boldsymbol{\sigma}(\mathbf{x})^\top + \mathcal{O}(\eta^4), \quad \mathbb{E}[\tilde{\Delta}^{\otimes 3}] = \mathcal{O}(\eta^4).$$

Splitting up the formula by indices proves the claim.  $\square$

### D.3 Verifying Condition 3

**Lemma D.6.** *Let  $P := \{1, 2, \dots, 2d\}$ . Then*

1. *There is a constant  $C_1 > 0$  (independent of  $\eta_e$ ) so that*

$$\|\mathbb{E}\Delta(\mathbf{x}, k)\|_P \leq C_1 \eta_e (1 + \|\mathbf{x}\|_P), \quad \|\mathbb{E}\Delta(\mathbf{x}, k)\|_R \leq C_1 \eta_e (1 + \|\mathbf{x}\|_P^2) (1 + \|\mathbf{x}\|_R),$$

for all  $k \leq N$  and  $\mathbf{x} \in \mathcal{X}_k$ .

2. For all  $m \geq 1$ , there is a constant  $C_{2m}$  (independent of  $\eta_e$ ) so that

$$\mathbb{E}\|\Delta(\mathbf{x}, k)\|_{\mathbb{P}}^{2m} \leq C_{2m}\eta_e^m(1 + \|\mathbf{x}\|_{\mathbb{P}}^{2m}), \quad \mathbb{E}\|\Delta(\mathbf{x}, k)\|_{\mathbb{R}}^{2m} \leq C_{2m}\eta_e^m(1 + \|\mathbf{x}\|_{\mathbb{P}}^{4m})(1 + \|\mathbf{x}\|_{\mathbb{R}}^{2m}),$$

for all  $k \leq N$  and  $\mathbf{x} \in \mathcal{X}_k$ .

*Proof.* By Lemma D.4, for all  $i \in [d]$ ,

$$\begin{aligned} \mathbb{E}[\Delta_i] &= -\nu_i\eta^2(m_i + c_1\eta^2(\partial_i f(\boldsymbol{\theta}) - m_i)) \\ \mathbb{E}[\Delta_{d+i}] &= c_1\eta^2(\partial_i f(\boldsymbol{\theta}) - m_i) \\ \mathbb{E}[\Delta_{2d+i}] &= c_2\eta^2((\partial_i f(\boldsymbol{\theta})/\sigma)^2 + \Sigma_{ii} - u_i). \end{aligned}$$

Combining this with the Lipschitzness of  $\nabla f(\boldsymbol{\theta})$  and the boundedness of  $\Sigma(\boldsymbol{\theta})$  proves Item 1.

By (15), for all  $i \in [d]$ , one can show that there exists a constant  $\hat{C}$  such that

$$\begin{aligned} |\Delta_i| &\leq \eta^2\hat{C}(1 + |m_i| + |\partial_i f(\boldsymbol{\theta})|)(1 + |z_i|) \\ |\Delta_{d+i}| &\leq \eta^2\hat{C}(1 + |m_i| + |\partial_i f(\boldsymbol{\theta})|)(1 + |z_i|) \\ |\Delta_{2d+i}| &\leq \eta^2\hat{C}(1 + |\partial_i f(\boldsymbol{\theta})|^2 + z_i^2)(1 + u_i) \end{aligned}$$

By the Lipschitzness of  $\nabla f(\boldsymbol{\theta})$  and the bounded moments condition for  $\mathcal{Z}_\sigma$ , we can prove Item 2 by taking powers and expectations on both sides of the above inequalities.  $\square$

## E Analysis of SVAG Operator

**Lemma E.1.** Let  $\mathcal{G}_\sigma = (f, \Sigma, \mathcal{Z}_\sigma)$  be a NGOS and  $\widehat{\mathcal{G}}_{\ell\sigma} = (f, \Sigma, \widehat{\mathcal{Z}}_{\ell\sigma})$  be the NGOS after applying the SVAG operator with hyperparameter  $\ell > 0$ . Then  $\widehat{\mathcal{G}}_{\ell\sigma}$  is indeed an NGOS. That is,  $\widehat{\mathcal{Z}}_{\ell\sigma}(\boldsymbol{\theta})$  is well-defined and has mean zero, covariance  $\Sigma(\boldsymbol{\theta})$ .

*Proof.* Let  $\widehat{\mathcal{Z}}_{\ell\sigma}(\boldsymbol{\theta})$  be the distribution of  $\hat{\mathbf{z}} := \frac{1}{\ell}(r_1(\ell)\mathbf{z}_1 + r_2(\ell)\mathbf{z}_2)$  when  $\mathbf{z}_1, \mathbf{z}_2 \sim \mathcal{Z}_\sigma(\boldsymbol{\theta})$ . Then it is easy to check that  $\hat{\mathbf{g}}$  has the same distribution as  $\nabla f(\boldsymbol{\theta}) + \ell\sigma\hat{\mathbf{z}}$ , since

$$\begin{aligned} \hat{\mathbf{g}} &= r_1(\ell)\mathbf{g}_1 + r_2(\ell)\mathbf{g}_2 \sim r_1(\ell)(\nabla f(\boldsymbol{\theta}) + \sigma\mathbf{z}_1) + r_2(\ell)(\nabla f(\boldsymbol{\theta}) + \sigma\mathbf{z}_2) \\ &= (r_1(\ell) + r_2(\ell))\nabla f(\boldsymbol{\theta}) + \sigma(r_1(\ell)\mathbf{z}_1 + r_2(\ell)\mathbf{z}_2) \\ &= \nabla f(\boldsymbol{\theta}) + \ell\sigma\hat{\mathbf{z}}, \end{aligned}$$

where the last equality uses the fact that  $r_1(\ell) + r_2(\ell) = 1$ . Hence  $\widehat{\mathcal{Z}}_{\ell\sigma}(\boldsymbol{\theta})$  is well-defined.

Now we check the mean and covariance of  $\hat{\mathbf{z}} \sim \widehat{\mathcal{Z}}_{\ell\sigma}(\boldsymbol{\theta})$ . By linearity of expectation and linearity of variance (for independent variables), we have

$$\begin{aligned} \mathbb{E}[\hat{\mathbf{z}}] &= \frac{1}{\ell}(r_1(\ell)\mathbb{E}[\mathbf{z}_1] + r_2(\ell)\mathbb{E}[\mathbf{z}_2]) = \frac{1}{\ell}(\mathbf{0} + \mathbf{0}) = \mathbf{0}, \\ \text{Cov}(\hat{\mathbf{z}}) &= \frac{1}{\ell^2}(r_1^2(\ell)\text{Cov}(\mathbf{z}_1) + r_2^2(\ell)\text{Cov}(\mathbf{z}_2)) = \frac{1}{\ell^2}(r_1^2(\ell) + r_2^2(\ell))\Sigma(\boldsymbol{\theta}) = \Sigma(\boldsymbol{\theta}), \end{aligned}$$

where the last equality uses the fact that  $r_1^2(\ell) + r_2^2(\ell) = \left(\frac{1+\sqrt{2\ell^2-1}}{2}\right)^2 + \left(\frac{1-\sqrt{2\ell^2-1}}{2}\right)^2 = \frac{1+2\ell^2-1}{2} = \ell^2$ .  $\square$

**Lemma E.2.** Let  $\mathcal{G}_\sigma = (f, \Sigma, \mathcal{Z}_\sigma)$  be a NGOS with scale  $\sigma$ . Applying the SVAG operator with hyperparameter  $\ell \geq 1$ , we obtain  $\widehat{\mathcal{G}}_{\hat{\sigma}} = (f, \Sigma, \widehat{\mathcal{Z}}_{\hat{\sigma}})$  with scale  $\hat{\sigma} = \ell\sigma$ . Fixing  $\sigma$  and changing  $\ell$  produces  $\widehat{\mathcal{G}}_{\hat{\sigma}}$  for all scales  $\hat{\sigma} \geq \sigma$ . If  $\mathcal{G}_\sigma$  is well-behaved and satisfies the bounded moments condition, then  $\widehat{\mathcal{G}}_{\hat{\sigma}}$  is also well-behaved and satisfies the bounded moments condition. Furthermore,  $\widehat{\mathcal{G}}_{\hat{\sigma}}$  satisfies the low-skewness condition.

*Proof.* The loss function  $f$  and covariance function  $\Sigma$  are not changed after applying the SVAG operator, so  $\widehat{\mathcal{G}}_{\hat{\sigma}}$  is well-behaved.

Now we verify the bounded moments condition. Let  $\hat{z} = \frac{1}{\ell} (r_1(\ell)z_1 + r_2(\ell)z_2)$ , where  $z_1, z_2 \sim \mathcal{Z}_\sigma(\theta)$ . Then we have

$$\begin{aligned} \mathbb{E}[\|\hat{z}\|_2^{2m}]^{\frac{1}{2m}} &\leq \frac{1}{\ell} \left( |r_1(\ell)| \mathbb{E}[\|z_1\|_2^{2m}]^{\frac{1}{2m}} + |r_2(\ell)| \mathbb{E}[\|z_2\|_2^{2m}]^{\frac{1}{2m}} \right) \leq \frac{1}{\ell} (|r_1(\ell)| + |r_2(\ell)|) \cdot \mathbb{E}[\|z_1\|_2^{2m}]^{\frac{1}{2m}} \\ &\leq (1 + \sqrt{2}) \mathbb{E}[\|z_1\|_2^{2m}]^{\frac{1}{2m}}. \end{aligned}$$

By the bounded moments condition for  $\mathcal{G}_\sigma$ , there exists a constant  $C_{2m}$  such that  $\mathbb{E}_{z \sim \mathcal{Z}_\sigma(\theta)}[\|z\|_2^{2m}]^{\frac{1}{2m}} \leq C_{2m}(1 + \|\theta\|_2)$  for all  $\theta \in \mathbb{R}^d$ . So  $\mathbb{E}[\|\hat{z}\|_2^{2m}]^{\frac{1}{2m}} \leq (1 + \sqrt{2})C_{2m}(1 + \|\theta\|_2)$  for all  $\theta \in \mathbb{R}^d$ .

We now verify the low skewness condition by showing that third moment of  $\hat{z}$  is  $\mathcal{O}(1/\ell)$ . By the bounded moments condition with  $m = 2$  and Jensen's inequality,

$$|\mathbb{E}[z_1^{\otimes 3}]| \leq \mathbb{E}[\|z_1\|_2^3] \leq \mathbb{E}[\|z_1\|_2^4]^{3/4} \leq (C_4(1 + \|\theta\|_2))^{3/4}.$$

So  $|\mathbb{E}[z_1^{\otimes 3}]|$  is bounded by  $\tilde{K}_3(\theta) := (C_4(1 + \|\theta\|_2))^{3/4}$  of polynomial growth.

Let  $r = \sqrt{2\ell^2 - 1}$ . Then  $r_1(\ell) = \frac{1}{2}(1 + r)$ ,  $r_2(\ell) = \frac{1}{2}(1 - r)$ . Since the third moments of two independent random vectors are additive,

$$\begin{aligned} \mathbb{E}[\hat{z}^{\otimes 3}] &= \frac{1}{8\ell^3} \mathbb{E} \left[ ((1+r)z_1 + (1-r)z_2)^{\otimes 3} \right] \\ &= \frac{1}{8\ell^3} (\mathbb{E}[(1+r)^3 z_1^{\otimes 3}] + \mathbb{E}[(1-r)^3 z_2^{\otimes 3}]) \\ &= \frac{1}{8\ell^3} ((1+r)^3 + (1-r)^3) \mathbb{E}[z_1^{\otimes 3}] \\ &= \frac{1}{8\ell^3} (2 + 6r^2) \mathbb{E}[z_1^{\otimes 3}] \\ &= \frac{1}{8\ell^3} (12\ell^2 - 4) \mathbb{E}[z_1^{\otimes 3}] \leq \frac{1}{\ell} \tilde{K}_3(\theta), \end{aligned}$$

where the 4th equality is due to  $(1+r)^3 + (1-r)^3 = (1+3r+3r^2+r^3) + (1-3r+3r^2-r^3) = 2+6r^2$ . Therefore, the low skewness condition is verified.  $\square$

## F Miscellaneous Theoretical Arguments

### F.1 How does the noise scale change with batch size?

We discuss how the noise scale  $\sigma$  in the NGOS (Definition 2.3) changes when the batch size changes: in particular,  $\sigma \sim 1/\sqrt{B}$ . The argument follows from the linearity of covariance and is an already well-known result - we reproduce it here for clarity. We first fix a parameter vector  $\theta$ . Let  $\mathbf{g}^{(1)}, \dots, \mathbf{g}^{(B)}$  be the gradients evaluated at data points from a batch of size  $B$ , where  $\mathbf{g}^{(b)} = \nabla f(\theta) + z^{(b)}$ , and every  $z^{(b)}$  is a gradient noise vector drawn i.i.d. from a distribution with mean  $\mathbf{0}$  and covariance  $\Sigma(\theta)$ . For sampling with replacement on a finite dataset of size  $n$ , where  $f_1(\theta), \dots, f_n(\theta)$  are the loss functions for the  $n$  data points (and the average of these  $n$  functions is  $f(\theta)$ ), this covariance matrix can be explicitly written as:

$$\Sigma(\theta) = \frac{1}{n} \sum_{i=1}^n (\nabla f_i(\theta) - \nabla f(\theta)) (\nabla f_i(\theta) - \nabla f(\theta))^\top.$$

The average gradient over the batch is  $\mathbf{g} := \frac{1}{B} \sum_{b=1}^B \mathbf{g}^{(b)} = \nabla f(\theta) + \frac{1}{B} \sum_{b=1}^B z^{(b)}$ . As  $z^{(1)}, \dots, z^{(B)}$  are sampled i.i.d., their average  $\frac{1}{B} \sum_{b=1}^B z^{(b)}$  has mean  $\mathbf{0}$  and covariance  $\Sigma(\theta)$  by linearity of expectation and covariance. We can set  $\mathcal{Z}_\sigma(\theta)$  to be the distribution of the random variable  $\frac{1}{\sqrt{B}} \sum_{b=1}^B z_b$ , where  $\sigma = \frac{1}{\sqrt{B}}$ , then  $\mathbf{g}$  has the same distribution as the stochastic gradient produced by the NGOS  $\mathcal{G}_\sigma = (f, \Sigma, \mathcal{Z}_\sigma)$ .

## F.2 What happens when the noise does not dominate the gradient?

We discuss the linear warm-up setting described in Section 4.1. Recall that when ignoring the effect of  $\epsilon$ , the RMSprop update can be written as

$$\theta_{k+1} \approx \theta_k - \eta \mathbf{g}_k \odot (\bar{\mathbf{g}}^2 + \sigma^2 \mathbf{1})^{-1/2}.$$

From the above equation, it is clear that the dynamics of  $\theta$  depends on the relationship between the noise scale  $\sigma$  and the gradient  $\|\bar{\mathbf{g}}\|$ . In Section 4.1, we discuss the case where  $\sigma \gg \|\bar{\mathbf{g}}\|$ , which is the regime where the SDE approximation can exist.

Here, we argue that when  $\sigma \ll \|\bar{\mathbf{g}}\|$ , no SDE approximation can exist for the discrete trajectory. In this case, the RMSprop update would instead be  $\theta_{k+1} \approx \theta_k - \eta \mathbf{U}^{-1} \mathbf{g}_k$ , where  $\mathbf{U} = \text{diag}(\sqrt{\bar{\mathbf{g}}^2})$ . Combining this with  $\mathbf{g}_k \sim \mathcal{N}(\bar{\mathbf{g}}, \sigma \mathbf{I})$  yields that  $\theta_{k+1} - \theta_k \sim \mathcal{N}(\eta \mathbf{U}^{-1} \bar{\mathbf{g}}, \eta^2 \sigma^2 \mathbf{U}^{-2})$  approximately. We can again take a telescoping sum to obtain the marginal distribution of  $\theta_k$ :  $\theta_k \sim \mathcal{N}(k\eta \mathbf{U}^{-1} \bar{\mathbf{g}}, k\eta^2 \sigma^2 \mathbf{U}^{-2})$  approximately.

However, it is impossible to make the above distribution fixed even as  $\sigma$  changes, so no SDE approximation exists. In particular, we need to make both  $k\eta$  and  $k\eta^2 \sigma^2$  fixed, so  $\eta\sigma$  must be a constant. If  $\sigma \ll \|\bar{\mathbf{g}}\|$ , then  $\frac{1}{\eta} \ll \|\bar{\mathbf{g}}\|$  too. This requirement on  $\eta$  implies that no SDE approximation exists when  $\sigma \ll \|\bar{\mathbf{g}}\|$ , and hence motivates us to study the case of  $\sigma \gg \|\bar{\mathbf{g}}\|$ .

## G Experimental Verification of Assumptions

In this section, we take measurements and perform experiments to verify that the various assumptions made in our theory do not harm the applicability of our findings to realistic settings.

### G.1 Noise Dominates the Gradient

Our analysis in Section 4.1 suggests that an SDE approximation cannot exist when the the gradient  $\bar{\mathbf{g}}$  dominates the noise scale  $\sigma$ . Note that Section 4.1 performs a rough analysis under the assumption of a linear loss function (i.e., fixed gradient throughout training), which is far from practice. In the more general setting, we require that for every step  $k$ ,  $\mathbb{E}\|z_k\|^2$  (i.e., the gradient variance) dominates  $\|\mathbb{E}\mathbf{g}_k\|$  (i.e., the norm of the average gradient), where the expectations are taken over sampling seeds, in order for the SDE approximation to exist. Figure 4 shows that our assumption holds for small batches and for large batches near the end of training.

### G.2 Using $v_k$ instead of $v_{k+1}$ in the update rule

In Definitions 2.1 and 2.2, we slightly modify the standard implementation of RMSprop and Adam by using  $v_k$  in the update rule instead of  $v_{k+1}$ . Here, we verify for Adam that this modification of the optimization algorithms does not significantly harm performance. Figure 6 shows the behavior of ResNet-50 and VGG-16 trained with Adam on CIFAR-10 with the above modification of the optimization algorithm. We observe a small drop ( $\approx 1\%$ ) in test accuracies. However, the behavior of the trajectories across different batch sizes for the proposed scaling rule stays the same, i.e. we observe a maximum of 3% test accuracy gap between training batch size 256 and 8192. Moreover, the behavior of the test functions match across the trajectories of different batch sizes.

## H SVAG Experiments

Recall that the SVAG algorithm (Definition 6.2) is a computationally efficient simulation of the SDEs corresponding to RMSprop and Adam. The SVAG algorithm requires a hyperparameter  $\ell$ , and the resulting parameters after  $k\ell^2$  steps should match the parameters on the corresponding discrete optimization trajectory after  $k$  steps. In particular, Theorem 6.3 shows that the SVAG algorithm is an order-1 weak approximation (Definition 2.4) of the SDE, and the approximation error scales as  $1/\ell$ . One may be initially concerned that realistic deep learning settings require  $1/\ell$  to be very small, which would make  $\ell$  large and hence computationally intractable. [11] showed that the SVAG trajectories appear to converge to the SDE trajectory for computationally tractable small values of  $\ell$ . We similarly find that our proposed SVAG-like algorithms in Definition 6.2 appear to converge for small  $\ell$  in various settings.

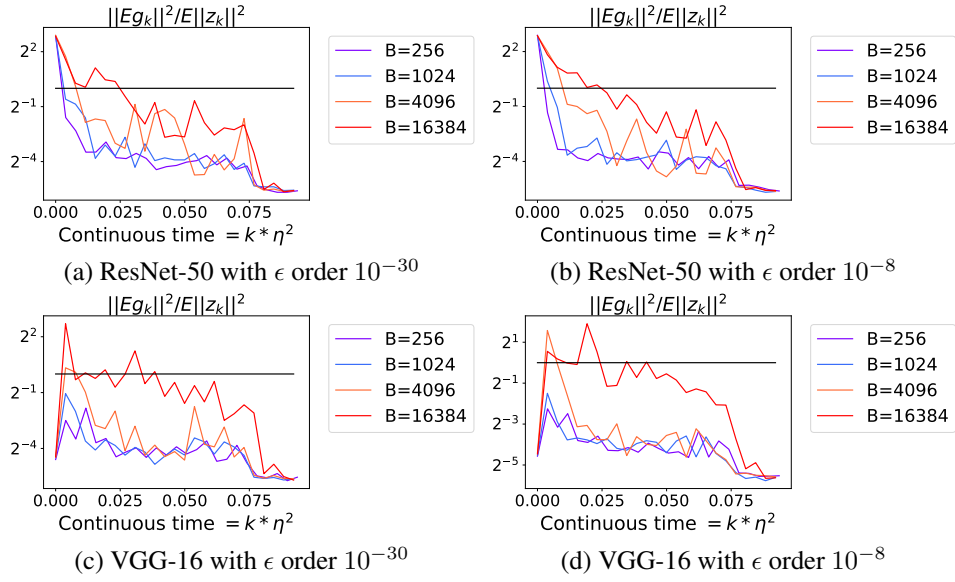


Figure 4: We compare the norm of the average gradient with the noise scale for different batch sizes during training of ResNet-50 and VGG-16 model with RMSprop on the CIFAR-10 dataset. Here,  $(\eta, \beta) = (10^{-3}, 0.999)$  for batch size 256 and scaled with our proposed square root scaling rule (Definition 5.1) for the other batch sizes. We show the results for  $\epsilon$  at both small (of order  $10^{-30}$ ) and large scale (of order  $10^{-8}$ ). We observe that for small batches, the noise in the gradient dominates the signal in the gradient, supporting our hypothesis. For larger batches, the hypothesis seems to hold true towards the end of training.

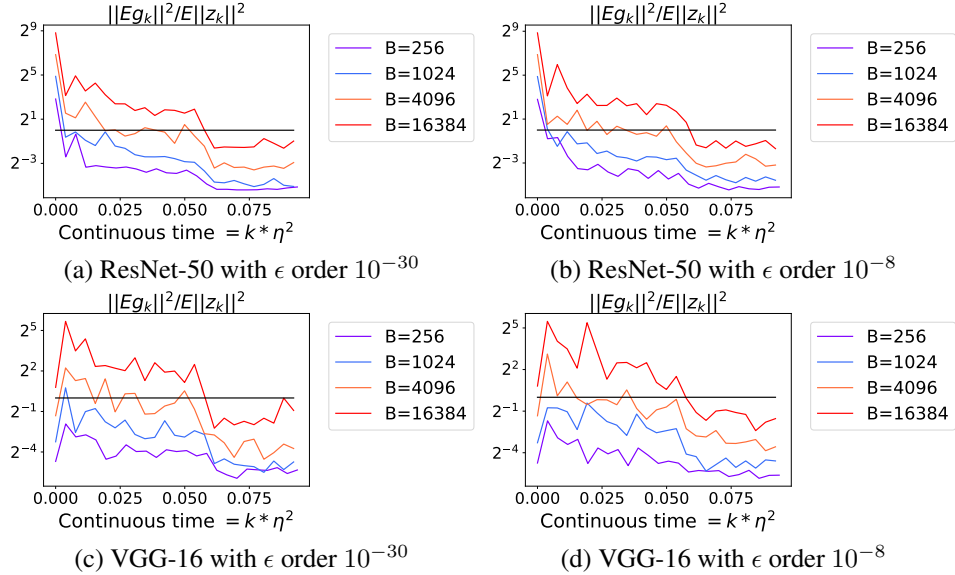
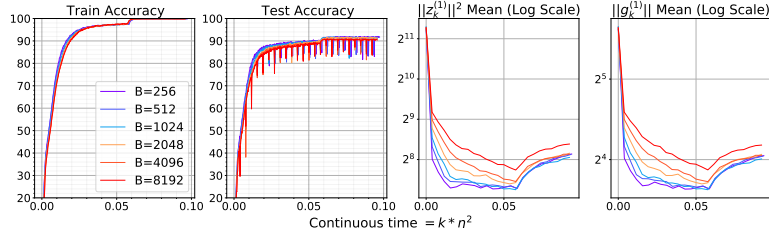
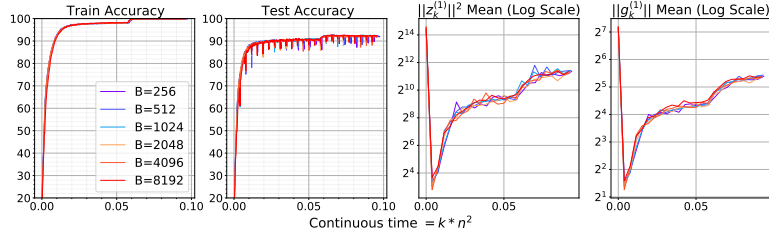


Figure 5: We compare the norm of the average gradient with the noise scale for different batch sizes during training of ResNet-50 model with Adam on the CIFAR-10 dataset. Here,  $(\eta, \beta_1, \beta_2) = (10^{-3}, 0.999, 0.999)$  for batch size 256 and scaled with our proposed square root scaling rule (Definition 5.1) for the other batch sizes. We show the results for  $\epsilon$  at both small (of order  $10^{-30}$ ) and large scale (of order  $10^{-8}$ ). We observe that for small batches, the noise in the gradient dominates the signal in the gradient, supporting our hypothesis. For larger batches, the hypothesis seems to hold true towards the end of training.



(a) ResNet-50



(b) VGG-16

Figure 6: We repeat the Square Root Scaling experiments with Adam for ResNet-50 and VGG-16 on CIFAR-10 dataset, where we slightly modify the standard implementation of Adam by using  $\mathbf{v}_k$  in the update rule instead of  $\mathbf{v}_{k+1}$ . For batch size 256,  $(\eta, \epsilon, \beta_1, \beta_2) = (10^{-3}, 10^{-8}, 0.999, 0.999)$  and the hyperparameters are scaled according to the square root scaling rule for other batch sizes. We observe a small drop ( $\approx 1\%$ ) in test accuracies. However, the behavior of the trajectories across different batch sizes stays the same.

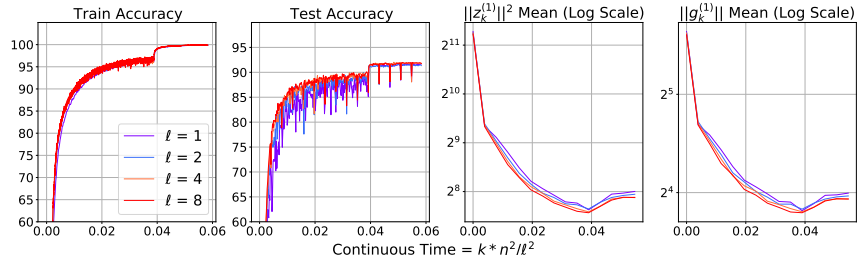


Figure 7: SVAG experiments on ResNet-50 trained on CIFAR-10 with RMSprop. We use batch size 256 and the hyperparameters  $\eta = 10^{-3}$ ,  $\beta = 0.999$ ,  $\epsilon = 10^{-30}$  and a weight decay of  $10^{-4}$ . Since SVAG takes  $\ell$  smaller steps to simulate the continuous dynamics in  $\eta$  time, we plot accuracy against continuous time defined as  $k \times \eta^2 / \ell^2$ .

**CIFAR-10.** Figures 7 and 8 show that SVAG converges and closely tracks RMSprop at smaller  $\epsilon (=10^{-30})$ , and at larger  $\epsilon (=10^{-8})$  respectively. Figures 3 and 9 show that SVAG converges and closely tracks Adam at smaller  $\epsilon (=10^{-30})$ , and at larger  $\epsilon (=10^{-8})$  respectively. All experiments follow the setting in Appendix J.1 for batch size 256.

**Wikipedia + Books (Academic BERT).** Figure 10 shows that SVAG converges and closely tracks Adam. We use the experimental setting for batch size 1024 in Appendix J.3 except the hyperparameters  $\beta_1$  and  $\beta_2$  are fixed at 0.9 and 0.98 respectively.

**WikiText-103 (GPT).** Figure 23 shows that SVAG converges and closely tracks Adam. We use the experimental setting for batch size 1024 in Appendix J.3 except the hyperparameters  $\beta_1$  and  $\beta_2$  are fixed at 0.9 and 0.98 respectively. Additionally, for computational reasons, we pretrain on sequences of length 64.

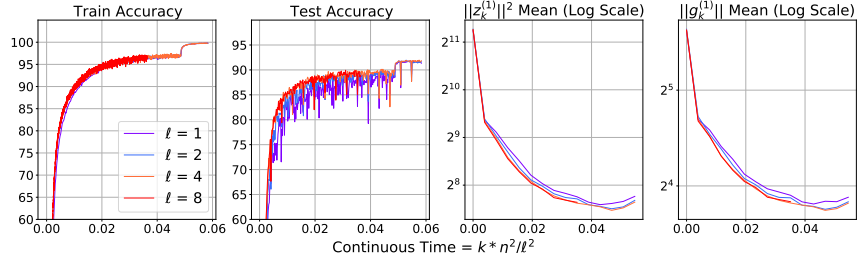


Figure 8: SVAG experiments on ResNet-50 trained on CIFAR-10 with RMSprop. We use batch size 256 and the hyperparameters  $\eta = 10^{-3}$ ,  $\beta = 0.999$ ,  $\epsilon = 10^{-8}$ , and a weight decay of  $10^{-4}$ . Since SVAG takes  $\ell$  smaller steps to simulate the continuous dynamics in  $\eta$  time, we plot accuracy against continuous time defined as  $k \times \eta^2 / \ell^2$ .

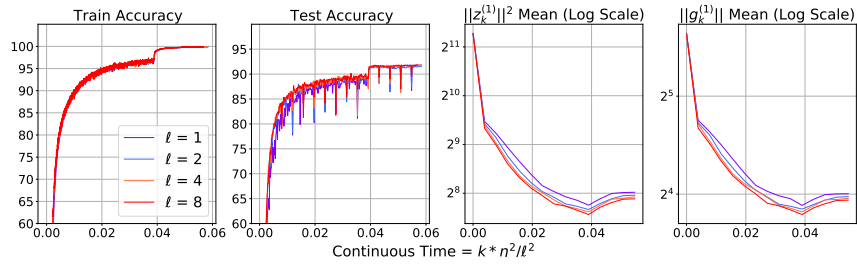


Figure 9: SVAG experiments on ResNet-50 trained on CIFAR-10 with Adam. We use batch size 256 and the hyperparameters  $\eta = 10^{-3}$ ,  $\beta_1 = 0.9$ ,  $\beta_2 = 0.999$ ,  $\epsilon = 10^{-8}$ , and a weight decay of  $10^{-4}$ . Since SVAG takes  $\ell$  smaller steps to simulate the continuous dynamics in  $\eta$  time, we plot accuracy against continuous time defined as  $k \times \eta^2 / \ell^2$ .

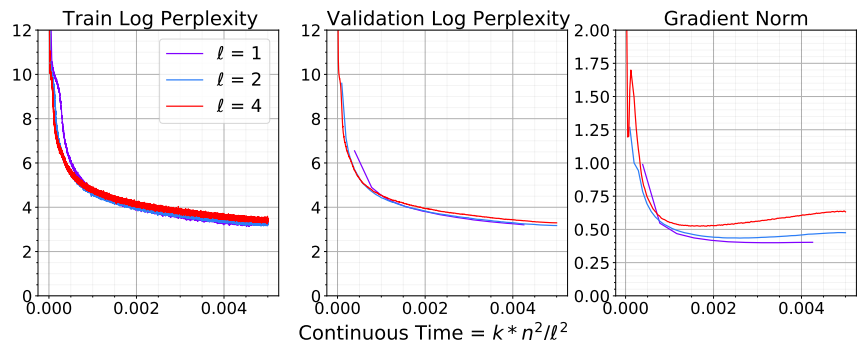


Figure 10: SVAG experiments on RoBERTa pretrained on Bookcorpus + Wikipedia dataset with Adam. We use batch size 1024 and the hyperparameters  $\eta = 10^{-3}$ ,  $\beta_1 = 0.9$ ,  $\beta_2 = 0.98$ ,  $\epsilon = 2 \times 10^{-6}$ . Since SVAG takes  $\ell$  smaller steps to simulate the continuous dynamics in  $\eta$  time, we plot accuracy against continuous time defined as  $k \times \eta^2 / \ell^2$ .

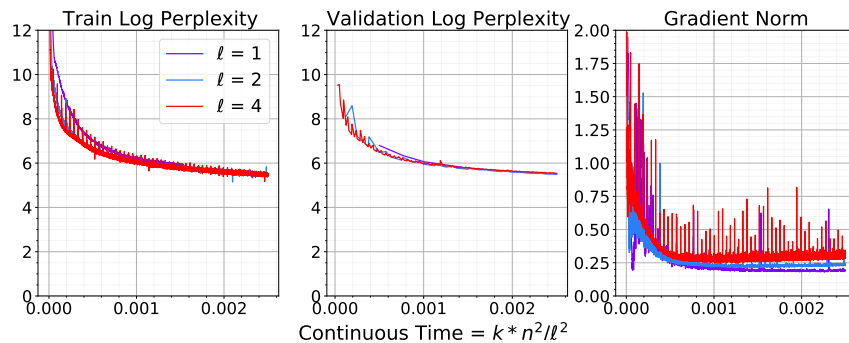


Figure 11: SVAG experiments on GPT pretrained on WikiText-103 with Adam. We use batch size 1024 and the hyperparameters  $\eta = 10^{-3}$ ,  $\beta_1 = 0.9$ ,  $\beta_2 = 0.98$ ,  $\epsilon = 2 \times 10^{-8}$ . Since SVAG takes  $\ell$  smaller steps to simulate the continuous dynamics in  $\eta$  time, we plot accuracy against continuous time defined as  $k \times \eta^2 / \ell^2$ . For computational constraints, we train on sequences of length 64.

## I Square Root Scaling Experiments

We experimentally evaluate the scaling rules proposed in Definitions 5.1 and 5.2 by training models with different batch sizes and modifying the optimization hyperparameters accordingly. The number of gradient steps were modified to keep the total amount of continuous time same across all the batches. The warmup schedule and the learning rate decay schedule were kept the same. See Appendix J for details about the baseline runs for each dataset.

We perform two types of ablation studies. In Appendix I.1, we compare our proposed scaling rule to variants that only scale some subset of the optimization hyperparameters. We find that our proposed scaling rule is the best at preserving the validation accuracy and the other test functions across different batch sizes. In Appendix I.2, we compare the proposed square root scaling rule to a linear one and find that they perform comparably on CIFAR-10, though the square root scaling significantly outperforms linear scaling on the ImageNet dataset. We hypothesize that for simpler datasets, like CIFAR-10, the differences between the two scaling rules is not reflected clearly in the validation accuracies because the task is too easy to learn.

**CIFAR-10.** Figures 12 and 14 show the performance of VGG-16 when trained with different batch sizes with RMSprop at smaller  $\epsilon (=10^{-30})$ , and at larger  $\epsilon (=10^{-8})$  respectively. Figures 13 and 15 show the performance of VGG-16 when trained with different batch sizes with Adam at smaller  $\epsilon (=10^{-30})$ , and at larger  $\epsilon (=10^{-8})$  respectively. For the corresponding experiments on ResNet-50, please refer to Figures 16 to 19. For the details on the experimental setting, please refer to Appendix J.1.

We observe that in all settings the test accuracies vary by at most 3% across batch sizes when using the proposed square root scaling rule. Moreover, the test functions stay close across multiple batch sizes, signifying that the trajectories stay close across the batch sizes using the Square root scaling rule.

**ImageNet.** Figures 20 and 21 show the performance of ResNet-50 when trained with different batch sizes with RMSprop at smaller  $\epsilon (=10^{-30})$ , and at larger  $\epsilon (=10^{-8})$  respectively. For the details on the experimental setting, please refer to Appendix J.2.

We observe that on the validation set, the loss and accuracy behavior for the model is very similar, when trained with different batch sizes. Moreover, the difference between the validation accuracies is at most 3% between the batch sizes 256, 1024, 4096, and 16384 for smaller  $\epsilon$ . The difference between the validation accuracies is at most 1.5% between the batch sizes 256, 1024, 4096, 16384, and 32768 for larger  $\epsilon$ .

**Wikipedia + Books (Academic BERT).** Figure 22 shows the performance of a RoBERTa model when pretrained with different batch sizes with ADAM. The scaling rule is applied to modify the



peak values of the optimization hyperparameters. We also evaluate the pretrained models on several downstream tasks, and show the results in Table 1. For the details on the setting for both pretraining and downstream experiments, please refer to Appendix J.3.

We observe that the log perplexity on the training and validation datasets matches across different batch sizes throughout pretraining. Moreover, we also observe that the gradient norms across different batch sizes remain close throughout the pretraining. Furthermore, the models pretrained across different batch sizes can achieve very similar performance in the downstream tasks.

**WikiText-103 (Academic GPT).** Figure 23 shows the log perplexity behavior of GPT on training and validation datasets, across different batch sizes of pretraining. We observe that the log perplexity matches across different batch sizes. Moreover, we also observe that the gradient norms across different batch sizes remain close throughout the training.

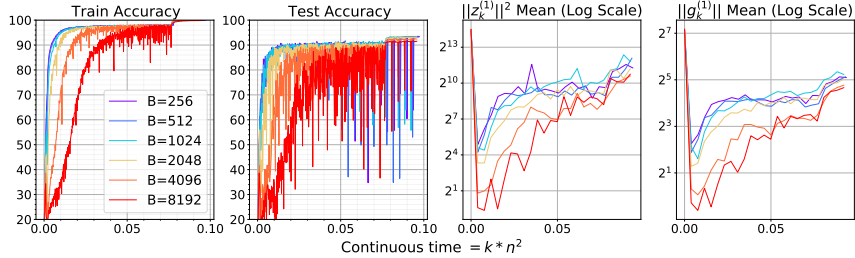


Figure 12: VGG-16 trained on CIFAR-10 using RMSprop are close for different batch sizes when the optimization hyperparameters are varied according to the proposed scaling rule for RMSprop (Definition 5.2). We use a baseline setting of  $\eta = 10^{-3}$ ,  $\epsilon = 10^{-8}$ , and  $(\beta_1, \beta_2) = (0.0, 0.999)$  for batch size 256. We use a weight decay factor of  $10^{-4}$ . We observe a gap of at most 3% among the different batch sizes under consideration.

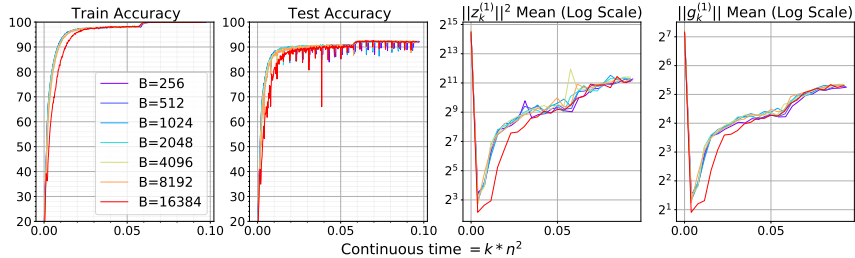


Figure 13: VGG-16 trained on CIFAR-10 using Adam are close for different batch sizes when the optimization hyperparameters are varied according to the proposed scaling rule for Adam (Definition 5.2). We use a baseline setting of  $\eta = 10^{-3}$ ,  $\epsilon = 10^{-8}$ , and  $(\beta_1, \beta_2) = (0.999, 0.999)$  for batch size 256. We use a weight decay factor of  $10^{-4}$ . We observe a gap of at most 3% among the different batch sizes under consideration.

### I.1 Ablation study on the proposed scaling rule

**CIFAR-10.** We conduct an ablation study on whether all the parameters  $\eta, \epsilon, \beta_1, \beta_2$  need to be scaled in our proposed scaling rule. To do so, we compare the performance of a ResNet-50 model trained with batch size 256 and hyperparameters ( $\epsilon = 10^{-8}, \beta_1 = 0.999, \beta_2 = 0.999$ ) with the performance at a larger batch size, across 5 runs representing 5 different scaling rules: (a) Scale  $\eta$ , keeping others fixed, (b) Scale  $\eta, \epsilon$ , keeping others fixed, (c) Scale  $\eta, \epsilon, \beta_1$ , keeping others fixed, (d) Scale  $\eta, \epsilon, \beta_2$ , keeping others fixed, and (e) Scale  $\eta, \epsilon, \beta_1, \beta_2$ . Please check the behaviors of the different scaling rules at batch size 2048, 4096, 8192 and 16384 in Appendix I.2. We found that (e) consistently beats others in terms of the test functions and the validation accuracies at all batch sizes. The closest scaling rule (c) involved scaling only  $\eta, \epsilon$ , and  $\beta_1$  while keeping  $\beta_2$  fixed.

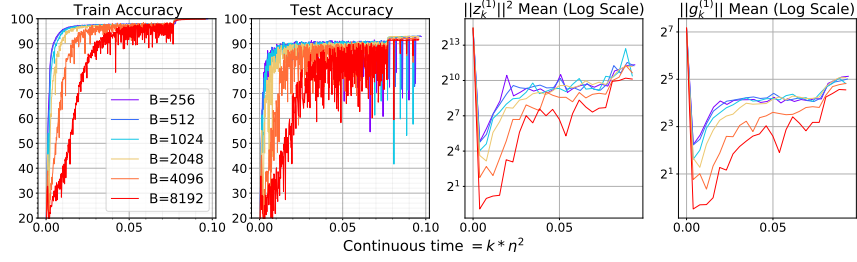


Figure 14: VGG-16 trained on CIFAR-10 using RMSprop are close for different batch sizes when the optimization hyperparameters are varied according to the proposed scaling rule for RMSprop (Definition 5.2). We use a baseline setting of  $\eta = 10^{-3}$ ,  $\epsilon = 10^{-30}$ , and  $(\beta_1, \beta_2) = (0.0, 0.999)$  for batch size 256. We use a weight decay factor of  $10^{-4}$ . We observe a gap of at most 3% among the different batch sizes under consideration.

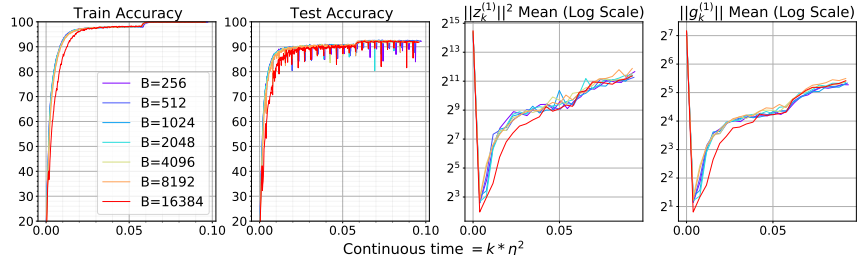


Figure 15: VGG-16 trained on CIFAR-10 using Adam are close for different batch sizes when the optimization hyperparameters are varied according to the proposed scaling rule for Adam (Definition 5.2). We use a baseline setting of  $\eta = 10^{-3}$ ,  $\epsilon = 10^{-30}$ , and  $(\beta_1, \beta_2) = (0.999, 0.999)$  for batch size 256. We use a weight decay factor of  $10^{-4}$ . We observe a gap of at most 3% among the different batch sizes under consideration.

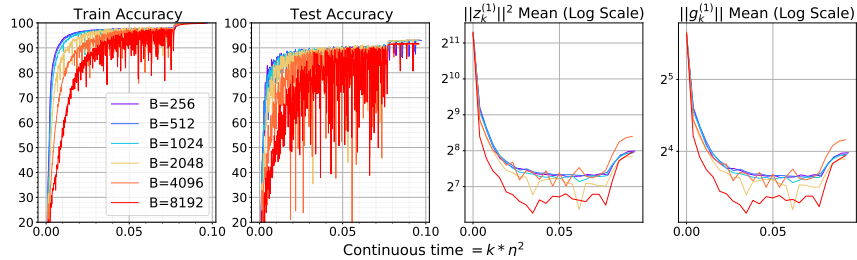


Figure 16: ResNet-50 trained on CIFAR-10 using RMSprop are close for different batch sizes when the optimization hyperparameters are varied according to the proposed scaling rule for RMSprop (Definition 5.2). We use a baseline setting of  $\eta = 10^{-3}$ ,  $\epsilon = 10^{-8}$ , and  $(\beta_1, \beta_2) = (0.0, 0.999)$  for batch size 256.  $\epsilon = 10^{-30} \approx 0$  for all experiments. We use a weight decay factor of  $10^{-4}$ . We observe a gap of at most 3% among the different batch sizes under consideration.

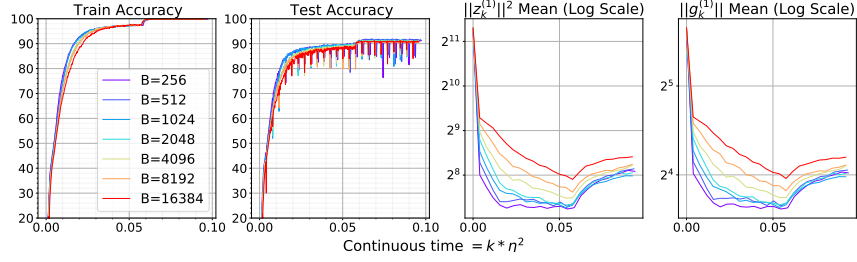


Figure 17: ResNet-50 trained on CIFAR-10 using Adam are close for different batch sizes when the optimization hyperparameters are varied according to the proposed scaling rule for Adam (Definition 5.2). We use a baseline setting of  $\eta = 10^{-3}$  and  $(\beta_1, \beta_2) = (0.999, 0.999)$  for batch size 256.  $\epsilon = 10^{-30} \approx 0$  for all experiments. We use a weight decay factor of  $10^{-4}$ . We observe a gap of at most 3% among the different batch sizes under consideration.

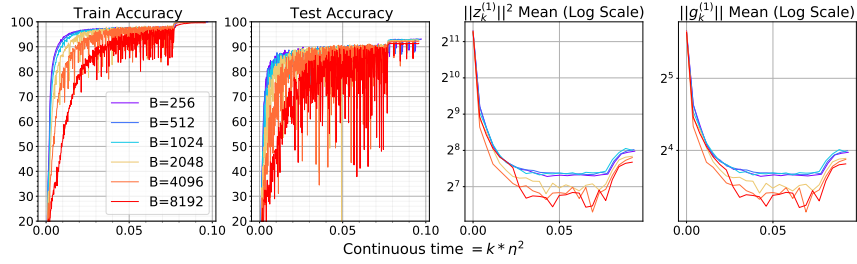


Figure 18: ResNet-50 trained on CIFAR-10 using RMSprop are close for different batch sizes when the optimization hyperparameters are varied according to the proposed scaling rule for RMSprop (Definition 5.2). We use a baseline setting of  $\eta = 10^{-3}$ ,  $\epsilon = 10^{-8}$ , and  $(\beta_1, \beta_2) = (0.0, 0.999)$  for batch size 256. We use a weight decay factor of  $10^{-4}$ . We observe a gap of at most 3% among the different batch sizes under consideration.

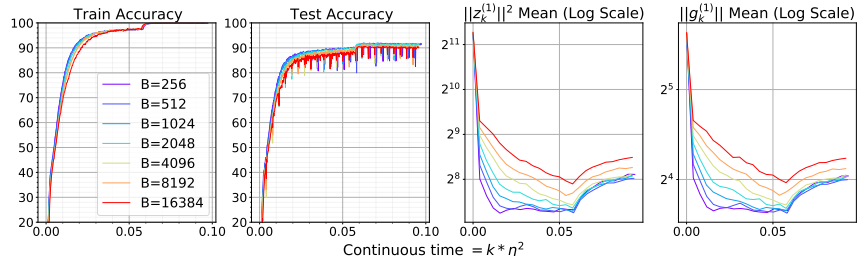


Figure 19: ResNet-50 trained on CIFAR-10 using Adam are close for different batch sizes when the optimization hyperparameters are varied according to the proposed scaling rule for Adam (Definition 5.2). We use a baseline setting of  $\eta = 10^{-3}$ ,  $\epsilon = 10^{-8}$ , and  $(\beta_1, \beta_2) = (0.999, 0.999)$  for batch size 256. We use a weight decay factor of  $10^{-4}$ . We observe a gap of at most 3% among the different batch sizes under consideration.

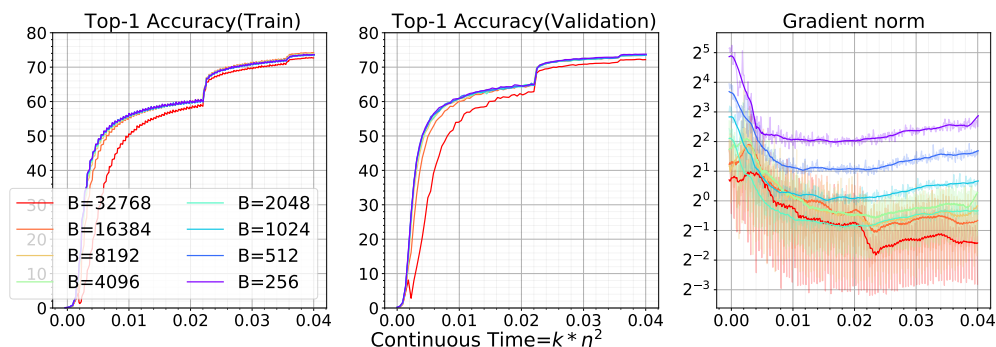


Figure 20: ResNet-50 trained on ImageNet using Adam are close for different batch sizes when the optimization hyperparameters are varied according to the proposed scaling rule for Adam (Definition 5.2). We use a baseline setting of  $\eta = 3 \times 10^{-4}$ ,  $\epsilon = 10^{-8}$ , and  $(\beta_1, \beta_2) = (0.999, 0.999)$  for batch size 256. We use a weight decay factor of  $10^{-4}$ . We achieve around 74% validation accuracy with batch size 256 and the accuracy drops by at most 1.5% at batch size 32768.

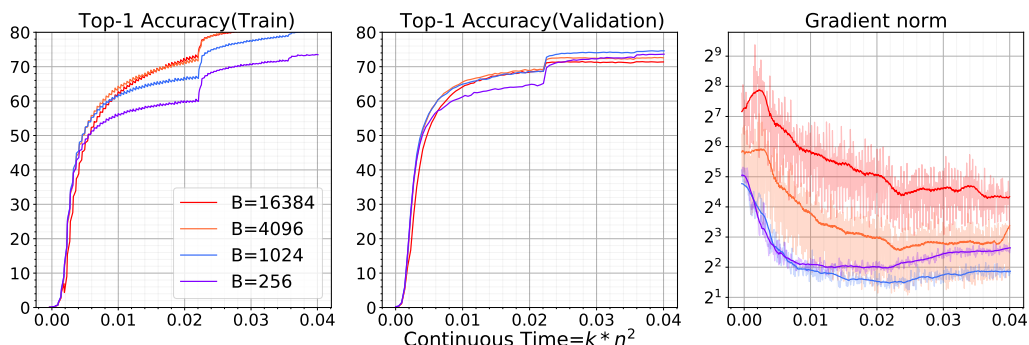


Figure 21: ResNet-50 trained on ImageNet using Adam are close for different batch sizes when the optimization hyperparameters are varied according to the proposed scaling rule for Adam (Definition 5.2). We use a baseline setting of  $\eta = 3 \times 10^{-4}$  and  $(\beta_1, \beta_2) = (0.999, 0.999)$  for batch size 256.  $\epsilon = 10^{-30} \approx 0$  for all experiments. We use a weight decay factor of  $10^{-4}$ . We achieve around 74% validation accuracy with batch size 1024 and the accuracy drops by at most 3% at batch size 16384.

Pretrain batch size $B$	CoLA	SST-2	MRPC	STS-B	QQP	MNLI	QNLI	RTE
1024	0.585	0.92	0.73	0.866	0.873	0.836	0.906	0.682
2048	0.563	0.928	0.803	0.869	0.875	0.826	0.897	0.653
4096	0.581	0.921	0.778	0.869	0.875	0.839	0.892	0.675
8192	0.626	0.929	0.778	0.884	0.877	-	0.9	0.675

Table 1: Performance of the pretrained RoBERTa models when finetuned on different downstream tasks in GLUE [40]. F1 scores are reported for QQP and MRPC, Spearman correlations are reported for STS-B, Matthews correlations for CoLA, and accuracy scores are reported for the other tasks. Here,  $B$  denotes the batch size used for pretraining. We run an extensive grid search (Table 4) to find the best performance of each pretrained model on each of the downstream tasks.

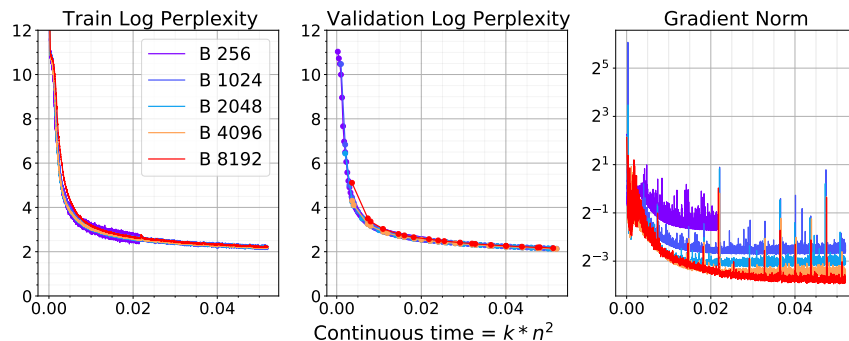


Figure 22: The train and validation log perplexities of RoBERTa-large trained on the Wiki+Books corpus using Adam (for 48 hours) are close for moderate batch sizes using the Square Root Scaling Rule on Adam.  $\eta = 10^{-3}$  and  $(\beta_1, \beta_2) = (0.99375, 0.996)$  for batch size 1024,  $\epsilon = 2 \times 10^{-6}$  for batch size 1024 and scaled likewise for other batch sizes. We achieve a validation log perplexity of  $2.1 \pm 0.1$  for batch size 1024, 2048, 4096 and 8192. Training with batch size 256 is computationally inefficient, but follows the same behavior during its 48-hour trajectory.

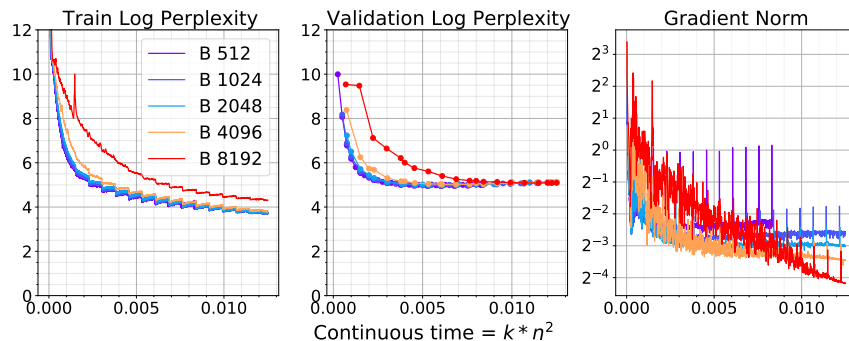


Figure 23: The train and validation perplexities of 12 layer GPT trained on the Wikitext corpus using Adam (for 48 hours) are close for moderate batch sizes Square Root Scaling Rule on Adam on RoBERTa-large.  $\eta = 10^{-3}$  and  $(\beta_1, \beta_2) = (0.9875, 0.996)$  for batch size 1024,  $\epsilon = 2 \times 10^{-8}$  for batch size 1024 and scaled likewise for other batch sizes. We achieve a validation log perplexity of  $5 \pm 0.1$  for all the batch sizes under consideration. Moreover, we observe an alignment in the behavior of the trajectories across the different batch sizes (except 8192 in the first half of the training).

## I.2 Ablation against linear scaling rules

**CIFAR-10.** We compared the proposed scaling rule against possible linear scaling rules, that scale the hyperparameters linearly with the increase in training batch size. We focused on ResNet-50 training with Adam. The linear scaling rules that we tried were: (a) Scale  $\eta$  linearly, keeping  $\beta_1, \beta_2, \epsilon$  fixed, (b) Scale  $\eta, 1 - \beta_1$  linearly, keeping  $\beta_2, \epsilon$  fixed, (c) Scale  $\eta, 1 - \beta_2$  linearly, keeping  $\beta_1, \epsilon$  fixed, and (d) Scale  $\eta, 1 - \beta_1, 1 - \beta_2$  linearly, keeping  $\epsilon$  fixed. Fig. 25 shows the behavior of these scaling rules at batch size 8192 and 16384, at different values of  $\epsilon$ .

The linear scaling rule in (d) seems to perform as well as the proposed Square Root scaling rule (Definition 5.2) in terms of validation accuracies. However, with a closer look on the train accuracy plots, we observe that the Square Root scaling rule tracks the smaller batch training trajectory better than the linear scaling rule. The linear scaling rules seem to catch up, only after the learning rate is decayed. Our hypothesis is that the CIFAR-10 dataset is simple enough for different scaling rules to work well.

**ImageNet.** We conduct ablation experiments on ResNet-50, trained with Adam on ImageNet, where we follow a linear scaling rule to scale the hyperparameters across batch sizes. Due to computational issues, we didn’t conduct extensive experiments, as was done for CIFAR-10. The linear scaling rule for Adam is as follows: the hyperparameters  $\eta$ ,  $1 - \beta_1$  and  $1 - \beta_2$  are scaled by  $\kappa$ , when the batch size is scaled by  $\kappa$ , and  $\epsilon$  isn’t scaled. As was noted earlier, the definition of continuous time will change to  $\eta \times \#\{\text{gradient steps}\}$ . We keep the number of training epochs equal to 90 as before, follow the same learning rate schedule, and show the performance of the models in Figure 26. We observe that scaling the hyperparameters to larger batch training with the proposed LSR results in a big drop in validation accuracies.

## J Experiment Configuration Details

### J.1 CIFAR-10

There are 50000 images in the training set and 10000 images in the validation set of CIFAR-10 [22].

**Architecture.** We used the architecture of ResNet-56 from [41] without modification. We used the same architecture of VGG-16 with batch normalization from [21]. However, we kept the final layer of the architecture fixed throughout training, to make the model 1-homogenous and avoid the optimization difficulties of 2-homogenous networks ([42]).

**RMSprop.** To fix a baseline to compare against, we first trained the models with batches of size 256, sampled with replacement, at peak learning rate  $\eta = 10^{-3}$  and  $\beta = 0.999$ . The model was trained for  $500 \times \lfloor (50000/256) \rfloor = 97500$  gradient steps (or 500 epochs). We followed an initial warmup for the first 2% of the total gradient steps. The learning rate schedule during the warmup phase is given by  $\eta \times 10^{-3} \times (10^3)^{\#\text{epochs}/10}$ . We also followed a learning rate decay schedule, the learning rate was decayed by 0.1 when the model reaches 80% (400 epoch) and 90% (450 epoch) of the total continuous time respectively. We did experiments at two values of  $\epsilon$ , small ( $= 1e - 30$ ) and large ( $= 1e - 8$ ).

We then made multiple runs of the same model with batches of varying sizes in  $\{1024, 4096, 16384\}$ , with the hyperparameters  $\eta$ ,  $\epsilon$  and  $\beta$  modified appropriately according to the scaling rule. The number of gradient steps were modified to keep the total amount of continuous time same across all the batches (which amounted to 500 epochs by the equivalence between continuous time and the number of training epochs). The warmup schedule and the learning rate decay schedule were kept the same.

**Adam.** We first trained the models with batches of size 256, sampled with replacement, at peak learning rate  $\eta = 10^{-3}$  and  $(\beta_1, \beta_2) = (0.999, 0.999)$ . The total continuous time of training (or number of epochs), the amount of continuous time in the warmup phase, and the learning rate schedule in the warmup phase were same as RMSprop. The only difference was the learning rate schedule after the warmup phase, the learning rate was decayed by 0.1 when the model reaches 60% of the total continuous time (or 300 epochs).

We then made multiple runs of the same model with batches of varying sizes in  $\{1024, 4096, 16384\}$ , with the hyperparameters  $\eta$ ,  $\epsilon$  and  $\beta_1, \beta_2$  modified appropriately according to the scaling rule. The number of gradient steps were modified to keep the total amount of continuous time same across all the batches. The warmup schedule and the learning rate decay schedule were kept the same.

### J.2 ImageNet

There are 1281167 images in the training set and 50000 images in the validation set of ImageNet [27].

**Architecture.** We trained a ResNet-50 [41] model without modification.

**Adam.** To fix a baseline to compare against, we first trained the models with batches of size 256, sampled with replacement, at learning rate  $\eta = 3 \times 10^{-4}$  and  $\beta = 0.999$ . The model was trained for a total of  $90 \times \lfloor (1281167/256) \rfloor = 450360$  gradient steps (or 90 epochs). We followed an initial warmup for the first  $\frac{1}{18}$  fraction of the total continuous time (or the first 5 epochs). The learning rate

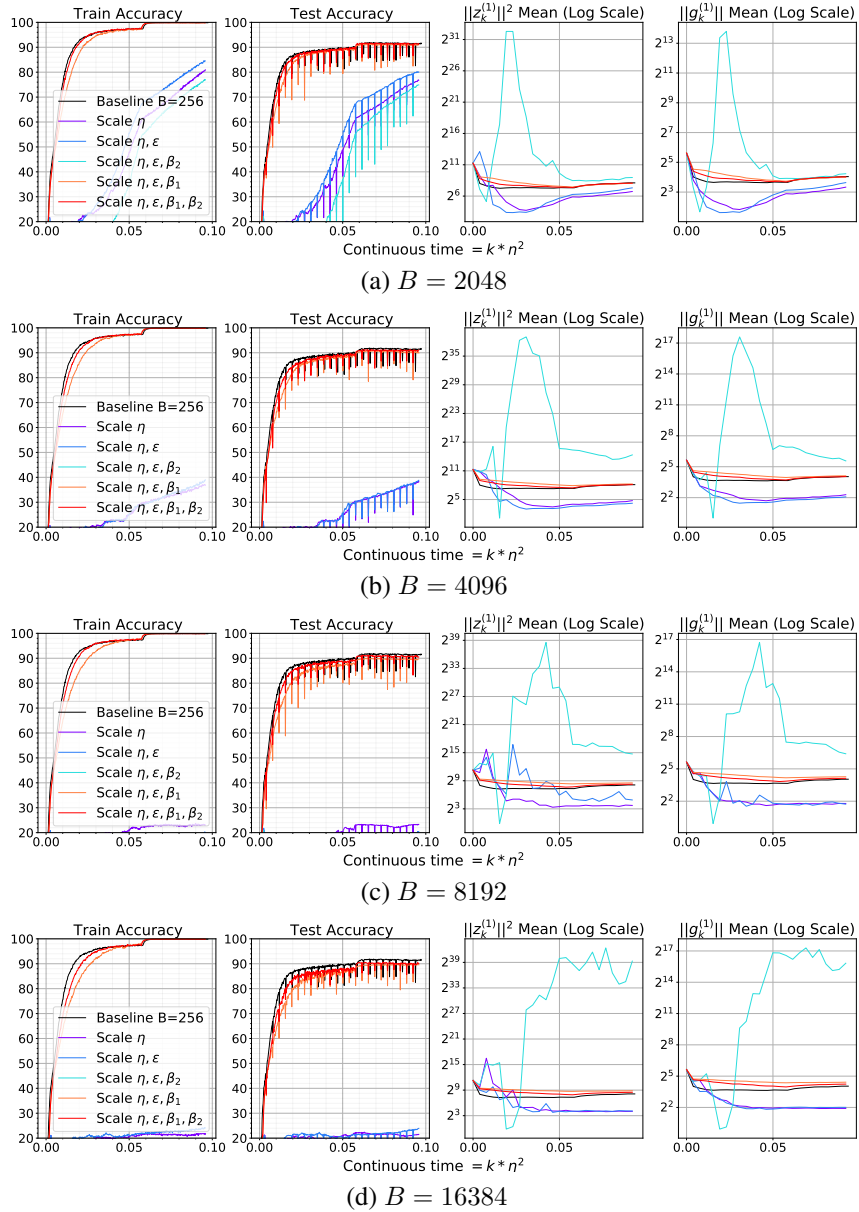
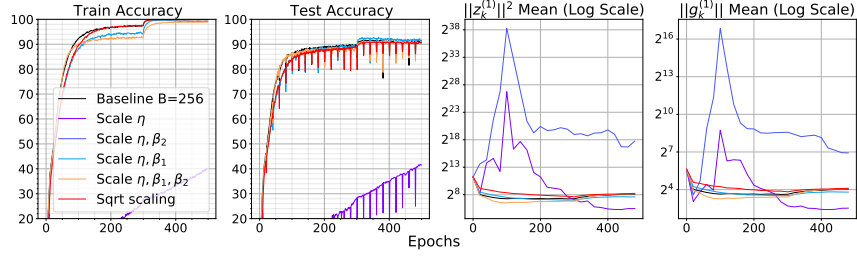
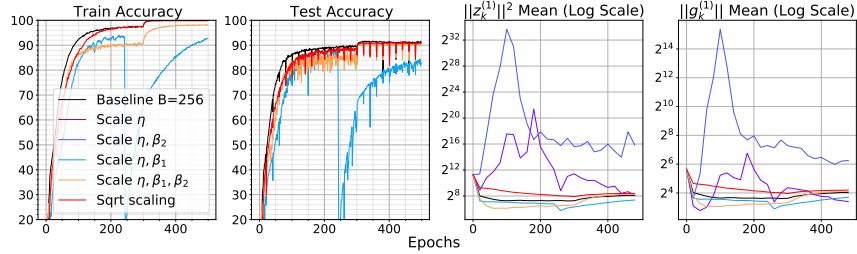


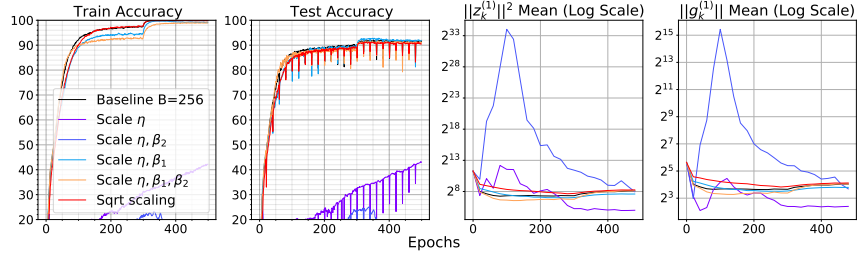
Figure 24: Ablation study for the square root scaling rule on Resnet-50 trained with Adam on CIFAR-10. We compare the performance of a model trained with batch size 256 and hyperparameters ( $\epsilon = 10^{-8}$ ,  $\beta_1 = 0.999$ ,  $\beta_2 = 0.999$ ) with the performance at a larger batch size, across 5 runs representing 5 variations of the square root scaling rule: (a) Scale  $\eta$ , keeping others fixed, (b) Scale  $\eta, \epsilon$ , keeping others fixed, (c) Scale  $\eta, \epsilon, \beta_1$ , keeping others fixed, (d) Scale  $\eta, \epsilon, \beta_2$ , keeping others fixed, and (e) Scale  $\eta, \epsilon, \beta_1, \beta_2$ . We use a weight decay of  $10^{-4}$  in all the experiments. We observe that scaling all the hyperparameters consistently gives better performance at higher batch size. Scaling rule (c) is close second.



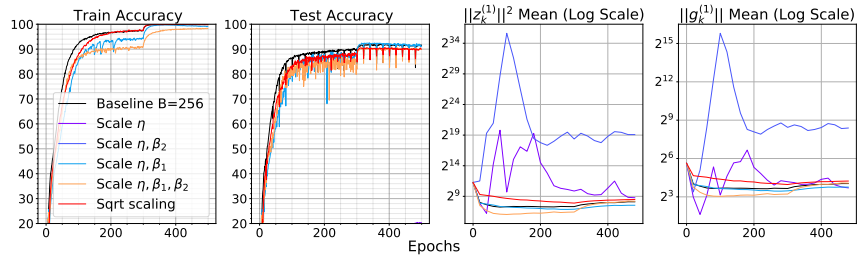
(a)  $B = 8192$ ,  $\epsilon$  of order  $10^{-30}$



(b)  $B = 16384$ ,  $\epsilon$  of order  $10^{-30}$



(c)  $B = 8192$ ,  $\epsilon$  of order  $10^{-8}$



(d)  $B = 16384$ ,  $\epsilon$  of order  $10^{-8}$

Figure 25: Ablation study against (possible) linear scaling rules on Resnet-50 trained with Adam on CIFAR-10. We compare the performance of a model trained with batch size 256 and hyperparameters ( $\epsilon = 10^{-8}/10^{-30}$ ,  $\beta_1 = 0.999$ ,  $\beta_2 = 0.999$ ) with the performance at a larger batch size, across 5 runs representing 5 possible linear scaling rules: (a) Scale  $\eta$  linearly, keeping  $\beta_1, \beta_2, \epsilon$  fixed, (b) Scale  $\eta, 1 - \beta_1$  linearly, keeping  $\beta_2, \epsilon$  fixed, (c) Scale  $\eta, 1 - \beta_2$  linearly, keeping  $\beta_1, \epsilon$  fixed, and (d) Scale  $\eta, 1 - \beta_1, 1 - \beta_2$  linearly, keeping  $\epsilon$  fixed. We use a weight decay of  $10^{-4}$  in all the experiments. We also compare the behavior of the linear scaling rules against the square root scaling rule. Since the continuous time definition varies across the scaling rules, we plot against the number of epochs trained. A closer look at the training accuracy plots shows that the square root scaling rule tracks the smaller batch training trajectory better than the linear scaling rule.



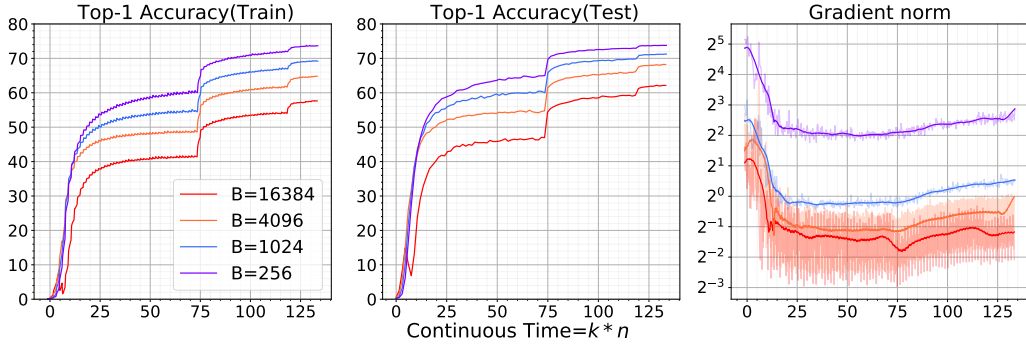


Figure 26: Ablation study against a (possible) linear scaling rule on Resnet-50 trained with Adam on Imagenet. We compare the performance of a model trained with batch size 256 and hyperparameters ( $\eta = 3 \times 10^{-4}$ ,  $\epsilon = 10^{-8}$ , and  $(\beta_1, \beta_2) = (0.999, 0.999)$ ) with the performance at a larger batch size, when the hyperparameters are scaled as follows: scale  $\eta, 1 - \beta_1, 1 - \beta_2$  by  $\kappa$ , if the batch size is scaled by  $\kappa$ , keeping  $\epsilon$  fixed. We use a weight decay factor of  $10^{-4}$ . We clearly observe a decrease in performance at larger batch size, in comparison to models trained with square root scaling rule (see Figure 20).

schedule during the warmup phase is increased linearly with epoch, i.e. the learning rate is given by  $\eta \times 10^{-3} \times (10^3)^{\#\text{epochs}/5}$ . We then followed a learning rate decay schedule, where the learning rate was decayed by 0.1 when the model reaches  $\frac{5}{18}$  fraction (or 50 epoch) and  $\frac{8}{9}$  fraction (or 80 epoch) of the total continuous time respectively. We use two different values for  $\epsilon$ , small  $\epsilon (= 1e - 30 \approx 0)$  and a larger  $\epsilon (= 1e - 8)$ .

### J.3 Books and Wikipedia (Academic BERT)

We use a combination of Bookcorpus [24] plus English Wikipedia, which totals 16 GB of uncompressed text. We split the data uniformly with a ratio 9 : 1, to create training and validation datasets for pretraining.

**Architecture.** We pretrain a 24-layer RoBERTa [23] model. We pretrain on sequences of length 128.

**Pre-training with Adam.** We use the code from [43]. We follow the optimization recipe from [28] for efficient pre-training. To fix a baseline, we first trained our model with batch size 1024, with the optimization parameters given in table 2. In the warmup phase, the learning rate is increased linearly over the interval, i.e. the learning rate at step  $k$  in the warmup phase is given by  $\frac{k}{k_{\text{warmup}}}\eta$ , where  $k_{\text{warmup}}$  denotes the total number of warmup steps and  $\eta$  denotes the peak learning rate. Moreover, after the warmup phase, the learning rate is decayed linearly to 0, i.e. the learning rate at step  $k$  after the warmup phase is given by  $\frac{k - k_{\text{warmup}}}{k_{\text{max}} - k_{\text{warmup}}}\eta$ , where  $\eta$  denotes the peak learning rate and  $k_{\text{max}}$  denotes the maximum number of gradient steps intended for pretraining.

**Fine-tuning with Adam:** We also validate the performance of the pretrained models from the previous section on the GLUE[40] datasets. For each downstream task, we run an extensive grid search on the hyperparameters for finetuning each pretrained model. We focused on the following hyperparameters for grid search: batch size, the peak learning rate and the total number of training epochs. Please see Table 4 for the hyperparameter grid. The rest of the hyperparameters are fixed for all the runs and are given in Table 3. We follow a similar learning rate schedule during the warmup phase as was used for pretraining: the learning rate at step  $k$  in the warmup phase is given by  $\frac{k}{k_{\text{warmup}}}\eta$ , where  $k_{\text{warmup}}$  denotes the total number of warmup steps and  $\eta$  denotes the peak learning rate. Moreover, after the warmup phase, the learning rate is decayed linearly to 0, i.e. the learning rate at step  $k$  after the warmup phase is given by  $\frac{k - k_{\text{warmup}}}{k_{\text{max}} - k_{\text{warmup}}}\eta$ , where  $\eta$  denotes the peak learning rate and  $k_{\text{max}}$  denotes the maximum number of gradient steps intended for finetuning.

Hyperparameter	Value
Dropout	0.1
Attention Dropout	0.1
Warmup Steps	5520
Peak Learning Rate	$10^{-3}$
Batch Size	1024
Weight Decay	$10^{-4}$
Max Steps	92000
Learning Rate Decay	Linear
Adam $\beta_1$	0.99375
Adam $\beta_2$	0.996
Adam $\epsilon$	$2 \times 10^{-6}$
Gradient Clipping	0.0
Position embeddings	128

Table 2: Optimization hyperparameters of baseline RoBERTa model during pretraining.

Hyperparameter	Value
Dropout	0.1
Attention Dropout	0.1
Warmup Steps	6% of total
Weight Decay	0.1
Learning Rate Decay	Linear
Adam $\beta_1$	0.9
Adam $\beta_2$	0.98
Adam $\epsilon$	$10^{-6}$
Gradient Clipping	0.0

Table 3: Optimization hyperparameters of all pretrained RoBERTa models during finetuning.

Dataset	Finetune batch size	Peak Learning rate	Total training epochs
CoLA	{16, 32}	$\{10^{-5}, 3 \times 10^{-5}, 5 \times 10^{-5}, 8 \times 10^{-5}\}$	{3, 5, 10}
SST-2	{16, 32}	$\{10^{-5}, 3 \times 10^{-5}, 5 \times 10^{-5}, 8 \times 10^{-5}\}$	{3, 5, 10}
MRPC	{16, 32}	$\{10^{-5}, 3 \times 10^{-5}, 5 \times 10^{-5}, 8 \times 10^{-5}\}$	{3, 5, 10}
STS-B	{16, 32}	$\{10^{-5}, 3 \times 10^{-5}, 5 \times 10^{-5}, 8 \times 10^{-5}\}$	{3, 5, 10}
RTE	{16, 32}	$\{10^{-5}, 3 \times 10^{-5}, 5 \times 10^{-5}, 8 \times 10^{-5}\}$	{3, 5, 10}
QQP	{32}	$\{5 \times 10^{-5}, 8 \times 10^{-5}\}$	{3, 5}
MNLI	{32}	$\{5 \times 10^{-5}, 8 \times 10^{-5}\}$	{3, 5}
QNLI	{32}	$\{5 \times 10^{-5}, 8 \times 10^{-5}\}$	{3, 5}

Table 4: Hyperparameter grid for pretrained RoBERTa on the downstream tasks.

Hyperparameter	Value
Dropout	0.1
Attention Dropout	0.1
Warmup Steps	1000
Peak Learning Rate	$10^{-3}$
Batch Size	1024
Weight Decay	$10^{-4}$
Max Steps	12500
Learning Rate Decay	Linear
Adam $\beta_1$	0.9875
Adam $\beta_2$	0.996
Adam $\epsilon$	$2 \times 10^{-8}$
Gradient Clipping	0.0
Position embeddings	128

Table 5: Optimization hyperparameters of baseline GPT model during pretraining.

#### J.4 WikiText-103 (GPT)

WikiText-103 [26] is a dataset with 103 million tokens extracted from Wikipedia. We split the data uniformly with a ratio 9 : 1, to create training and validation datasets for pretraining. We use Adam [6] optimization algorithm.

**Architecture.** We pretrain a 12-layer GPT [25] model without modification. The model has 12 layers with hidden dimension 768, feedforward network dimension 3072, 12 attention heads in each attention layer, and attention head size 64. We pretrain on sequences of length 128 (unless stated otherwise).

**Adam.** We use the code from [43]. To fix a baseline, we first trained our model with batch size 1024, with the optimization parameters given in Table 5. In the warmup phase, the learning rate is increased linearly over the interval, i.e. the learning rate at step  $k$  in the warmup phase is given by  $\frac{k}{k_{\text{warmup}}}\eta$ , where  $k_{\text{warmup}}$  denotes the total number of warmup steps and  $\eta$  denotes the peak learning rate. Moreover, after the warmup phase, the learning rate is decayed linearly to 0, i.e. the learning rate at step  $k$  after the warmup phase is given by  $\frac{k - k_{\text{warmup}}}{k_{\text{max}} - k_{\text{warmup}}}\eta$ , where  $\eta$  denotes the peak learning rate and  $k_{\text{max}}$  denotes the maximum number of gradient steps intended for pretraining.